

Extreme & High Synchrotron Peak Blazars beyond 4FGL: The 2BIGB γ -ray catalogue

B. Arsioli^{1,2*}, Y-L. Chang^{2,3} B. Musiimenta⁴

¹*Instituto de Física Gleb Wataghin, Universidade Estadual de Campinas UNICAMP, Rua Sérgio Buarque de Holanda 777, Campinas, Brazil*

²*ICRANet, P.zza della Repubblica 10, I-65122, Pescara, Italy*

³*Tsing-Dao Lee Institute, Shanghai Jiao Tong University, 800 Dongchuan RD. Minhang District, 200240, Shanghai, China*

⁴*Mbarara University of Science and Technology, Department of Physics, P.O. box 1410, Mbarara, Uganda*

Accepted 2020 January 31. Received 2019 November 19; in original form

ABSTRACT

This paper presents the results of a γ -ray likelihood analysis over all the extreme and high synchrotron peak blazars (EHSP & HSP) from the 3HSP catalogue. We investigate 2013 multifrequency positions under the eyes of Fermi Large Area Telescope, considering 11 years of observations in the energy range between 500 MeV to 500 GeV, which results in 1160 γ -ray signatures detected down to the TS = 9 threshold. The detections include 235 additional sources concerning the Fermi Large Area Telescope Fourth Source Catalog (4FGL), all confirmed via high-energy TS maps, and represent an improvement of $\sim 25\%$ for the number of EHSP & HSP currently described in γ -rays. We build the γ -ray spectral energy distribution for all the 1160 2BIGB sources, plot the corresponding γ -ray logN-logS, and measure their total contribution to the extragalactic gamma-ray background, which reaches up to $\sim 33\%$ at 100 GeV. Also, we show that the γ -ray detectability improves according to the synchrotron peak flux as represented by the Figure of Merit (FOM) parameter, and note that the search for TeV peaked blazars may benefit from considering HSP and EHSP as a whole, instead of EHSPs only. The 2BIGB acronym stands for ‘Second Brazil-ICRANet Gamma-ray Blazars’ catalogue, and all the broadband models and spectral energy distribution data-points will be available on public data repositories (OpenUniverse, GitHub, and Brazilian Science Data Center-BSDC).

Key words: radiation mechanisms: non-thermal, galaxies: active, BL Lacertae objects: general, gamma-rays: galaxies, catalogues

1 INTRODUCTION

The Fermi Large Area Telescope (LAT, Atwood et al. 2009) produced our most detailed picture of the gamma-ray sky and has opened a window to investigate high & very-high energy¹ processes throughout the universe. Since the delivery of its first source catalogue (Abdo et al. 2010a,b), the *Fermi*-LAT mission has identified blazars as the main population of extragalactic γ -ray emitters. There are 5066 γ -ray point sources reported in the latest *Fermi*-LAT catalogue (4FGL, The Fermi-LAT collaboration 2019a, gll-pcs-v20.fit), all detected with significance $>4\sigma$ (TS>25) covering 8 years of observations, and integrating over the 50 MeV to 1 TeV energy band. According to the Fourth catalogue of active galactic nuclei detected with *Fermi*-LAT (4LAC, The Fermi-LAT collaboration 2019b), there are 3647 4FGL sources out of the galactic plane (at $|b| > 10^\circ$), from which 79% are confident counterparts of active

galactic nuclei (AGN). Given all those gamma-ray AGNs, 98% are blazars. At energies larger than 1 TeV, there is a similar dominance, as follows from the latest version of TeVcat². The TeVcat lists 225 TeV detected sources, and nearly 90% of the extragalactic ones (72 out of 81) are blazars.

Blazars are relatively rare objects with nearly 4000 optically confirmed sources -with available optical spectrum- as listed in 5BZcat and 3HSP catalogues (Massaro et al. 2015; Chang et al. 2019). The 5BZcat lists 3651 confirmed blazars of all types, while the 3HSP lists 2013 objects with a focus to high synchrotron peak blazars and blazar-candidates. Within the 3HSP catalogue there are 657 blazars already listed in 5BZcat, 257 are newly confirmed blazars (out of 5BZcat), and 1099 are blazar-candidates (high confident blazars missing optical identification). Blazars are well estab-

* E-mail: arsioli@ifi.unicamp.br, bruno.arsioli@gmail.com

¹ We use high-energy (HE) for the 0.2-100 GeV range, and very high-energy (VHE) for E > 100 GeV.

² TeVcat:<http://tevcat.uchicago.edu/> is a regularly updated list of TeV detected astrophysical sources. The TeVcat reports on 81 extragalactic TeV sources, which includes 72 blazars, 3 Starbursts, 1 Globular Cluster, 2 AGNs of unknown type and 3 gamma-ray bursts.

lished as the dominant population of extragalactic γ -ray sources, but yet a significant fraction lack detection at HE and VHE.

According to the unification scheme for active galactic nuclei, blazars are AGNs producing relativist jets that happen to point close to our line of sight (Urry & Padovani 1995; Giommi et al. 2012; Padovani et al. 2017). The jets are launched from the AGN's core and composed of relativistic charged particles trapped within the jet's magnetic field. This configuration is most likely powered by accretion into supermassive black holes (Dermer 2015; Petropoulou & Dermer 2016), and gives rise to non-thermal (synchrotron) spectral emission extending through the entire electromagnetic spectra, from radio up to TeV γ -rays.

Blazars can be classified according to the frequency associated with their synchrotron peak and called as low, intermediate, high, and extremely-high synchrotron peak sources (respectively: LSP for $\nu_{\text{peak}}^{\text{syn.}} < 10^{14} \text{ Hz}$, ISP for $10^{14} < \nu_{\text{peak}}^{\text{syn.}} < 10^{15} \text{ Hz}$, HSP for $10^{15} < \nu_{\text{peak}}^{\text{syn.}} < 10^{17} \text{ Hz}$, and EHSP for $\nu_{\text{peak}}^{\text{syn.}} > 10^{17} \text{ Hz}$). The EHSP and HSP sources have -on average- a hard³ photon index $\langle \Gamma \rangle = 1.85 \pm 0.01$ as probed by *Fermi*-LAT (Arsioli et al. 2015; Ackermann et al. 2015b) in the MeV to GeV window. For this reason, EHSP and HSP blazars are considered promising for VHE observations with the Cherenkov Telescope Arrays (Actis et al. 2011; Cherenkov Telescope Array Consortium et al. 2019), and the community dedicates significant attention to characterize their SEDs via multifrequency observation campaigns (Ahnen et al. 2017a,b; Paiano et al. 2017; Aleksić et al. 2014; Takahashi et al. 2000).

This work aims to contribute to the description of blazars at HE & VHE by presenting new γ -ray detections, describing their SEDs, and studying their population properties. We use the position from blazars and blazar-candidates as multifrequency seeds for a likelihood analysis with the *Fermi*-LAT Science Tools, to search for associated γ -ray signatures. The 3HSP catalogue (Chang et al. 2019) is used as reference blazar-database, and is currently the most extensive compilation of EHSP and HSP sources.

Given the spectral characteristics of 3HSP sources, our analysis focuses on a particular blazars subsample, which is more likely to be detectable at the VHE band. In fact, 925 3HSPs sources already have a 4FGL counterpart (we call them 3HSP-4FGL) meaning that the 3HSP source lies within the 95% error region reported in 4FGL. So by studying the entire 3HSP catalogue under *Fermi*-LAT eyes, we can compare results with 4FGL to show the stability of our analysis and the robustness of all new detections. We compute high-energy TS maps for the new sources and confirm that those signatures emerge from a low TS background with points-like TS distribution, avoiding spurious detections with origin related to underestimated background.

The results of this large-scale analysis is the Second Brazil-ICRANet Gamma-ray Blazar catalogue, 2BIGB, which lists 1160 γ -ray excess signatures (Table 1) with significance down to $\text{TS} = 9$. Our broadband analysis integrates over the 500 MeV up to 500 GeV energy range along 11 years of observations with *Fermi*-LAT (Aug. 2008 to Aug. 2019), and we compute the γ -ray SED for all detected sources. Therefore, the 2BIGB catalogue brings an updated review for all the 925 3HSP-4FGL sources and describes the γ -ray spectrum of 235 3HSPs in addition to 4FGL (226 are entirely new and never reported in *Fermi*-LAT catalogues).

This work is a followup from a series of previous efforts dedicated to the γ -ray detection of blazars. The series includes the

First version of the Brazil-ICRANet Gamma-ray Blazar catalogue (1BIGB, Arsioli & Chang 2017), the computation of the 1BIGB γ -ray SEDs (Arsioli et al. 2018), and the use of multifrequency seeds for the detection of LSP blazars (Arsioli & Polenta 2018). To mention, the 1BIGB catalogue involved the analysis of 400 γ -ray candidates from the 2WHSP catalogue Chang et al. (2017), selecting only those with synchrotron peak flux $\nu f_{\nu} \geq 10^{-12.1} \text{ ergs/cm}^2/\text{s}$ and not yet detected by *Fermi*-LAT at the time. The 1BIGB study lead to the detection of 150 γ -ray signatures with significance down to $\text{TS} = 10$, from which 85 had $\text{TS} > 25$.

The 2BIGB catalogue goes beyond 4FGL for the description of EHSP & HSP blazars since all 3HSP-4FGLs now have their γ -ray spectrum modeled with 11 years of available data, in contrast to 8 years for 4FGL. Besides, this work provides a list of newly detected 3HSPs, which represents an improvement of $\sim 25\%$ for the number of EHSP & HSP described in γ -rays.

2 MOTIVATIONS

2.1 An overview of the gal. & extragal. gamma-ray sky

A clear understanding of the γ -ray sky depends on our ability to account for both galactic and extragalactic components and describe each of them in detail so that new features can be unveiled.

Concerning the galactic content, the *Fermi*-LAT mission was essential to map and model point-like sources such as pulsars, supernovae remnants (SNR), pulsar wind nebulae (PWN), globular clusters, etc ($\sim 239, 40, 18, 30$, etc. objects according to the 4FGL catalogue), as well as a diffuse γ -ray component produced by cosmic-ray interactions with the Milk Way gas (Biswas & Gupta 2019). Still, around 90 galactic sources remain unassociated but are likely related to SNR and PWN.

In 2010, the finding of a bipolar component called “Fermi Bubbles” was unexpected (Su et al. 2010). It resembles a jet structure that emanates from the center of our galaxy, extending nearly 8 kpc perpendicular to the galactic plane, in what could be the result of past accretion process in the galactic center black hole (Ko et al. 2019). This structure has well-defined edges in coincidence with X-ray signatures seen by the ROSAT mission in the 1990s (Ponti et al. 2019), and a microwave excess in the same region known as “WMAP haze” (Finkbeiner 2004; Rubtsov & Zhezher 2018). Proper modeling of this component allowed to account for an excess diffuse emission, which covered a significant fraction of the γ -ray sky. As a result, it improves the sensitivity for detecting new point sources in that region.

Within the open question involving observations from *Fermi*-LAT, there is a long-standing debate related to the GeV excess at $\sim 1.5\text{-}3.0$ kpc from the galactic center (Hooper et al. 2013; Mirabal 2013; Leane & Slatyer 2019). This feature could result from multiple unresolved point-like sources as millisecond pulsars (Calore et al. 2014), or the integrated γ -ray emission from our galactic dark matter (DM) halo via annihilation or decay channels (Goodenough & Hooper 2009; Daylan et al. 2016; Karwin et al. 2017). A combination of both contributions, including unresolved sources and DM signatures, are also considered in this contest.

All current debate concerning the galactic γ -ray content is crucial for proper modeling of the extragalactic content. The extragalactic emission (γ_{ExtraGal}) is the remaining radiation when the total galactic contribution (γ_{Gal}) is subtracted from the entire γ -ray content (γ_{Tot}) seen by *Fermi*-LAT; ($\gamma_{\text{ExtraGal}} = \gamma_{\text{Tot}} - \gamma_{\text{Gal}}$). The total γ_{ExtraGal} is usually referred to in the literature as extragalactic γ -ray background (EGB, Ackermann et al. 2015a).

³ We refer to hard (and soft) photon index meaning $\Gamma < 2.0$ (and $\Gamma > 2.0$).

The EGB is a combination of well-resolved point-like sources with a diffuse -and isotropic- γ -ray content. Detailed simulations of the CR interaction with the galactic disk shows that the isotropic diffuse component seen off the galactic plane must have extragalactic roots (Biswas & Gupta 2019). This component, usually called isotropic γ -ray background (IGRB, Ackermann et al. 2015a), could well be the result of an unresolved population of faint γ -ray emitters, including blazars (Giommi & Padovani 2015; Arsioli & Chang 2017; Di Mauro et al. 2014b). Nevertheless, the fact is, the community is still building an understanding of the total EGB composition.

If one considers the IGRB as a sum of unresolved point-like sources plus an actual diffuse component, the increasing number of detectable blazars from 3LAC to 4LAC (Ackermann et al. 2015b; The Fermi-LAT collaboration 2019b) indicates an ever-shrinking space for the remaining diffuse component. Besides, direct searches for new γ -ray sources as in 1BIGB and 2BIGB (this work) proof the existence of a relevant underlying population of faint γ -ray emitters, with direct impact over the diffuse component intensity.

A diffuse component could be the signature of annihilation or decay processes associated with DM particles, happening throughout the universe. A clear understanding of IGRB content may allow us to probe DM parameters like the cross-section associated with processes (annihilation or decay), producing diffuse γ -rays (Liu et al. 2017; Cohen et al. 2017; Di Mauro & Donato 2015; Di Mauro 2015). Contributions to the EGB coming from misaligned AGNs (Inoue 2011; Di Mauro et al. 2014a) and Star Forming Galaxies (Storm et al. 2012) are also present. They certainly account for a significant fraction that could be well constrained via stacking analysis as in Paliya et al. (2019). Moreover, the IGRB could also contain a pure diffuse emission as a result of ultra-high-energy cosmic rays (UHECR) interaction with the extragalactic background light (Gavish & Eichler 2016). In this context, the identification of faint γ -ray emitter is essential to resolve the diffuse content into point-sources and constrain the parameter space available for other possible contributions.

2.2 Blazars as multifrequency seeds to investigate the gamma-ray sky

The 3HSP catalogue lists a total of 2013 sources, and nearly half of them (1088) have no γ -ray counterpart according to the latest release of the *Fermi*-LAT point source catalogue, 4FGL. Fig. 1 shows the distribution of the log synchrotron peak flux $\log(\nu f_\nu)$ for the 3HSP detected and undetected γ -ray sources according to 4FGL. As seen, the 4FGL has unveiled most of the bright 3HSPs with $\log(\nu f_\nu) > -12.2$ [ergs/cm²/s], and many of the undetected 3HSPs have a synchrotron component as bright as the detected ones.

Besides, the 1BIGB catalogue shows clearly how the ‘fraction of *Fermi*-LAT detected sources’ varies according to the synchrotron peak flux $\log(\nu f_\nu)$, and that a dedicated search for new γ -ray sources can improve the detected fraction down to the faintest blazars (see Fig. 6 at Arsioli & Chang 2017). Therefore, the overlap in Fig. 1 for detected and undetected sources at $\log(\nu f_\nu)$ [erg/cm²/s] between -13.0 to -12.2, hints for a population of blazars that are just within reach of *Fermi*-LAT, close to the detectability threshold.

Those facts alone are compelling enough to motivate a dedicated *Fermi*-LAT analysis based on the entire 3HSP catalogue, using them as multifrequency seed positions to unveil new γ -ray sources. Also, we rely on the availability of 11 years of *Fermi*-LAT data, in contrast to 8 years used to build the 4FGL catalogue. The 1BIGB catalogue was done over this same and straightforward idea, and lead to the detection of nearly 150 new γ -ray sources,

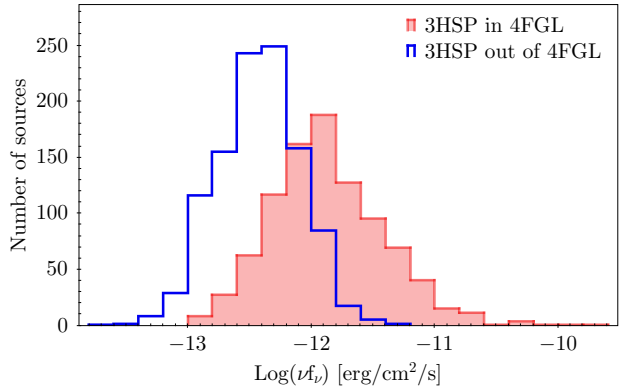


Figure 1. The distribution of log synchrotron peak flux $\log(\nu f_\nu)$ [erg/cm²/s] for the 3HSP sources, with the 925 objects detected in 4FGL (full bars in light-red), and the 1088 undetected ones (blue line). The intersection between histograms suggests that multiple sources are close to the *Fermi*-LAT detection threshold.

from which the 3FHL catalogue has confirmed 34 (Ajello et al. 2017), and a total of 99 are well within the 95% error ellipses from 4FGL sources.

The method applied to build the 2BIGB catalogue is a follow-up from previous works (Arsioli et al. 2018; Arsioli & Chang 2017; Arsioli & Polenta 2018) where multifrequency data is used as a complementary tool to select seed positions in the sky for further analysis with the Fermi Science Tools. Mostly, we reproduce what the Cerenkov Telescope community already does in search of new TeV sources, which means, to actively aim to seed-candidates selected from multifrequency data. One of the latest detections from the Major Atmospheric Gamma Imaging Cherenkov - MAGIC (MAGIC Collaboration et al. 2019a) is a clear example of that, where a new TeV signature is confirmed when aiming at 2WHSP J073326.7+515354, which is well characterized at lower energies and previously selected as a promising TeV target from multifrequency considerations.

The search for new γ -ray sources as in 1 & 2BIGB catalogues can also contribute to studies of astrophysical neutrinos in connection to γ -ray blazars. Recently in MAGIC Collaboration et al. (2019c); Padovani et al. (2018), the authors dedicate attention to the identification and modeling of dim γ -ray sources in regions associated with IceCube muon-track events. With no doubt, proper identification of faint GeV-TeV sources is of high relevance. Also, a source can be weak in terms of photon counts but still relevant in the VHE window, especially for cases where the *Fermi*-LAT only probes the rising tail of the higher-energy SED peak.

3 METHODOLOGY

3.1 The Gamma-ray data analysis

For the broadband data analysis, we use the Fermi Science Tools version v11r5p3 and Pass 8 data (P8R3, Bruel et al. 2018; Atwood et al. 2013) corresponding to 11 years of observations, from Aug 2008 to Aug. 2019. We build an all-sky pre-selection of photons with energy between 300 MeV up to 900 GeV, and use the clean-event type (evtype=256) with its corresponding instrument response function (IRF) P8R3-CLEAN-V2. The use of clean-event type is desirable in our case since it provides an improved lower-

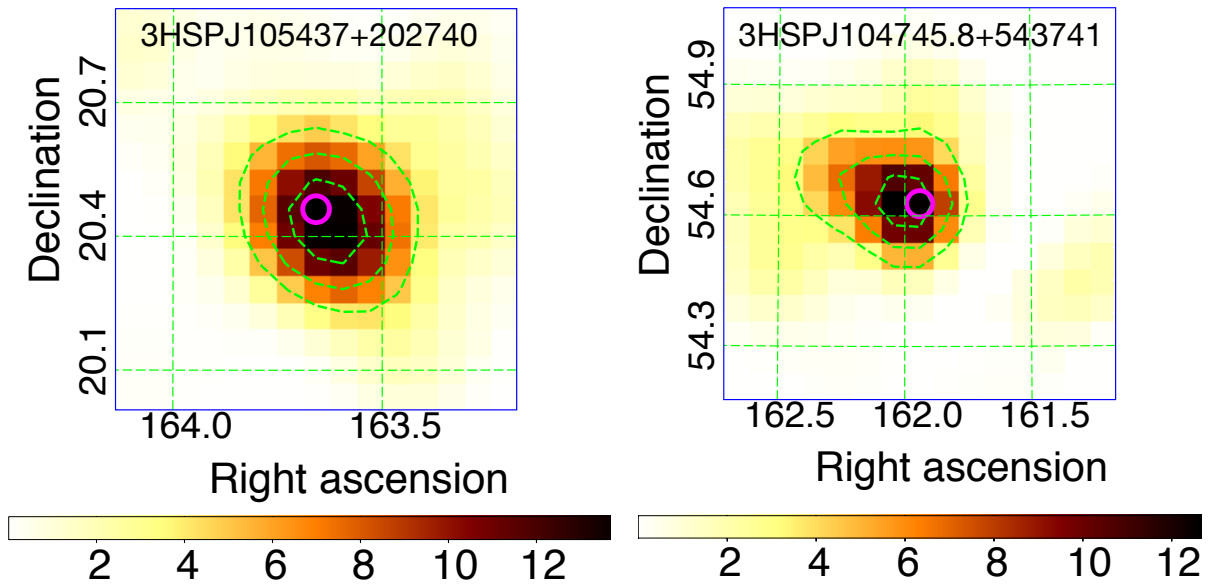


Figure 2. The high-energy TS map center at 3HSP J105437.9+202740 (right) and 3HSP J104745.8+543741 (left), integrating over 10.5 years of data only considering photons with $E > 2$ GeV. Those are examples of γ -ray signatures close to the detection threshold. The green dashed lines correspond to the 68%, 95%, and 99% containment region for the γ -ray signature (from inner to outer lines). The TS values are smoother over two pixels with a 2σ Gaussian function and are color-coded corresponding to the bottom legend.

level background at $E > 3$ GeV; therefore, more sensitive to hard spectrum sources as the HSP blazars. The all-sky photon file (our pre-selection) speeds up the gselec routine, which is the first step of the analysis, and repeated for each object.

After the pre-selection, we set a broadband binned analysis in the 500 MeV to 500 GeV energy band, considering a region of interest (ROI) of 15° around the position of a 3HSP γ -ray candidate. The investigation for each 3HSP object is independent, meaning that each analysis probe only one γ -ray candidate at a time. We accomplish the coverage over the entire 3HSP catalogue by parallel computing in computer clusters as Planck and Feynman from CCJDR Unicamp BR, and Joshua from ICRA-Net IT.

The cut at 500 MeV serves two purposes: On one hand, it is meant to improve the computational time of the analysis, which gets heavier when considering low-energy photons (those are relatively more abundant). On the other hand, it improves the robustness of the results while avoiding low-energy photons that have the largest point spread function (PSF) in the database. The low-energy cut is desirable in our case given the focus on EHSP & HSP sources, which are characterized by relatively hard γ -ray spectrum and more relevant at the highest energies. Also, cutting off the low-energy photons let the analysis free of computing energy dispersion at energy levels lower than 300 MeV, which would significantly increase the computational burden.

The cut at 500 GeV follows recommendations from the *Fermi*-LAT team for broadband analysis (in “data preparation” section at <https://fermi.gsfc.nasa.gov/>). Also, the 4FGL paper (their sec. 3.2, [The Fermi-LAT collaboration 2019a](#)) comment on the fact that for hard sources, integrating up to energies of 1 TeV in a broadband analysis systematically increases the uncertainty for parameters such as the photon and energy fluxes. Therefore, with a cut at 500 GeV the analysis avoids uncertainties for the broadband flux, and prevent spurious detections that could arise from poor modeling of the VHE diffuse background.

A zenith angle-cut of 105° is used to avoid contamination with

Earth’s limb γ -ray photons, which are induced by cosmic-ray interactions with the atmosphere and are known as a strong source of background for the low-energy band of *Fermi*-LAT. With the gtmktime routine, we generate a list of good time intervals, selecting events with flags (DATA-QUAL>0) and (LAT-CONFIG==1), which guarantees to only consider data acquired in normal science data-taking mode. Then, with the gtbin routine, we generate counts maps (CMAP) and counts cubes (CCUBE) of 300×300 and 210×210 pixels with $0.1^\circ/\text{pixel}$, respectively. The CCUBE is a series of CMAPs, each one having photons within 37 logarithmic equally-spaced energy bins along 0.5–500 GeV. The livetime cube is build with the gltcube routine, selecting $\cos(\theta)=0.025^\circ$ as recommended.

The γ -ray sky models are build with the make4FGLxml.py⁴ script, which includes information on all point and extended sources in the ROI region, together with the galactic and extra-galactic diffuse components. For the point sources, we use the latest version of the *Fermi*-LAT catalogue gll-psc-v20.fit, which we call 4FGLv20. For the diffuse galactic background model and the isotropic component, versions gll-iem-v07.fit and iso-P8R3-CLEAN-V2-v1.txt are used, respectively. All sources within 8.0° from the center ROI have spectral parameters -normalization and photon index- set free to vary, which is essential to adapt the 4FGL models (based in eight years) to the 11 years of integration time used in this work. This is necessary for a proper description of the ROI region and to avoid spurious signatures associated with our candidates.

Then, a model map is prepared with the gtsrcmaps routine, which holds information about all spectral components and sources within the ROI region. Each 3HSP object is placed in the ROI model as a point-like source, and described with a power-law type

⁴ The makeFGLxml.py is a python routine written by T. Johnson, 2015, and provided by the *Fermi*-LAT team as a user contribution tool.

Table 1. Power-law model for the top 10 2BIGB-3HSP new γ -ray sources. Note that a complete table with all the 1160 2BIGB source is available in the on-line version of this paper, and also at public repositories; Github <https://github.com/BrunoArsioli>. The first three columns show the 2BIGB names, right ascension R.A. and declination Dec. in degrees (J2000), respectively. The fourth column shows the reported redshifts from literature (Shaw et al. 2013b; Pita et al. 2014; Furniss et al. 2013; Danforth et al. 2010; Shaw et al. 2013a; Masetti et al. 2013; Sbarufatti et al. 2005; Massaro et al. 2015), with a right uppercase flag where (1) correspond to cases with a robust redshift value, (2) for values reported as uncertain, (3) for lower limits reported in 3HSP catalogue, and for a photometric estimate by fitting a Giant Elliptical host galaxy template we have (4) when a featureless optical spectrum is available, and (5) when no optical spectrum is available but only photometric data points. The parameters reported in columns are the normalization N_0 (eq. 1), which is given in units of $\text{ph}/\text{cm}^2/\text{s}/\text{MeV}$; the photon spectral index Γ ; the column Flux shows the photon counts integrated over 0.5–500 GeV in units of $\text{ph}/\text{cm}^2/\text{s}$; the pivot energy E_0 ; and the TS is the Test Statistic value.

2BIGB name	R.A. (deg)	Dec. (deg)	z	Γ	$N_0 (10^{-15})$	$\text{Flux}_{0.5-500 \text{ GeV}}^{<10^{-11}}$	$E_0 (\text{GeV})$	TS
210415.9+211808	316.06633	21.30228	⁵ 0.36	1.91±0.14	13.2±2.3	59.6±17.5	5.0	122.3
235955.0+314600	359.98042	31.76667	⁵ 0.33	1.85±0.12	8.54±1.38	35.6±7.0	5.0	96.8
111717.5+000633	169.32308	0.10931	¹ 0.451	1.76±0.13	7.85±1.50	29.6±7.4	5.0	74.3
230848.7+542611	347.20308	54.43644	-	1.71±0.12	2.55±0.47	30.1±7.8	10.0	66.9
083015.1-094455	127.56308	-9.74883	⁵ 0.5	1.85±0.15	15.8±3.7	25.6±7.4	3.0	53.1
225613.3-330338	344.05546	-33.06064	¹ 0.243	1.99±0.17	15.9±4.4	28.5±10.2	3.0	51.6
030103.7+344101	45.26558	34.68367	¹ 0.246	2.13±0.17	21.5±4.1	44.4±11.6	3.0	49.8
235917.0+021520	359.8210	2.25564	-	1.85±0.14	5.40±1.20	22.5±6.1	5.0	48.3
173044.8+380454	262.68663	38.08192	⁵ 0.22	1.79±0.17	4.64±1.18	18.0±6.6	5.0	40.9
101724.4+253956	154.35158	25.66556	¹ 0.417	1.40±0.19	0.96±0.30	7.54±3.14	10.0	40.6

of spectrum as follows:

$$\frac{dN}{dE} = N_0 \left(\frac{E}{E_0} \right)^{-\Gamma}, \quad (1)$$

where N_0 is the normalization constant (prefactor) in units of photons/cm²/s/MeV and represents the flux density calculated at the pivot-energy E_0 , with Γ to represent the photon spectral index.

In cases where a 4FGL is already counterpart of the 3HSP, we remove the 4FGL form the ROI model and place a new γ -ray candidate using the 3HSP position as seed. For all cases, the position associated with the γ -ray source (or candidate) is fixed, therefore lowering the uncertainty related to source position. This is the main advantage of considering multifrequency data to select seed positions. Given that the 2BIGB analysis avoids two degrees of freedom concerning a blind search, we can lower the detection threshold.

In fact, the detection of a new class of γ -ray emitter demands large significance, given the analysis cannot avoid the uncertainty on the source position when deduced from γ -ray information only. From Mattox et al. (1996), the χ^2 distribution with four degrees of freedom shows that a Test Statistic (TS) of 25 corresponds to a detection with $\sim 4\sigma$, just as the detection threshold defined in the 4FGL catalogue⁵. In this case, there are two degrees of freedom related to source position (R.A. and Dec.), and another two related to the normalization N_0 and the photon spectral index Γ , which are free parameters of the power-law model.

Following Mattox et al. (1996) (their sec. 3.2), a γ -ray signature with statistical significance of the order of $\sim 3\sigma$ is sufficient for the detection of blazars, because blazars are the most relevant class of extragalactic gamma-ray emitter. A lower detection threshold is acceptable, given the analysis has less two degrees of freedom

⁵ The Test Statistic parameter is defined as $-2\ln(L_{(\text{no-source})} / L_{(\text{source})})$, where $L_{(\text{no-source})}$ is the likelihood of observing a given photon count only due to background (null-hypothesis), and $L_{(\text{source})}$ is the likelihood of observing a given photon count considering a source exists in a particular position (Mattox et al. 1996).

(R.A. and Dec. are set as fixed to avoid the uncertainty related to the source location). For a broadband analysis with two degrees of freedom, a 3σ detection corresponds to TS~13. In our analysis, we lower the threshold down to TS = 9 ($\sim 2.3\sigma$) to include faint detections for future follow-up⁶. Given that we investigate ~ 2000 seed positions, the total number of spurious detections expected is of the order of $\frac{2000}{10^{2.3}} \sim 10$. Moreover, the number of spurious detection might be even lower, given that we evaluate the TS distribution of all new detections, and actively removed all likely-spurious cases which did not reveal itself as a point-like source.

Since the prefactor term N_0 corresponds to the flux density at the pivot energy E_0 , we scan over the E_0 space, running the likelihood analysis with E_0 set as fixed for 1 GeV, 3 GeV, 5 GeV and 10 GeV to evaluate the best condition for modeling each source. This particular step allows to select a pivot-energy that minimizes the error associated to N_0 . For cases where the 3HSP has a 4FGL counterpart, the pivot-energy corresponds to 4FGLv20. We perform the analysis with E_0 set as fixed so that N_0 and Γ could be estimated with much lower uncertainty.

The likelihood analysis goes through two steps with the gtlike routine, following recommendations from the *Fermi*-LAT analysis threads. First, the gtlike runs with the fitting optimizer DRMNFB to generate enhanced sky models, better describing all sources with free parameters. After this first interaction, the model map is rebuilt with the enhanced source-input list, and feed the gtlike routine, now with the NEWMINUIT optimizer, to generate the final model.

3.2 Building the 2BIGB catalogue

With the results of our likelihood analysis, we set the requirement of TS>9 to select the preliminary list of sources with significant γ -

⁶ The correspondence between the TS value, the number of degrees of freedom, and the significance of a γ -ray signature can be calculated according to <https://github.com/BrunoArsioli/TS-DegFreedom-Sigma-relation-FermiLAT>.

ray signature. This list included all 925 3HSPs with a counterpart in 4FGL, which are considered as firm detections. It also included ~270 cases with no counterpart in 4FGL, and that could turn out to be new γ -ray detections. Therefore, in addition to the TS requirement, we build high-energy TS maps with an energy cut of $E > 2 \text{ GeV}$ for all cases with no counterpart in 4FGL.

A TS map is a grid of pixels where the existence of a point-like γ -ray source is tested separately in each point of the grid. The grids have $\sim 18 \times 18$ pixels with $0.06^\circ/\text{pixel}$. If a pixel match with the position of a point source, the TS signature is maximized (large TS values), and if there is a slight offset between the pixel and the exact position of the point-source, the reported TS values are depleted. Therefore, a point source is expected to reveal itself as a smooth Gaussian-like distribution of TS values around a TS peak, as seen in Fig. 2 (build with DS9 software, Joye & Mandel 2003). With this procedure we confirmed 235 sources out of the 270 candidates, clearly showing point-like signatures emerging from a smooth and low TS background as in Fig. 2.

Finally, the 2BIGB catalogue has a total of 1160 sources with a broadband excess signature corresponding to $\text{TS} > 9$, from which 925 have a 4FGL counterpart, and 235 are new-detections concerning 4FGL. Table 1 shows a sub-sample of 10 new-detection with the most significant TS values. A list with the total 1160 sources is available in the on-line version of this paper, and also in public repositories; Github <https://github.com/BrunoArsioli>. For simplicity, we define the acronyms:

- 3HSP-2BIGB corresponds to the total 1160 3HSP sources detected in our broadband analysis over 11 years of *Fermi*-LAT observations, along the 0.5–500 GeV energy band.
- 3HSP-4FGL corresponds to the 925 3HSPs sources that already have a 4FGL counterpart, as of version gll-psc-v20.
- 2BIGB_{new} refers to the 235 2BIGB sources which are new with respect to 4FGL. Moreover, 226 were never reported in previous γ -ray catalogues, including 1-2-3-4FGL & 1-2-3FHL (Abdo et al. 2010a; Nolan et al. 2012; Ackermann et al. 2015c; The Fermi-LAT collaboration 2019a; Ackermann et al. 2013, 2016b; Ajello et al. 2017).

3.3 The gamma-ray Spectral energy distribution

The 2BIGB catalogue presents a SED description for all its 1160 sources, with estimated flux values (or Upper Limits) for ten energy bands, with data-points ranging from 1 GeV to 170 GeV. Note that the broadband analysis is updated to the latest version of the point-source catalogue 4FGLv20 (gll-psc-v20.fit) and integrated over 11 years. However, the γ -ray SED is built considering 10.5 years of observations, and having 4FGLv19 (gll-psc-v19.fit) as the library of point-sources to build the sky models.

In *Fermi*-LAT catalogues, the energy bins are defined by dividing the broadband window in equally spaced logarithmic values, which tends to produce mostly UL values in faint γ -ray sources. However, in the 2BIGB catalogue, the fluxes are estimated by integrating over superposed energy windows (as listed in Table 2), which are larger than equally spaced logarithmic bins. By doing so, we incorporate valuable broadband information into the SED description, following the same approach as in previous work (Arsioli et al. 2018), and allowing us to extract SED information even for the faint sources. To fit each SED data-points, both N_0 and Γ are left free to vary, setting an independent power-law model for each energy bin. This way, the SED final shape is more sensitive to the actual spectral curvature, and not bound to the broadband

Table 2. The column ‘Integrated over’ shows the definition of the energy bins used for the spectral analysis. We estimate the flux density N_0 [ph/cm²/s/MeV] for each pivot-energy E_0 within its corresponding bin, and the analysis-type binned/unbinned is also listed.

E_0 [GeV]	Integrated over [GeV]	Analysis-Type
1.0	0.7 - 5.0	binned
1.7	0.8 - 10.0	binned
3.0	0.9 - 17.0	binned
5.0	1.0 - 30.0	binned
10.0	1.7 - 50.0	binned
17.0	3.0 - 100.0	unbinned
30.0	5.0 - 170.0	unbinned
50.0	10.0 - 300.0	unbinned
100.0	30.0 - 500.0	unbinned
170.0	50.0 - 800.0	unbinned

power-law modeling (500 MeV to 500 GeV). In the case of 4FGL, for example, only N_0 is allowed to vary (fit) in each energy bin, and the Γ parameter is set fixed according to its broadband power-law modeling (The Fermi-LAT collaboration 2019a).

To build a spectral description for all 1160 2BIGB sources represents a massive load of nearly 12k likelihood analysis to complete, divided between binned and unbinned for the lower and higher energy bands, respectively. Table 2 lists the pivot-energies (E_0) at which the fluxes are calculated, by integrating over the correspondent energy band. We choose those E_0 values to be close to logarithmic equally spaced SED data points when plotting on commonly used spectrum planes for blazars, like $\log(\nu)$ vs. $\log(\nu f_\nu)$. Therefore E_0 increases from 1 GeV up to 170 GeV with increments of the order of $\sim 10^{0.25}$.

For the highest energy bands (17 GeV up to 170 GeV), we applied unbinned analysis, which is more compute-intensive but better suited for cases where the photon count is low. This approach follows from the 1BIGB paper data analysis, which showed that a binned analysis could lead to an underestimated flux at 100 GeV when compared to sources detected in 2FHL and 3FHL. Although a cut at 500 GeV was set for the broadband analysis, the use of photons with $E > 500$ GeV is valuable to estimate the flux at the very-high-energy bins. Especially for bright and extreme sources, which can be detected by *Fermi*-LAT up to the energy level of 100 GeV and larger, we do integrate from 50 GeV up to 800 GeV to build the largest energy data-point at 170 GeV. In this case, the uncertainties related to VHE photon/energy fluxes are contained in the last bin and adequately accounted for by the flux error estimate.

For the data analysis, all sources within 8° from the 2BIGB position have free spectral parameters to fit, just as in the broadband analysis. Given the choice of E_0 for each bin, we get a reliable calculation for the normalization parameter N_0 , which is the differential flux at that specific energy. In other words, the SED data points are direct outputs from the likelihood analysis, only by converting N_0 [ph/MeV/cm²/s] to flux [erg/cm²/s]; $\text{Flux}(E_0) = N_0 \cdot E_0^2 \cdot 1.602 \times 10^{-6}$, where the factor 1.602×10^{-6} is to convert MeV to erg. Whenever a band reaches $\text{TS} < 6.0$, an upper limit value is assigned. Especially, for the largest energies of 100 GeV and 170 GeV, we raise the UL threshold to $\text{TS} < 10.0$ to be more conservative and only report on confident VHE flux estimates. For the upper limit values, we use the Broadband-Flux-

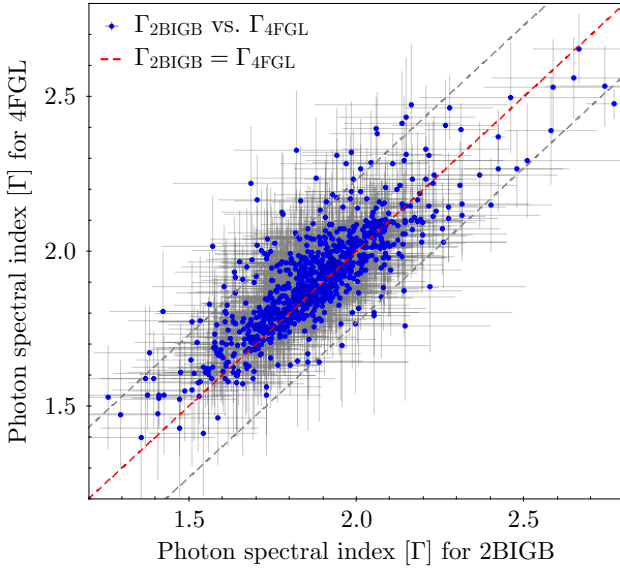


Figure 3. Scatter plot comparing the photon spectral index for the 925 2BIGB sources with counterparts in 4FGL (the 3HSP-4FGL sources). Dashed red represent the $\Gamma_{2\text{BIGB}} = \Gamma_{4\text{FGL}}$ line, and dashed gray represents the 2σ confinement region.

Sensitivity-l0-b30 (for P8R3-V2 and 10 years of exposure), which are conservative compared to larger galactic latitudes⁷.

The SED data points from the 2BIGB catalogue are suitable to identify the mean spectral shape over time, given the large integration window of 10.5 years, but also smooth in terms of energy, given the superposed energy bins. Fine spectral structure derived from this data-set in combination with TeV data from Cherenkov Telescopes should be considered with care and case by case, especially to evaluate the influence of spectral variability along time. If not properly accounted, short-time flaring events can mimic spectral structure when integrating over a large time window.

4 RESULTS & DISCUSSION

4.1 A comparison between 2BIGB and 4FGL

We chose to investigate the entire 3HSP catalogue with *Fermi*-LAT to update the power-law fitting parameters for all the 925 3HSP-4FGL sources, now based on 11 years of observations. Besides, it is possible to compare all 3HSP-4FGL with the 3HSP-2BIGB sources, and evaluate the agreement between the main fitting parameters Γ and N_0 . Fig. 3 shows the scatter plot of the photon spectral index from 3HSP-4FGL ($\Gamma_{4\text{FGL}}$) versus the 3HSP-2BIGB sources ($\Gamma_{2\text{BIGB}}$). And Fig. 4 shows the normalization parameter $N_0^{4\text{FGL}}$ vs. $N_0^{2\text{BIGB}}$. In both cases, we consider all 925 3HSP-4FGL sources that have a 2BIGB counterpart, and compare their power-law fitting parameters. A certain degree of scattering is expected, as seen in Fig. 3 and 4.

Note that the 2BIGB broadband analysis covers the 500 MeV to 500 GeV energy window, whereas 4FGL covers 50 MeV up to 1 TeV. The 2BIGB avoids the lower energy band (from 50 MeV

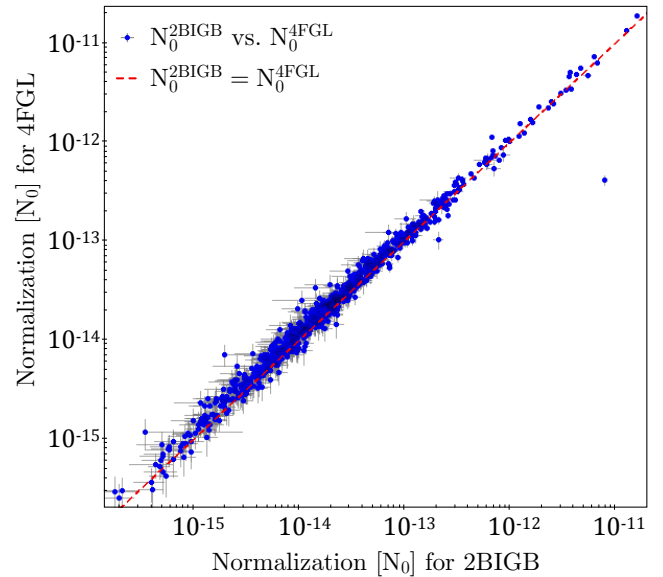


Figure 4. Scatter plot comparing the normalization parameter N_0 for the 925 3HSP-4FGL sources with counterparts in 2BIGB. Red dashed represent the $N_0^{2\text{BIGB}} = N_0^{4\text{FGL}}$ line, which shows good agreement along five decades.

to 500 GeV), which is a source of uncertainty given the broader PSF of low energy photons. Also, the 2BIGB incorporates an additional three years of observations concerning 4FGL, and intrinsic variability becomes another source of data spread. The scattering for the Γ plane is well confined within 2σ deviation, and there is good agreement between 2BIGB and 4FGL for the N_0 parameter along five decades in flux⁸. We conclude that our 2BIGB analysis is robust and consistent with the results reported in 4FGLv20, and this agreement supports the validity of our 235 new detections (2BIGB_{new}) associated with 3HSP sources.

4.2 Detectability and sensitivity limit according to FOM

The Fig. 5 shows the photon spectral index (Γ) versus the integral flux (0.5–500 GeV) from where it is possible to perceive the improvement in sensitivity limit when going from the 3FGL setup to 4FGL, and finally to 2BIGB. Besides, the overlap between 2BIGB and 4FGL sources shows the improvement in completeness close the faint end of the 3HSP-4FGL sample. The dashed lines are qualitative representations of the flux-limit and its dependence with respect to Γ , for both the 3HSP-2BIGB and 3HSP-4FGL samples. The improvements seen for the 2BIGB catalogue result from the extra three years of data, the use of multifrequency information, and the adoption of a lower detection threshold to search for new sources.

Each 3HSP source has an associated Figure of Merit (FOM) parameter. The Figure of Merit is defined as a ratio between the synchrotron peak flux $v f_\nu$ of a given source, and the faintest $v f_\nu$ associated to a TeV detected HSP source ($v f_\nu = 2.5 \times 10^{-12}$ erg/cm²/s, $\log(v f_\nu) = -11.6$). Therefore, the FOM is a parameter connected to the likelihood of TeV detectability (see Chang et al. 2019, for more

⁷ The *Fermi*-LAT performance is described at https://www.slac.stanford.edu/exp/glast/groups/canda/lat_Performance.htm.

⁸ The single outlier is 3HSP J224910.7-130002, which is detect in 2BIGB with TS~15000, while detected with TS~121 in 4FGL, therefore a source which probably went flaring between Oct 2016 to Oct 2019.

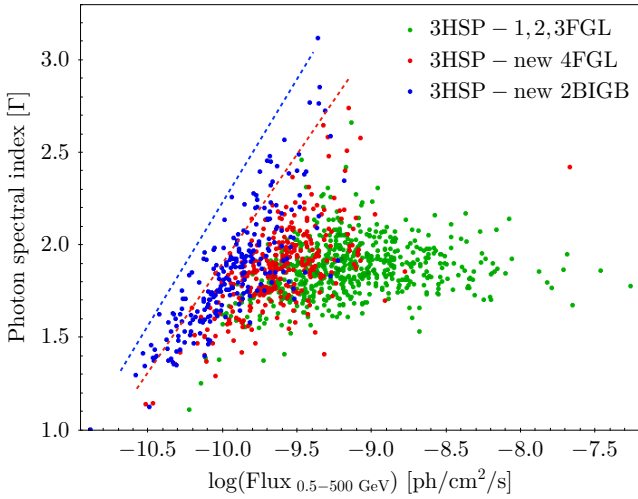


Figure 5. The photon spectral index (Γ) versus $\log(\text{flux})$ for the energy range 0.5–500 GeV. Green, red, and blue colors represent respectively 3HSP sources with counterparts from 1,2,3FGL, only 4FGL, and the new detections from the 2BIGB catalogue. The dashed lines represent a qualitative flux limits

reached by the 4FGL (red) and the 2BIGB (blue) catalogues.

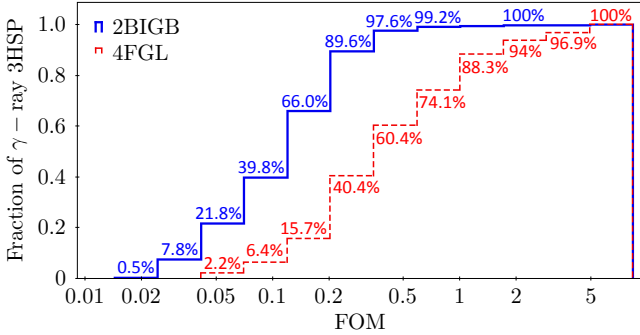


Figure 6. Histogram for the cumulative fraction of 3HSP sources detected in γ -rays for each FOM logarithmic bin. The 2BIGB sources are shown in blue and the 4FGL in red. Note that the last bin to the right condense all 3HSP sources with $\text{FOM} > 5$. Here, $\text{FOM} = \log(vf_v)/-11.6$ [erg/cm²/s].

details) and here we show it indeed works as a reliable proxy for the γ -ray detectability with *Fermi*-LAT.

Figure 6 shows that the fraction of γ -ray detected sources increases with the FOM value, for both 2BIGB and 4FGL catalogues. Moreover, Fig. 6 shows that the 2BIGB catalogue brings an improvement in sensitivity concerning 4FGL, contributing to the γ -ray detection of a larger fraction of blazars in every FOM bin.

4.3 The photon spectral index & flux distribution

Fig. 7 (top) shows the photon spectral index distribution for all the 925 3HSP-4FGL and compare it to the 1160 3HSP-2BIGB sources. We also plot the distribution for the 235 2BIGB_{new} sources, which are new detections concerning 4FGL. A Kolmogorov-Smirnov (KS) test shows that the 3HSP-4FGL and 3HSP-2BIGB normalized histograms are similar, with a p-value of 0.587. Also, the normalized distribution of 3HSP-4FGL and 3HSP-2BIGB_{new} are similar under the KS test, with a p-value of 0.174. Therefore, at 5% level

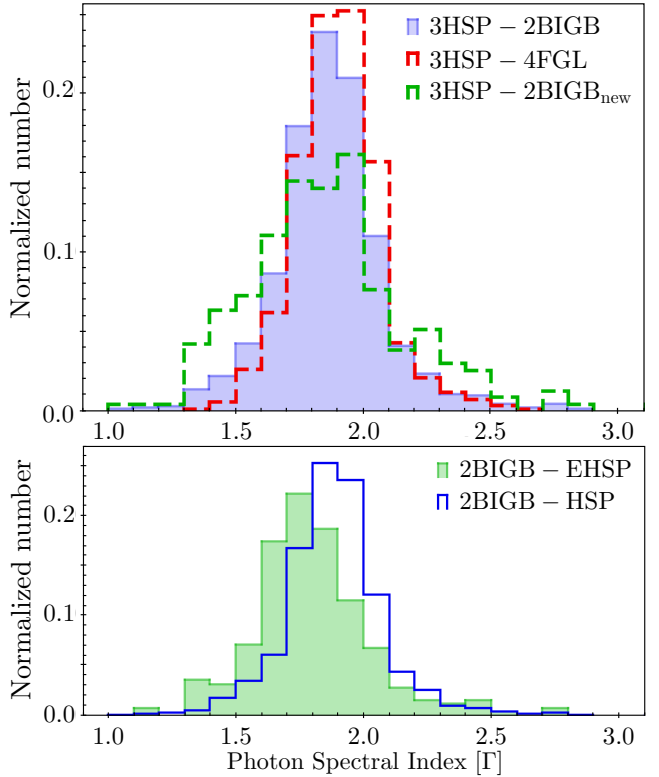


Figure 7. (Top) Normalized histogram to compare the photon index Γ distribution for the samples 3HSP-2BIGB (full indigo bars), 3HSP-4FGL (red dashed), and 2BIGB_{new} (green dashed). In the case of 3HSP-4FGL sources, the Γ values correspond to 4FGLv20. (Bottom) Normalized histogram to compare Γ for 2BIGB sources divided into HSP and EHSP subsamples, respectively, with 908 and 252 objects.

(p-value > 0.05), the photon index distributions are alike and consistent with a single-parent population.

The γ -ray photon index deduced from the 2BIGB analysis agree with 4FGL, for both the entire 2BIGB sample and the 2BIGB_{new} subsample. The mean values ($\langle \Gamma \rangle$) and the distribution width ($\pm 1\sigma$) for each sample are $\langle \Gamma_{3\text{HSP}-2\text{BIGB}} \rangle = 1.87 \pm 0.21$, $\langle \Gamma_{2\text{BIGB}-\text{new}} \rangle = 1.86 \pm 0.32$, and $\langle \Gamma_{3\text{HSP}-4\text{FGL}} \rangle = 1.90 \pm 0.17$. Moreover, the $\langle \Gamma_{3\text{HSP}-4\text{FGL}} \rangle$ parameter (as derived from the associations done in this work, Table 1) is in full agreement with the value obtained in 4LAC (The Fermi-LAT collaboration 2019b) for the HSP population, $\langle \Gamma_{\text{HSP}-4\text{LAC}} \rangle = 1.90 \pm 0.17$.

In Fig. 7 (bottom), we divide the 2BIGB catalogue into subsamples of HSPs (908 objects) and EHSPs (252 objects) to compare their photon index $\Gamma_{0.5-500\text{GeV}}$ histograms. A KS test to compare the normalized histograms shows that the distributions are alike (p-value of 0.838), and with compatible mean values ($\pm 1\sigma$) of $\langle \Gamma_{2\text{BIGB}-\text{HSP}} \rangle = 1.89 \pm 0.20$ and $\langle \Gamma_{2\text{BIGB}-\text{EHSP}} \rangle = 1.80 \pm 0.25$. The $\langle \Gamma \rangle$ values measured for the HSP and EHSP subsamples are similar, in agreement with a flattening in the $\log(v_{\text{syn-peak}})$ vs. Photon Index plane, which is observed in 4LAC (The Fermi-LAT collaboration 2019b) for sources with synchrotron peak $v_{\text{syn-peak}} > 10^{15}$ Hz.

Fig. 8 shows the Photon Index vs. $\log(v_{\text{syn-peak}})$ relation for the 3HSP-2BIGB sample and confirm the flattening at $v_{\text{syn-peak}} > 10^{15}$ Hz. We find a relatively weak trend of hardening $\Gamma = -0.056 \times \log(v_{\text{syn-peak}}) + 2.78$, with increasing synchrotron peak frequency. However, according to 4LAC paper The Fermi-

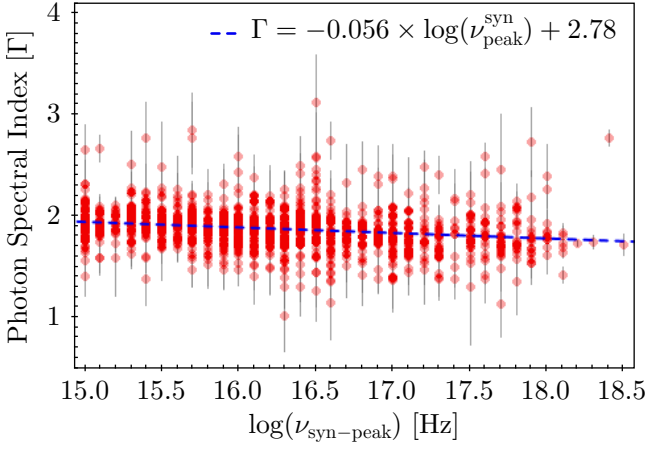


Figure 8. Scatter plot with the 0.5–500 GeV photon spectral index Γ versus the log of synchrotron peak $\log(\nu_{\text{syn-peak}})$ for the 3HSP-2BIGB sample. The blue dashed line is a linear fit to the data.

LAT collaboration (2019b), the hardening trend is stronger when considering the entire blazar population, with $\langle \Gamma \rangle \sim 2.6$ at $\log(\nu_{\text{syn-peak}}) = 12.0$ [Hz], and $\langle \Gamma \rangle \sim 1.9$ at $\log(\nu_{\text{syn-peak}}) = 16.0$ [Hz].

We note that there is no relevant correlation between redshift and photon spectral index for the 2BIGB sample alone⁹. Nevertheless, when considering all blazar families as in 4LAC paper, this correlation shows up as an average γ -ray spectral softness for sources with large redshift. The 4LAC attributes this effect to the intrinsic spectral curvature at the high energy end, which is redshifted to lower energies as z increases, and result in softer spectrum. However, a significant fraction of the γ -ray detected BL Lacs have no spectroscopic redshift measurements. Taking the 2BIGB catalogue as an example, only 377 out of 1160 3HSP-2BIGB sources (32.5%) have a reliable redshift measurement (redshift flag-1 in Table 1). Therefore any correlation with redshift or derived quantities, like source luminosity, could be under heavy bias.

The Fig. 9 (top) shows the integral flux distribution $S_{0.5-500 \text{ GeV}}$ for the 3HSP-4FGL sample and to compare with the 2BIGB_{new}, from where it is seen that the 2BIGB_{new} detections represent an underlying population of faint γ -ray emitters. Fig. 9 (bottom) shows the $S_{0.5-500 \text{ GeV}}$ distribution, dividing the entire 2BIGB catalogue into HSP and EHSP subsamples, with 908 and 252 objects, respectively. A KS test to compare the normalized histograms confirms the distributions are similar (p -value = 0.681) and shows that EHSPs are not necessarily fainter than HSPs concerning the photon-counts in the *Fermi*-LAT band.

Also, for the 3HSP-2BIGB sample, we study the synchrotron peak versus the gamma-ray flux plane, $\nu_{\text{syn-peak}}$ vs. $S_{0.5-500 \text{ GeV}}$, and report in null correlation (or very weak), with a Pearson correlation coefficient of ~ -0.2 . Given the absent correlation between synchrotron $\nu_{\text{syn-peak}}$ with $S_{0.5-500 \text{ GeV}}$ and the flattening concerning $\Gamma_{0.5-500 \text{ GeV}}$, we find that the HE spectral characteristics of HSPs and EHSPs are similar. Therefore, the search for TeV peaked blazars (or Extreme TeV BL Lacs) as done in MAGIC Collaboration et al. (2019b) may benefit from considering both HSP & EHSP blazars as TeV candidates, instead of EHSPs only. In agreement to

⁹ The 4LAC paper (The Fermi-LAT collaboration 2019b) also reports on the absent (or low significance) correlation between redshift and Γ when considering blazar subclasses alone.

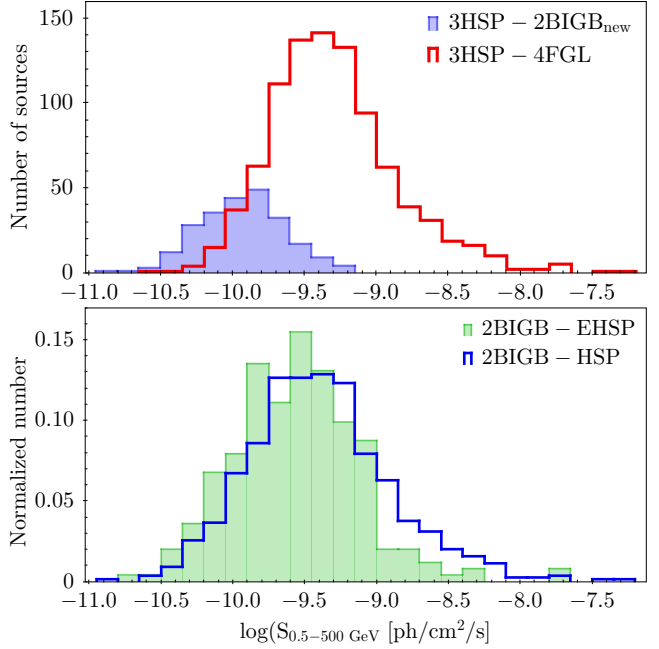


Figure 9. (Top) Histogram to compare the log of integral γ -ray flux $\log(S_{0.5-500 \text{ GeV}})$ for the 3HSP-4FGL (red line) and 2BIGB_{new} (full indigo bars). (Bottom) Histogram to compare the integral γ -ray flux for 2BIGB sources divided in HSP (blue line) and EHSP (full green bars) subsamples.

that, Costamante (2019) who searches for TeV peaked blazars considering spectral properties of the entire 5BZcat and Sedentary catalogues (Massaro et al. 2015; Giommi et al. 1999), and delivers a list with 47 Extreme TeV BL Lacs candidates.

We call attention to the argument that “EHSPs might peak at $E > 1 \text{ TeV}$ while the HSP population is more likely to peak at the energy window covered by *Fermi*-LAT”, which is not precise. As reported in Foffano et al. (2019), the HE properties of TeV detected EHSP sources are very similar but can be substantially different at VHE. The VHE spectrum of EHSP sources comprises a mix of cases peaking at hundreds of GeV and cases where it is possible to observe a hard & continuum spectrum from HE to VHE¹⁰.

4.4 The contribution of HSP & EHSP blazars to the EGB

Here we investigate the total - measured - contribution of HSP & EHSP blazars to the extragalactic gamma-ray background. We build a stacked SED with the high galactic latitude 2BIGBs ($|b| > 10^\circ$) as a sum of fluxes for each bin E_0 (all UL fluxes are removed from the sum), and the stacked flux for each energy E_0 is averaged over the sky area $A_{|b| > 10^\circ} = 34,110.3 \text{ deg}^2 = 10.39 \text{ sr}$. Fig. 10, shows the integral spectral contribution of HSP + EHSP blazars to the total extragalactic γ -ray content (EGB). The total EGB flux is measured for high galactic latitude ($|b| > 20^\circ$) and considers the foreground model A from Ackermann et al. (2015a); Di Mauro (2015). Note that Fig. 10 represents a direct and unprecedented measurement of the emission produced by resolved HSP & EHSP blazars, down to the faintest γ -ray signatures at the TS > 9 level.

Table 3 shows the 2BIGB improvement regards to solving the

¹⁰ All VHE spectra considered in Foffano et al. (2019) are deabsorbed with the EBL model from Franceschini & Rodighiero (2017).

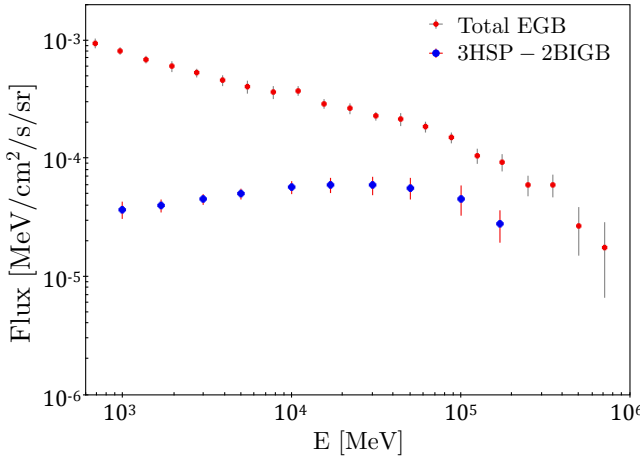


Figure 10. The contribution of 3HSP-2BIGB sources to the EGB. The blue points represent the stacked γ -ray SED for the entire 3HSP-2BIGB population at $|b| > 10^\circ$, and red for the total extragalactic gamma-ray content (EGB, Ackermann et al. 2015a). The signals are averaged over the sky area at $|b| > 10^\circ$, and $|b| > 20^\circ$, respectively.

extragalactic component into point sources. We add 235 new γ -ray emitters to the known population of 925 3HSP-4FGL sources, which brings a relatively small -but not negligible- contribution to the total intensity already solved by 4FGL. The 2BIGB represents an improvement of $\sim 25\%$ for the number of 3HSP blazars detected in γ -rays. However, the entire group of 2BIGB_{new} sources only populate the faint end of the $\log(S_{0.5-50\text{ GeV}})$ flux distribution (see Fig. 9), meaning that the most intense 3HSP-4FGL sources already dominate the stacked fluxes. The extra contribution solved into 2BIGB_{new} sources ranges from 1.2% up to 3.4% along the 1 GeV to 170 GeV band (column ‘I(%)’ in Table 3) peaking around the 17-30 GeV energy band.

There is, in fact, an underlying population of faint gamma-ray sources that contribute to the EGB with a spectral index characteristic of HSP blazars. Moreover, the total contribution of HSP & EHSP blazars to the EGB gets more relevant with increasing energy (column ‘Tot(%)’, Table 3), reaching up to 33.5% at 100 GeV. This trend is in agreement with predictions from (Giommi et al. 2013; Giommi & Padovani 2015; Di Mauro et al. 2014b), which argue that HSP blazars are the dominant fraction of isotropic γ -ray background at the $E > 10$ GeV. Besides, Di Mauro et al. (2018) concludes that the blazar population may represent up to (42±8)% of the total EGB at $E > 10$ GeV.

The measured fraction of the EGB due to HSP blazars, drop from 33.5% -at 100 GeV- to 29.9% -at 170 GeV- in what could be the result of lower detection efficiency at the highest energy bands. Also, we adopt a more restrictive upper limit threshold ($TS < 6 \rightarrow TS < 10$) for the 100 GeV and 170 GeV bins. Even though knowing this would affect the detection efficiency at those bands, this is done to assure the VHE detections are robust. For the same reasons, the flux fraction associated with 2BIGB_{new} sources ($\text{Flux}_{\text{2BIGB-new}} / \text{Flux}_{\text{2BIGB}}$, column ‘I(%)’ in Table 3) reaches 3.3% at 50 GeV, but also see a drop for the largest energy bins of 100 GeV and 170 GeV. There are indeed significant uncertainties at VHE for both the EGB and the 2BIGB integral fluxes. Notably, at 170 GeV, the errors are enough to absorb the observed drop in ‘Tot(%)’ flux-ratio ($\text{Flux}_{\text{2BIGB}} / \text{Flux}_{\text{EGB}}$) as a fluctuation.

Note that the flux at each pivot-energy is calculated over the

Table 3. The total contribution of HSP & EHSP blazars to the EGB content as measured from the 3HSP-2BIGB and 3HSP-4FGL samples. Flux in [$\text{MeV}/\text{cm}^2/\text{s}/\text{sr}$], for the Total EGB, and for the resolved contribution from 3HSP-2BIGB and 3HSP-4FGL sources. The ‘I(%)’ column shows the relative improvement of the 2BIGB concerning 4FGL for solving the EGB, and the ‘Tot’ column list the total fraction (%) of the EGB solved into HSP & EHSP blazars given the 2BIGB data.

EGeV	Flux _{EGB} $\times 10^{-4}$	Flux _{4FGL} $\times 10^{-5}$	Flux _{2BIGB} $\times 10^{-5}$	I(%)	Tot(%)
1.0	8.11 ± 0.52	3.56 ± 0.53	3.65 ± 0.57	2.71	$4.5^{+1.0}_{-0.93}$
1.7	6.30 ± 0.46	3.88 ± 0.42	3.99 ± 0.47	2.78	$6.3^{+1.3}_{-1.1}$
3.0	5.13 ± 0.39	4.38 ± 0.38	4.50 ± 0.44	2.98	$8.7^{+1.6}_{-1.4}$
5.0	4.16 ± 0.45	4.84 ± 0.42	4.99 ± 0.48	3.14	$11.9^{+2.7}_{-2.2}$
10	3.66 ± 0.34	5.51 ± 0.58	5.69 ± 0.66	3.23	$15.5^{+3.6}_{-3.0}$
17	2.83 ± 0.25	5.79 ± 0.69	5.99 ± 0.78	3.44	$21.1^{+5.1}_{-4.2}$
30	2.33 ± 0.17	5.78 ± 0.91	5.98 ± 1.01	3.43	$25.6^{+6.7}_{-5.8}$
50	2.05 ± 0.21	5.43 ± 0.10	5.61 ± 1.10	3.33	$27.3^{+9.1}_{-7.4}$
100	1.34 ± 0.14	4.36 ± 0.12	4.49 ± 1.24	2.84	$33.5^{+14.2}_{-11.5}$
170	0.937 ± 0.14	2.74 ± 0.79	2.78 ± 0.82	1.23	$29.9^{+15.7}_{-11.6}$

E-bins listed in Table 2. The fit for each E-bin had both Normalization N_0 and Photon Index Γ free to vary. Note, the SED analysis is not required to be bound to the broadband fit over 0.5-500 GeV, and therefore it is more sensitive to the spectrum curvature at the highest energy bands. Alternatively, if one uses the power-law broadband fit (0.5-500 GeV) to estimate fluxes at the high-energy bands, the risk is to be overestimated.

The power-law broadband fit is dominated by the lower energy photons (The Fermi-LAT collaboration 2019b), which have larger counts-rate and tend to determine the broadband photon index at a regime where the absorption due to EBL is not relevant. As a result, the power-law broadband fit tends to overestimate the VHE flux since the spectrum curvature is not described properly. Our approach avoids this bias, given that the SED data-points are computed based on multiple energy-bands that adjust well to the observed spectrum curvature. Therefore the SEDs provide a confident way to measure the integral contribution of point-sources to the very high-energy EGB.

Note that our work does not rely on extrapolations of the γ -ray SED or correlations to other wavebands (as in, Di Mauro et al. 2013, 2014a), neither detection efficiency corrections (as in, Di Mauro et al. 2018). An alternative and robust approach based on stacking analysis is discussed in Paliya et al. (2019), and has similarities to our work, given that multifrequency selected seeds drive the search for the stacked signature.

Accurate measurement of the EGB content produced by γ -ray resolved blazars can be accomplished by large-scale spectrum analysis (as done here), looking for signatures down to a low detection threshold and for the entire blazar population. The advantage is to produce detailed descriptions for individual sources while solving the EGB content. This allows to cross-check the measured flux at each energy bin with the estimates and extrapolations from other works, which should converge.

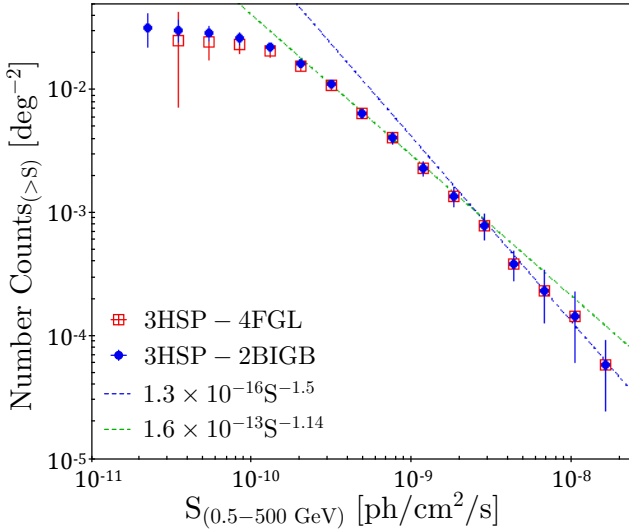


Figure 11. The γ -ray logN-logS for the 3HSP population detected in 2BIGB (blue) and in 4FGL (red), plotting the cumulative density of sources N with flux larger than the integral flux $S_{0.5-500 \text{ GeV}}$, only considering high galactic latitude sources at $|b|>10^\circ$.

4.5 The gamma-ray logN-logS of 2BIGB sources

The number counts plot (logN-logS) is a valuable tool to visualize and test if a population of astrophysical sources is uniformly distributed at low redshift. If the cumulative distribution follows the so-called Euclidean trend $\propto S^{-1.5}$, it is a strong indicative the sample is complete and non-evolving at least down to the flux-limit where it detaches from that trend. The measured number count is expected to deviate from the Euclidean slope at lower fluxes because of cosmological effects. However, it can also detach at intermediary fluxes as a result of the luminosity evolution of the population along time (Shanks et al. 1984).

The logN-logS interpretation can suffer from strong bias introduced by sample incompleteness, given that faint sources can be overwhelmingly numerous and hard to detect or select in its totality. Sample incompleteness can originate from multiple instrumental and source-selection limitations, and a clear understanding of those inefficiencies is crucial to derive conclusions from the logN-logS shape. To understand how a population evolves along with cosmic history, one needs to rely on a complete sample with robust redshift information. Though, a significant fraction of HSP blazars (68%, 1373 out of 2013 3HSPs) has no spectroscopic redshift, which hinders the understanding of blazar's evolution.

For blazars, it is not clear where to expect deviations from the Euclidean trend in the number counts, and here we look into that. The observed γ -ray logN-logS associated to 3HSP sources is shown, and also for the HSP and EHSP subsamples alone. The main features observed are discussed in details, and future works could apply improvements, e.g., to consider the effects of detection efficiency and k-correction.

Fig. 11 shows the γ -ray logN-logS for the 3HSP population detected in 2BIGB and in 4FGL, and only consider sources at $|b|>10^\circ$ where the 3HSP selection is homogeneous. This encloses a sky-area of 34110.3 deg^2 , which holds the majority of 3HSP sources (1925 out of 2013), from where 1073 are 3HSP-2BIGB, and 840 are 3HSP-4FGL.

As in previous work (Arsioli & Chang 2017), we observe an early-break in the $S^{-1.5}$ Euclidean trend at $\sim 2.5 \times 10^{-9}$. One could

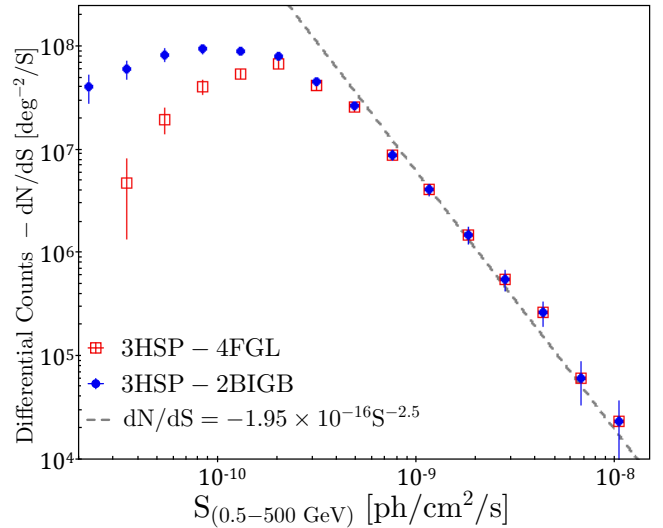


Figure 12. The differential number counts ($-dN/dS$) in γ -ray for the 3HSP population, comparing the 3HSP-2BIGB (blue) and 3HSP-4FGL (red) samples. The dashed line is the derivative of $N = 1.3 \times 10^{-16} S^{-1.5}$, which is the Euclidean fit to the number counts from Fig. 11.

argue that this might be a bias because of the *Fermi*-LAT exposure, which is not constant along the entire sky. If it were the case, our analysis would have seen improvements concerning completeness at the level of $S_{0.5-500 \text{ GeV}} < 2.5 \times 10^{-9} \text{ ph/cm}^2/\text{s}$, since the 2BIGB catalogue considers extra three years of observations when compared to 4FGL.

The 1BIGB paper reported this same early-break feature, which also highlights the existence of previous logN-logS data from the 3LAC paper (Ackermann et al. 2015b) that has similar characteristics as in here (see footnote 19 at Arsioli & Chang (2017)). The existence of an early break in the γ -ray logN-logS plane is intriguing, and its origin is not clear. However, it could well be the result of γ -ray variability, incompleteness from the 3HSP catalogue itself, absorption, or the need to apply k-correction to the observed flux. Therefore, proper treatment needs to add corrections to the γ -ray logN-logS, which should impact further discussions related to source evolution (see Ackermann et al. (2016a) as an example). To mention in more details:

- Gamma-ray flares. When integrated along 11 years of observations, a flare event in γ -rays gets diluted, which overestimates the mean flux concerning the non-flaring state of the source. This bias could act to exaggerate the number of sources in the bright end of γ -ray logN-logS.

- 3HSP incompleteness. As mentioned in 1BIGB paper (for the case of 2WHSP catalogue), the early-break could be a manifestation of incompleteness from the 3HSP catalogue that increasingly affects the selection of fainter sources as their synchrotron peak flux gets lower. Currently available radio surveys (SUMMS and NVSS) and the poor all-sky coverage in X-rays could be the actual limitations. The 3HSP paper reports on blazars with yet undetected radio counterpart, most likely with a faint radio-flux, which is lower than the flux-limit from SUMMS, NVSS, and FIRST radio surveys (Chang et al. 2019). An estimate for the number of similar cases is still to be evaluated, and could represent a significant fraction of the HSP & EHSP population.

- Absorption. This is a $\gamma\gamma$ process where a VHE photon

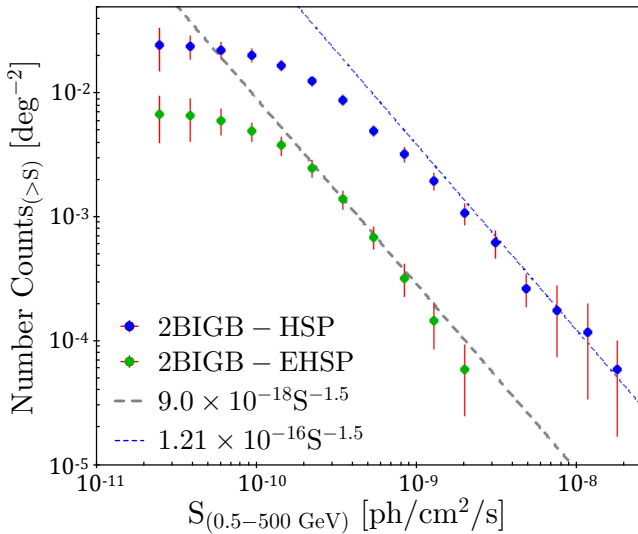


Figure 13. The γ -ray logN-logS for the entire 3HSP-2BIGB population, considering the integral flux $S_{0.5-500 \text{ GeV}}$ and separating between the HSP (blue) and EHSP (green) subsamples. Blue and gray dashed lines are fits to the HSP and EHSP logN-logS respectively, following the $S^{-1.5}$ slope for a non-evolving population.

in a head-on collision to extragalactic background light (EBL) annihilates to create electron-positron pairs. Absorption affects high redshift sources more heavily and steepens the observed spectrum, depleting the $S_{0.5-500 \text{ GeV}}$ flux. As highlighted by Costamante (2013), the critical energy above which at least 5% of the emitted photons are absorbed due to EBL is given by $E_{\text{crit}(z)} = 170(1+z)^{-2.38} \text{ GeV}$ (Ackermann et al. 2012), based on EBL model from Franceschini et al. (2008). Given that the 3HSP catalogue has confident lower-limit redshifts up to 0.7, the $E_{\text{crit}(z)}$ can be as low as 48 GeV.

- *Fermi*-LAT exposure. The *Fermi*-LAT data taken mode is turned off during passages along the South Atlantic Anomaly, inducing up to 15% sensitivity difference between the north and south hemisphere. As mention previously, this does not seem to be the main driver for the early-break in the γ -ray logN-logS.

- K-correction. To properly apply k-correction to the observed γ -ray flux, a redshift survey for the entire 3HSP catalogue is necessary. Indeed, the lack of spectroscopic (robust) redshift measurements for $\sim 68\%$ of the 3HSPs is a limitation. The use of photometric redshifts can help to close that gap, although introducing a certain degree of uncertainty. The 3HSP catalogue has estimated photometric redshifts for 930 objects, but still, nearly 1/4 of the sources lack a redshift estimate. One way to apply the correction is to compute the intrinsic gamma-ray flux $S_{E'_i-E'_f}$ given that the observed energy interval (E_i to E_f , selected to integrate over) gets corrected based on redshift according to $E_i=E'_i/(1+z)$ and $E_f=E'_f/(1+z)$. This way, one can probe the same intrinsic energy range, from E'_i to E'_f . The selection of a suitable energy range can minimize the effect of absorption due to EBL.

In Fig. 12, the differential counts dN/dS vs. S is shown, and a fast drop for $S < 2 \times 10^{-10} \text{ ph/cm}^2/\text{s}$ is seen. This drop is most likely because the detection efficiency decreases with flux, meaning that faint sources are harder to detect. Moreover, when comparing the 3HSP-4FGL to the 3HSP-2BIGB sample, there are gains concerning completeness for fluxes close to $\sim 2 \times 10^{-10} \text{ ph/cm}^2/\text{s}$ and lower.

This is because of the larger exposure from 2BIGB (11 years) regarding 4FGL (8 years).

Apart from the early-break feature, the γ -ray sample seems complete down to the flux level of $\sim 2 \times 10^{-10} \text{ ph/cm}^2/\text{s}$. From there on to lower fluxes, the 2BIGB catalogue introduce improvements in the differential number counts compared to 4FGL. The 2BIGB is indeed more complete than 4FGL in the lower flux end, as expected from Fig. 9.

Considering that the 2BIGB catalogue is currently the most sensitive γ -ray survey over the HSP & EHSP populations, it is also suitable to study the sky-density of each blazar class. Fig. 13 shows the number counts for the 2BIGB catalogue dividing between HSP and EHSP blazars. Here we consider only the 3HSPs at high galactic latitude $|b| > 10^\circ$, with a total of 838 2BIGB-HSP and 235 2BIGB-EHSP objects.

From Fig. 13 we conclude that the density of γ -ray detected HSPs is $\sim 13.4\times$ larger compared to EHSPs, and that the incompleteness of the EHSP γ -ray sample starts at $\sim 2 \times 10^{-10} \text{ ph/cm}^2/\text{s}$; Apart from the early-break feature, this is similar to what is seen in Fig. 12 for the entire 2BIGB catalogue. Also, the HE number counts of HSP and EHSP sources -at the bright end- are compatible to the Euclidean trend, indicating that both classes are homogeneously distributed in space.

Concerning the γ -ray detectability of HSP vs. EHSP sources, the fraction f of each class within the 4FGL and 2BIGB catalogues is very similar, with (f_{HSP} & f_{EHSP}) of (0.789 & 0.209) for 4FGL, and (0.781 & 0.219) for 2BIGB. Therefore, we expect that observational improvements in γ -ray sensitivity and exposure time may unveil new gamma-ray blazars independent of its blazar class.

5 SUMMARY AND CONCLUSIONS

The 2BIGB catalogue has 1160 sources and is the result of a γ -ray analysis of the entire 3HSP catalogue. The position of 3HSP sources are used as multifrequency seeds where we test for the existence of a γ -ray signature. Such an approach has a low number of free parameters, allowing to lower the detection threshold down to $TS > 9$ without compromising the final catalogue. The likelihood analysis fits only two free parameters (Normalization and Photon index) given the source position is set as fixed.

All 2BIGB detections result from a broadband 0.5-500 GeV analysis integrating over 11 years of observations with *Fermi*-LAT. We confirm and update the fitting parameters for the 925 2BIGB sources that have a counterpart in 4FGL. Also, the 2BIGB catalogue includes 235 sources that are new detections concerning 4FGL (226 of them were never reported in previous *Fermi*-LAT catalogues).

The fact that 925 2BIGB sources are already part of the 4FGL catalogue allowed us to compare results and to validate our analysis, supporting the robustness of the new γ -ray detections presented in this work. Moreover, all 2BIGB_{new} were evaluated with high-energy TS maps and confirmed as point sources.

The γ -ray photon index distribution of 3HSP-4FGL, 3HSP-2BIGB, and 2BIGB_{new} sources, are compared via KS test and show to be compatible with a single parent population. In particular, the 235 new detections have spectral properties that are well representative of the HSP population, excluding the possibility of heavy contamination for the 2BIGB_{new} sample.

We have built the γ -ray spectral energy distribution for all 2BIGB sources, covering the 1-170 GeV energy range with 10.5 years of observations with *Fermi*-LAT, and integrating over super-

posed energy bins. The SED data-points are available at <https://github.com/BrunoArsioli> with a template to upload at the ASDC-ASI portal and visualize with the SED Builder Tool <https://tools.ssdc.asi.it/>. The data will soon be available at OpenUniverse <http://www.openuniverse.asi.it/> and BSDC <http://bsdc.icranet.org/> portals¹¹.

This work revealed an underlying population of γ -ray emitters at the threshold detectability for *Fermi*-LAT. Those sources are not necessarily of low relevance and contribute to the EGB with photon index characteristic of HSP blazars, however, with fainter flux. Many of them have a hard photon spectral index, and only seen at the largest energy bands. Those cases can be relevant at higher energies and likely at reach for the upcoming Cherenkov Telescope Array (CTA). Therefore, this work delivers a complementary description of the γ -ray sky, which could impact on VHE population studies for CTA.

Regarding the γ -ray background, we show that the measured contribution of 3HSP blazars (HSP+EHSP) to the total EGB increases with energy, and reach 33.5% at 100 GeV. The 235 new detections serve to solve a fraction of the EGB into point sources, shrinking the available space for an actual extragalactic diffuse γ -ray component. When considering the additional 2BIGB_{new} sources, the resolved fraction of the EGB flux at 50 GeV is improved by 3.3%. The enhancements for other energy bands are lower, but of the same order, and listed in Table 3.

We plot the γ -ray number counts (logN-logS), and also, the differential number counts for the 3HSP-2BIGB sources, and compare to the 3HSP-4FGL sample. It is shown that the γ -ray sample is likely complete down to $S_{0.5-500\text{ GeV}} \sim 2 \times 10^{-10} \text{ ph/cm}^2/\text{s}$. We report on an early break in the logN-logS number counts at $\sim 2.5 \times 10^{-9} \text{ ph/cm}^2/\text{s}$, which can not be associated with incompleteness of the γ -ray sample. This could be a bias arising from γ -ray variability, incompleteness from the 3HSP catalogue itself, or the need for a proper k-correction. This particular feature in the γ -ray number counts for HSPs is present since early works (Arsioli & Chang 2017; Ackermann et al. 2015b) and demands more investigation. Also, we study the γ -ray number counts for the HSP and EHSP subclasses. Their distribution in space is relatively homogeneous (compatible with the Euclidean trend at the bright end), and the density of γ -ray detected HSPs is $\sim 13.4 \times$ larger than EHSPs.

Foffano et al. (2019) shows that EHSPs are not all necessarily TeV peaked blazars, but a mix of sources peaking at few to hundreds of GeV, with cases that have a hard photon index from HE to VHE, with a peak at $> 1 \text{ TeV}$ to $> 10 \text{ TeV}$. For the 2BIGB catalogue, we could compare the distribution of HE flux $S_{0.5-500\text{ GeV}}$ and photon index Γ for the HSP and EHSP subclasses, and found they are similar. Therefore, given the HE spectral similarities between those subclasses, the search for Extreme TeV BL Lac candidates may benefit from considering both HSPs and EHSPs as a whole, as done by Costamante (2019). Alternatively, at least, by lowering the synchrotron frequency threshold to incorporate candidates with $\nu_{\text{syn-peak}} < 10^{17} \text{ Hz}$. Methods to select TeV-peaked blazars from the entire 3HSP catalogue (i.e. HSP + EHSP) can also incorporate considerations about HE variability, since TeV-peaked blazars have shown to be remarkably stable (or long-term) HE & VHE sources (Costamante et al. 2018).

We show that a direct search for gamma-ray sources driven by

multiplex selected seeds is indeed fruitful and complementary to the official *Fermi*-LAT catalogue releases. An extension of current work is highly motivated, intending to account for the totality of blazars and blazar-candidates.

6 ACKNOWLEDGEMENTS

During this work, BA was supported by São Paulo Research Foundation (FAPESP) with grant n. 2017/00517-4. BA would like to thank Prof. Marcelo M. Guzzo for his support to this research proposal. BM thank Uppsala University International Science Programme (ISP) for the financial support towards developing this work. We thank the Centro de Computação John David Rogers (CCJDR) at IFGW Unicamp, Campinas-Brazil, for granting access to the Feynman and Planck Clusters. We thank IcraNet, Prof. Remo Ruffini and Prof. Carlo Bianco for the cooperation and granted access to Joshua Computer Cluster (Rome-Italy). The availability of computational resources was key to the development of our work. The VO publication of our data (vo.bsdc.icranet.org) is made by the Brazilian Science Data Center (BSDC) service maintained at CBPF, Rio de Janeiro, and accessible through the United Nations Open Universe Initiative at <http://www.openuniverse.asi.it>. We thank the entire *Fermi*-LAT collaboration for maintaining a public mission database, which promotes discoveries involving the entire γ -ray community in a multitude of scientific efforts. We thank J. Biteau for his help in obtaining VHE data from published papers which is now available via OpenUniverse and SSDC-ASI Data Science portals. We make use of archival data and bibliographic information obtained from the NASA-IPAC Extragalactic Database (NED), data, and software facilities maintained by the Space Science Data Center (SSDC) from the Italian Space Agency. We thank the anonymous Referee for all comments, which helped to improve the discussion and presentation of the paper.

REFERENCES

- Abdo A. A., et al., 2010a, *ApJS*, 188, 405
- Abdo A. A., et al., 2010b, *ApJ*, 715, 429
- Ackermann M., et al., 2012, *Science*, 338, 1190
- Ackermann M., et al., 2013, *ApJS*, 209, 34
- Ackermann M., et al., 2015a, *ApJ*, 799, 86
- Ackermann M., et al., 2015b, *ApJ*, 810, 14
- Ackermann M., et al., 2015c, *ApJ*, 810, 14
- Ackermann M., et al., 2016a, *Physical Review Letters*, 116, 151105
- Ackermann M., et al., 2016b, *ApJS*, 222, 5
- Actis M., et al., 2011, *Experimental Astronomy*, 32, 193
- Ahnen M. L., et al., 2017a, *A&A*, 603, A25
- Ahnen M. L., et al., 2017b, *A&A*, 603, A25
- Ajello M., et al., 2017, *ApJS*, 232, 18
- Aleksić J., et al., 2014, *A&A*, 564, A5
- Arsioli B., Chang Y.-L., 2017, *A&A*, 598, A134
- Arsioli B., Polenta G., 2018, *A&A*, 616, A20
- Arsioli B., Fraga B., Giommi P., Padovani P., Marrese P. M., 2015, *A&A*, 579, A34
- Arsioli B., Barres de Almeida U., Prandini E., Fraga B., Foffano L., 2018, *MNRAS*, 480, 2165
- Atwood W. B., et al., 2009, *ApJ*, 697, 1071
- Atwood W., et al., 2013, preprint, (<arXiv:1303.3514>)
- Biswas S., Gupta N., 2019, arXiv e-prints, p. <arXiv:1907.03102>
- Bruel P., Burnett T. H., Digel S. W., Johannesson G., Omodei N., Wood M., 2018, arXiv e-prints, p. <arXiv:1810.11394>
- Calore F., Di Mauro M., Donato F., 2014, *ApJ*, 796, 14
- Chang Y.-L., Arsioli B., Giommi P., Padovani P., 2017, *A&A*, 598, A17

¹¹ Find more information about the Open Universe Initiative at Giommi et al. (2019), and about the Brazilian Science Data Center BSDC at de Almeida et al. (2017).

- Chang Y.-L., Arsioli B., Giommi P., Padovani P., Brandt C., 2019, arXiv e-prints, p. [arXiv:1909.08279](#)
- Cherenkov Telescope Array Consortium et al., 2019, Science with the Cherenkov Telescope Array. Published by World Scientific Publishing Co. Pte. Ltd., doi:[10.1142/10986](#)
- Cohen T., Murase K., Rodd N. L., Safdi B. R., Soreq Y., 2017, *Phys. Rev. Lett.*, **119**, 021102
- Costamante L., 2013, *International Journal of Modern Physics D*, **22**, 1330025
- Costamante L., 2019, arXiv e-prints, p. [arXiv:1911.05027](#)
- Costamante L., Bonnoli G., Tavecchio F., Ghisellini G., Tagliaferri G., Khangulyan D., 2018, *MNRAS*, **477**, 4257
- Danforth C. W., Keeney B. A., Stocke J. T., Shull J. M., Yao Y., 2010, *ApJ*, **720**, 976
- Daylan T., Finkbeiner D. P., Hooper D., Linden T., Portillo S. K. N., Rodd N. L., Slatyer T. R., 2016, *Physics of the Dark Universe*, **12**, 1
- Dermer C. D., 2015, *Mem. Soc. Astron. Italiana*, **86**, 13
- Di Mauro M., 2015, in 5th International Fermi Symposium Nagoya, Japan, October 20-24, 2014. ([arXiv:1502.02566](#)), <https://inspirehep.net/record/1343480/files/arXiv:1502.02566.pdf>
- Di Mauro M., Donato F., 2015, *Phys. Rev. D*, **91**, 123001
- Di Mauro M., Donato F., Calore F., 2013, arXiv e-prints, p. [arXiv:1305.4200](#)
- Di Mauro M., Calore F., Donato F., Ajello M., Latronico L., 2014a, *ApJ*, **780**, 161
- Di Mauro M., Donato F., Lamanna G., Sanchez D. A., Serpico P. D., 2014b, *ApJ*, **786**, 129
- Di Mauro M., Manconi S., Zechlin H. S., Ajello M., Charles E., Donato F., 2018, *ApJ*, **856**, 106
- Finkbeiner D. P., 2004, *ApJ*, **614**, 186
- Foffano L., Prandini E., Franceschini A., Paiano S., 2019, *MNRAS*, **486**, 1741
- Franceschini A., Rodighiero G., 2017, *A&A*, **603**, A34
- Franceschini A., Rodighiero G., Vaccari M., 2008, *A&A*, **487**, 837
- Furniss A., et al., 2013, *ApJ*, **768**, L31
- Gavish E., Eichler D., 2016, *ApJ*, **822**, 56
- Giommi P., Padovani P., 2015, *MNRAS*, **450**, 2404
- Giommi P., Menna M. T., Padovani P., 1999, *MNRAS*, **310**, 465
- Giommi P., Padovani P., Polenta G., Turriziani S., D'Elia V., Piranomonte S., 2012, *MNRAS*, **420**, 2899
- Giommi P., Padovani P., Polenta G., 2013, *MNRAS*, **431**, 1914
- Giommi P., et al., 2019, arXiv e-prints, p. [arXiv:1904.06043](#)
- Goodenough L., Hooper D., 2009, arXiv e-prints, p. [arXiv:0910.2998](#)
- Hooper D., Cholis I., Linden T., Siegal-Gaskins J. M., Slatyer T. R., 2013, *Phys. Rev. D*, **88**, 083009
- Inoue Y., 2011, *ApJ*, **733**, 66
- Joye W. A., Mandel E., 2003, in Payne H. E., Jedrzejewski R. I., Hook R. N., eds, *Astronomical Society of the Pacific Conference Series Vol. 295, Astronomical Data Analysis Software and Systems XII*. p. 489
- Karwin C., Murgia S., Tait T. M. P., Porter T. A., Tanedo P., 2017, *Phys. Rev. D*, **95**, 103005
- Ko C. M., Chernyshov D. O., Cheng H., Dai L., Dogiel V. A., 2019, arXiv e-prints, p. [arXiv:1904.03958](#)
- Leane R. K., Slatyer T. R., 2019, arXiv e-prints, p. [arXiv:1904.08430](#)
- Liu W., Bi X.-J., Lin S.-J., Yin P.-F., 2017, *Chinese Physics C*, **41**, 045104
- MAGIC Collaboration et al., 2019a, arXiv e-prints, p. [arXiv:1909.11621](#)
- MAGIC Collaboration et al., 2019b, arXiv e-prints, p. [arXiv:1911.06680](#)
- MAGIC Collaboration et al., 2019c, *MNRAS*, **490**, 2284
- Masetti N., et al., 2013, *A&A*, **559**, A58
- Massaro E., Maselli A., Leto C., Marchegiani P., Perri M., Giommi P., Piranomonte S., 2015, *Ap&SS*, 357
- Mattox J. R., et al., 1996, *ApJ*, **461**, 396
- Mirabal N., 2013, *MNRAS*, **436**, 2461
- Nolan P. L., et al., 2012, *ApJS*, **199**, 31
- Padovani P., et al., 2017, *A&ARv*, **25**, 2
- Padovani P., Giommi P., Resconi E., Glauch T., Arsioli B., Sahakyan N., Huber M., 2018, *MNRAS*, **480**, 192
- Paiano S., Falomo R., Landoni M., Treves A., Scarpa R., 2017, *Frontiers in Astronomy and Space Sciences*, **4**, 45
- Paliya V. S., Domínguez A., Ajello M., Franckowiak A., Hartmann D., 2019, *ApJ*, **882**, L3
- Petropoulou M., Dermer C. D., 2016, *ApJ*, **825**, L11
- Pita S., et al., 2014, *A&A*, **565**, A12
- Ponti G., et al., 2019, *Nature*, **567**, 347
- Rubtsov G., Zhezher Y., 2018, arXiv e-prints, p. [arXiv:1812.05228](#)
- Sbarufatti B., Treves A., Falomo R., Heidt J., Kotilainen J., Scarpa R., 2005, *AJ*, **129**, 559
- Shanks T., Stevenson P. R. F., Fong R., MacGillivray H. T., 1984, *MNRAS*, **206**, 767
- Shaw M. S., Filippenko A. V., Romani R. W., Cenko S. B., Li W., 2013a, *AJ*, **146**, 127
- Shaw M. S., et al., 2013b, *ApJ*, **764**, 135
- Storm E. M., Jeltema T. E., Profumo S., 2012, *ApJ*, **755**, 117
- Su M., Slatyer T. R., Finkbeiner D. P., 2010, *ApJ*, **724**, 1044
- Takahashi T., et al., 2000, *ApJ*, **542**, L105
- The Fermi-LAT collaboration 2019a, arXiv e-prints, p. [arXiv:1902.10045](#)
- The Fermi-LAT collaboration 2019b, arXiv e-prints, p. [arXiv:1905.10771](#)
- Urry C. M., Padovani P., 1995, *PASP*, **107**, 803
- de Almeida U. B., Bodmann B., Giommi P., Brandt C. H., 2017, in *International Journal of Modern Physics Conference Series*. p. 1760075 ([arXiv:1702.06828](#)), doi:[10.1142/S2010194517600758](#)

Table 4: Power-law model for the 1160 2BIGB-3HSP sources in the 0.5-500 GeV energy band, integrating over 11 years of Fermi-LAT observations. It includes 935 3HSPs with counterpart in 4FGL (3HSP-4FGL sources), and another 235 which are new with respect to 4FGL (in fact, 226 are completely new and were never reported in previous 1-2-3FGL and 1-2-3FHL). The first three columns show respectively the 2BIGB names, right ascension R.A. and declination Dec. in degrees (J2000), all based in 3HSP astrometry data. The fourth column shows the reported redshifts from literature (Shaw et al. 2013b; Pita et al. 2014; Furniss et al. 2013; Danforth et al. 2010; Shaw et al. 2013a; Masetti et al. 2013; Sbarufatti et al. 2005; Massaro et al. 2015), with a right uppercase flag where (1) correspond to cases with a robust redshift value, (2) for values reported as uncertain, (3) for lower limits reported in 3HSP catalog, and for a photometric estimate by fitting a Giant Elliptical host galaxy template we have (4) when a featureless optical spectrum is available, and (5) when no optical spectrum is available but only photometric data points. The column ‘4FGL’ lists the counterpart name from the catalog’s version gll-psc-v20, meaning the the corresponding 3HSP seed position is within the 95% 4FGL error region. Whenever a 2BIGB source is new with respect to 4FGL, this column will show the ‘new’ flag. The power-law parameters (see eq. 1) are described in the following columns: The normalization ‘ N_0 ’ is given in units of $\text{ph}/\text{cm}^2/\text{s}/\text{MeV}$; ‘ Γ ’ is the photon spectral index; the pivot energy ‘ E_0 ’ is given in MeV and represents the optimum energy at which both N_0 and Γ are estimated with the lowest level of uncertainty; and TS is the Test Statistic value from the likelihood analysis over 11 years of Fermi-LAT data. All spectral information is at disposal on public data repositories as GitHub.

2BIGB Jname	R.A.(deg)	Dec.(deg)	z	4FGL J	$N_0 (10^{-15})$	Γ	$E_0 (\text{MeV})$	TS
000132.7-415525	0.38642	-41.92364	–	0001.6-4156	2.30 ± 0.27	1.76 ± 0.08	3475.9	218.9
000215.2-672653	0.56329	-67.44817	0.52 ³	0002.1-6728	1.26 ± 0.15	1.83 ± 0.09	4380.8	187.0
000236.1-081532	0.65025	-8.259	0.39 ⁵	new	0.341 ± 0.118	2.01 ± 0.26	5000.0	18.0
000319.6-524727	0.8315	-52.79094	0.37 ⁵	0003.1-5248	2.10 ± 0.22	1.92 ± 0.08	3921.0	245.1
000626.9+013610	1.61208	1.60294	0.787 ²	0006.4+0135	2.21 ± 0.54	2.03 ± 0.18	2459.6	33.0
000835.4-233927	2.14742	-23.65772	0.147 ¹	0008.4-2339	0.593 ± 0.098	1.70 ± 0.11	6084.1	121.5
000922.7+503028	2.34479	50.50797	0.25 ⁵	0009.3+5030	125.85 ± 4.32	2.02 ± 0.02	1310.5	3124.8
000949.7-431650	2.45729	-43.28058	0.23 ⁴	0009.8-4317	5.09 ± 0.75	2.21 ± 0.14	1959.5	95.3
000957.2+134058	2.48842	13.68303	0.43 ⁵	new	0.446 ± 0.129	2.08 ± 0.22	5000.0	25.7
001328.1+094930	3.37	9.82514	0.29 ⁵	new	1.59 ± 0.43	1.92 ± 0.18	3000.0	39.5
001356.0-185406	3.4835	-18.90181	0.094 ¹	0013.9-1854	3.75 ± 0.52	1.94 ± 0.10	2609.2	149.8
001411.5-502234	3.54771	-50.37636	0.01 ²	0014.1-5022	4.34 ± 0.49	2.12 ± 0.10	2545.1	180.1
001442.1+580201	3.67538	58.03367	0.35 ⁵	0014.7+5801	0.246 ± 0.017	1.71 ± 0.03	9809.6	68.2
001528.0+353639	3.86654	35.611	0.43 ⁵	0015.2+3537	0.656 ± 0.189	1.90 ± 0.20	3627.4	33.5
001540.1+555144	3.91721	55.86242	0.15 ⁵	0015.6+5551	0.953 ± 0.128	1.66 ± 0.08	5870.8	171.3
001827.8+294730	4.61579	29.79189	0.1 ²	0018.4+2946	0.945 ± 0.133	1.66 ± 0.09	5379.7	163.1
002200.1-514024	5.50033	-51.67339	0.25 ¹	0021.9-5140	20.56 ± 1.42	2.07 ± 0.06	1691.6	598.5
002201.0+000658	5.50396	0.11611	0.306 ¹	0022.0+0006	0.058 ± 0.017	1.29 ± 0.20	18064.9	62.5
002611.6-073115	6.54842	-7.52097	0.5 ⁵	0026.1-0732	2.16 ± 0.40	2.01 ± 0.14	2877.5	65.4
002635.6-460109	6.64838	-46.01936	0.25 ⁵	0026.6-4600	2.24 ± 0.31	1.88 ± 0.10	2976.1	129.8
002928.1+205333	7.36917	20.89269	0.367 ¹	0029.4+2051	0.094 ± 0.024	1.73 ± 0.16	13235.6	50.2
003020.4-164713	7.58508	-16.78694	0.237 ¹	0030.2-1647	1.47 ± 0.20	1.72 ± 0.09	4143.7	151.6
003119.1+072453	7.83212	7.41483	–	0031.3+0726	1.15 ± 0.29	1.80 ± 0.16	3216.9	39.2
003120.5-233401	7.83558	-23.56706	0.34 ⁴	new	0.491 ± 0.137	2.20 ± 0.19	5000.0	46.6
003222.6-472536	8.09404	-47.42669	0.44 ⁵	new	0.568 ± 0.206	1.61 ± 0.19	3000.0	31.6
003322.5-203908	8.34362	-20.65228	0.073 ¹	new	0.266 ± 0.096	1.79 ± 0.22	5000.0	20.3
003334.4-192132	8.39317	-19.35914	0.506 ³	0033.5-1921	96.42 ± 3.29	1.77 ± 0.02	1503.9	4634.2
003358.8+390631	8.49508	39.10881	0.58 ⁵	0033.9+3858	69.78 ± 10.8	2.73 ± 0.17	791.1	74.6
003514.1+151504	8.81129	15.25117	0.64 ³	0035.2+1514	13.51 ± 0.76	1.85 ± 0.04	2775.3	1007.9
003552.6+595004	8.96929	59.83453	0.086 ²	0035.9+5950	29.32 ± 0.91	1.73 ± 0.02	3176.7	4180.8
003908.2-222001	9.78421	-22.33372	0.064 ¹	0039.1-2219	1.57 ± 0.22	1.74 ± 0.10	3772.8	143.6
004013.1+405004	10.05754	40.83458	0.24 ⁵	0040.3+4050	0.851 ± 0.171	1.74 ± 0.14	4425.9	77.4
004123.0+375855	10.34596	37.98214	0.38 ¹	0041.4+3800	0.548 ± 0.159	1.67 ± 0.19	4382.0	52.0
004141.2-160747	10.42171	-16.12978	0.43 ⁵	0041.7-1607	0.128 ± 0.045	1.88 ± 0.26	8115.2	25.3
004147.0-470136	10.44592	-47.02692	0.15 ¹	new	0.285 ± 0.084	1.64 ± 0.18	5000.0	34.5
004208.1+364113	10.53375	36.68694	0.33 ⁵	0042.0+3640	2.85 ± 0.61	2.02 ± 0.16	2303.6	53.5
004334.1-044300	10.89217	-4.71678	0.48 ³	0043.5-0442	1.21 ± 0.22	1.97 ± 0.15	4035.9	71.6
004348.7-111607	10.95271	-11.26861	0.264 ¹	0043.7-1116	2.69 ± 0.44	1.91 ± 0.12	2769.7	90.0
004519.3+212740	11.33033	21.46114	0.35 ³	0045.3+2128	30.56 ± 1.48	1.82 ± 0.03	2028.3	1811.0
004752.0+544746	11.96687	54.79611	0.26 ⁵	0047.9+5448	0.043 ± 0.019	1.25 ± 0.29	19779.0	44.8
004755.2+394857	11.98008	39.816	0.252 ¹	0047.9+3947	13.55 ± 0.93	1.95 ± 0.05	2198.1	639.7
004859.2+422351	12.24646	42.39753	0.37 ⁵	0049.1+4223	0.465 ± 0.112	1.81 ± 0.15	4959.9	39.3
004938.9-415137	12.41204	-41.86047	0.38 ⁵	0049.5-4150	0.847 ± 0.244	1.91 ± 0.22	3229.0	33.0

Continued on next page

Table 4 – continued from previous page

2BIGB Jname	R.A.(deg)	Dec.(deg)	z	4FGL J	N₀ (10⁻¹⁵)	Γ	E₀ (GeV)	TS
005116.6-624204	12.81925	-62.70119	0.3 ³	0051.2-6242	25.15 ± 0.94	1.74±0.02	2497.1	3546.4
005347.7-664517	13.44892	-66.75494	0.31 ⁵	new	0.301 ± 0.083	1.77±0.18	5000.0	33.0
005446.7-245529	13.69475	-24.92472	0.12 ³	0054.7-2455	11.07 ± 0.79	1.76±0.05	2436.3	744.7
005542.1+450701	13.92792	45.11706	0.46 ⁵	0055.7+4507	0.117 ± 0.050	1.66±0.24	6487.0	12.1
005620.1-093630	14.08358	-9.6085	0.1 ¹	0056.3-0935	7.69 ± 0.58	1.84±0.05	3000.1	584.9
005758.4+632639	14.49325	63.44425	0.18 ⁵	0057.9+6326	0.175 ± 0.030	1.58±0.12	14527.7	89.0
005816.8+172313	14.56992	17.38708	0.42 ⁵	new	0.560 ± 0.250	1.49±0.19	3000.0	31.2
005916.9-015017	14.8205	-1.83819	0.114 ¹	0059.3-0152	0.878 ± 0.141	1.70±0.11	5331.9	129.6
005931.5-351049	14.88112	-35.18031	0.31 ⁴	0059.5-3512	2.30 ± 0.40	1.96±0.13	2533.9	76.1
010142.0-545547	15.42504	-54.92983	0.28 ⁵	0101.7-5455	0.085 ± 0.024	1.63±0.20	10507.6	39.1
010250.9-200158	15.71225	-20.03281	0.27 ²	0102.7-2001	0.112 ± 0.037	1.54±0.21	8409.6	28.6
010325.9+533713	15.85787	53.62039	0.15 ⁵	0103.5+5337	2.35 ± 0.17	1.78±0.05	5449.7	496.6
010326.0+152624	15.85833	15.44019	0.246 ¹	0103.5+1526	12.15 ± 3.08	2.13±0.17	1235.7	44.4
010956.6-402050	17.48571	-40.34747	0.313 ¹	0110.0-4019	0.998 ± 0.169	1.86±0.12	4039.0	83.4
011004.1+414950	17.52004	41.83078	0.096 ¹	new	0.264 ± 0.101	1.46±0.19	5000.0	37.3
011050.0-125503	17.70825	-12.91764	0.23 ¹	0110.7-1254	2.23 ± 0.35	2.13±0.15	3186.8	90.6
011130.2+053627	17.87579	5.60753	0.346 ¹	0111.4+0534	0.621 ± 0.184	1.84±0.21	3868.0	26.8
011231.4-750617	18.13083	-75.10494	0.3 ⁵	0112.8-7506	3.18 ± 0.36	1.93±0.08	2901.7	182.8
011232.8-320141	18.1365	-32.02828	0.48 ⁴	new	0.782 ± 0.247	1.93±0.20	3000.0	19.4
011501.7-340027	18.75717	-34.00756	0.482 ¹	0114.9-3400	0.167 ± 0.034	1.64±0.13	10327.9	82.0
011546.1+251953	18.94225	25.33153	0.375 ¹	0115.8+2519	25.83 ± 1.12	1.87±0.03	2469.9	1836.2
011555.5-274431	18.98108	-27.74206	0.7 ³	0116.0-2745	0.350 ± 0.072	1.88±0.14	6862.7	68.3
011637.1-281146	19.15442	-28.19636	0.32 ⁴	0116.5-2812	1.95 ± 0.82	2.14±0.29	1940.1	13.6
011747.0-244333	19.44583	-24.72603	0.279 ¹	0117.5-2442	0.163 ± 0.056	1.66±0.22	6293.0	23.2
011904.6-145858	19.76921	-14.98289	0.29 ⁴	0119.0-1458	2.17 ± 0.26	1.77±0.08	3846.3	221.1
012152.7-391544	20.46954	-39.26228	0.3 ⁵	0121.8-3916	2.16 ± 0.25	1.92±0.09	3501.2	192.2
012203.8-300509	20.51583	-30.08592	0.44 ⁵	new	0.062 ± 0.028	1.35±0.27	10000.0	28.1
012308.6+342048	20.78596	34.34681	0.27 ¹	0123.1+3421	0.643 ± 0.092	1.68±0.10	6441.1	169.6
012338.3-231058	20.90979	-23.18294	0.404 ¹	0123.7-2311	5.03 ± 0.43	1.87±0.06	3200.3	432.8
012340.4+421017	20.91829	42.17161	0.186 ¹	new	0.040 ± 0.025	1.35±0.32	10000.0	17.4
012443.7-314342	21.18217	-31.72856	0.4 ⁴	new	0.639 ± 0.258	2.22±0.34	3000.0	9.54
012657.2+330730	21.73846	33.12508	0.45 ⁵	0127.1+3310	2.89 ± 0.92	1.87±0.19	1923.9	37.3
012713.9+032300	21.80808	3.38353	–	0127.2+0324	8.20 ± 0.84	2.01±0.08	2262.2	234.6
013025.7-212838	22.60725	-21.47747	0.3 ⁵	0130.4-2129	1.35 ± 0.27	2.02±0.16	3131.4	55.3
013107.2+612033	22.78013	61.34258	–	0131.1+6120	7.99 ± 0.42	1.78±0.03	4185.6	1139.1
013113.8+554513	22.80758	55.75361	0.036 ¹	0131.2+5547	5.29 ± 0.57	2.06±0.09	2894.6	167.8
013241.1-080404	23.17138	-8.06803	0.149 ¹	0132.7-0804	1.58 ± 0.26	1.89±0.12	3647.4	87.6
013309.3-453524	23.28867	-45.59	–	0133.2-4533	0.090 ± 0.027	1.69±0.24	9390.4	32.3
013312.1-351916	23.30054	-35.32128	0.174 ¹	new	0.240 ± 0.088	2.24±0.28	5000.0	15.9
013428.2+263843	23.61746	26.64528	0.26 ³	0134.5+2637	10.51 ± 0.70	1.93±0.05	2775.9	648.6
013507.0+025542	23.77933	2.9285	0.372 ¹	0135.1+0255	0.160 ± 0.051	1.59±0.20	7994.5	35.1
013523.6-272813	23.84842	-27.47031	0.248 ¹	new	0.681 ± 0.244	2.39±0.30	3000.0	12.6
013632.6+390559	24.13579	39.09978	–	0136.5+3906	90.43 ± 2.20	1.70±0.01	1922.0	8915.6
013750.5+581411	24.46029	58.23647	–	0137.9+5814	14.33 ± 0.65	1.95±0.03	3251.0	1301.2
013801.1+224808	24.50467	22.80242	0.26 ⁴	0138.0+2247	3.64 ± 0.38	1.94±0.08	3421.6	232.4
014040.9-075849	25.17029	-7.98031	0.36 ⁴	0140.6-0758	0.840 ± 0.192	1.78±0.15	4029.3	47.1
014347.4-584551	25.94746	-58.76425	–	0143.7-5846	14.69 ± 0.70	1.81±0.03	2551.0	1601.0
014648.6-520233	26.70237	-52.04261	0.098 ¹	0146.9-5202	7.46 ± 0.83	2.05±0.09	1983.0	192.4
014753.7-602811	26.97358	-60.46992	0.38 ⁵	new	0.062 ± 0.021	1.84±0.22	10000.0	19.4
014820.3+520204	27.08471	52.03469	0.24 ⁵	0148.2+5201	2.42 ± 0.20	1.85±0.06	4777.3	385.1
014833.8+012901	27.14083	1.48372	0.94 ²	0148.6+0127	5.17 ± 0.95	2.12±0.16	1983.6	71.2
015044.1-545005	27.68542	-54.83472	0.28 ⁵	0150.6-5448	1.44 ± 0.29	1.90±0.14	2845.5	61.5
015239.6+014717	28.165	1.78817	0.08 ¹	0152.6+0147	10.98 ± 0.79	1.92±0.05	2533.8	613.6
015307.4+751742	28.28071	75.29522	–	0153.0+7517	3.14 ± 0.35	2.00±0.09	3337.5	176.1
015313.2-110627	28.30488	-11.10753	0.32 ⁴	new	0.089 ± 0.030	1.67±0.23	10000.0	26.4
015325.9+711506	28.35771	71.25178	0.02 ¹	0153.4+7114	0.537 ± 0.089	1.84±0.12	6767.5	83.9

Continued on next page

Table 4 – continued from previous page

2BIGB Jname	R.A.(deg)	Dec.(deg)	z	4FGL J	$N_0 (10^{-15})$	Γ	$E_0 (\text{GeV})$	TS
015402.8+082351	28.5115	8.3975	0.68 ²	0153.9+0823	60.25 ± 3.08	1.97 ± 0.04	1500.8	1329.5
015624.5-242003	29.10225	-24.33436	–	0156.3-2420	3.40 ± 0.40	2.00 ± 0.09	2909.2	168.6
015646.0-474417	29.19171	-47.73811	0.22 ⁴	0156.8-4744	15.52 ± 1.95	2.14 ± 0.10	1378.3	160.8
015658.0-530159	29.24163	-53.03328	0.25 ⁵	0156.9-5301	3.22 ± 0.26	1.74 ± 0.05	3892.5	535.1
015700.7-323529	29.25283	-32.59153	0.33 ⁵	new	0.042 ± 0.021	1.75 ± 0.38	10000.0	10.9
015809.9+251540	29.54142	25.26136	0.158 ¹	new	0.228 ± 0.110	1.52 ± 0.25	5000.0	16.9
015934.4+104705	29.89325	10.78494	0.195 ¹	0159.5+1046	23.78 ± 1.50	2.02 ± 0.05	2017.2	707.5
020020.9-410935	30.08725	-41.15992	0.5 ²	0200.3-4109	1.83 ± 0.25	1.86 ± 0.10	3419.3	148.6
020106.2+003400	30.27567	0.56675	0.298 ¹	0201.1+0036	0.310 ± 0.101	1.83 ± 0.23	5230.5	23.7
020110.9-434655	30.2955	-43.78203	0.45 ⁵	0201.1-4347	0.095 ± 0.029	1.82 ± 0.19	9398.5	28.6
020226.4+084913	30.61013	8.82044	0.35 ⁵	0202.4+0849	0.847 ± 0.153	1.86 ± 0.12	5034.3	78.5
020252.2-022320	30.71758	-2.38908	0.25 ⁵	0202.9-0225	1.23 ± 0.25	1.93 ± 0.17	3722.1	56.9
020412.9-333340	31.05383	-33.56136	0.617 ¹	0204.0-3334	1.10 ± 0.25	1.77 ± 0.14	3164.9	50.3
020416.4-314457	31.06842	-31.74931	0.31 ⁵	0204.3-3140	1.55 ± 0.38	2.04 ± 0.21	2630.3	35.7
020421.5+241750	31.08975	24.29742	0.18 ⁵	0204.3+2417	0.569 ± 0.146	1.91 ± 0.18	4533.0	32.8
020615.9-095717	31.56621	-9.95486	0.166 ¹	0206.0-0958	0.306 ± 0.087	1.85 ± 0.20	5642.3	30.3
020838.2+352312	32.159	35.38692	0.318 ¹	0208.6+3523	1.05 ± 0.18	1.83 ± 0.12	4282.0	83.2
020917.1+444946	32.32121	44.82956	0.27 ⁵	0209.3+4449	2.42 ± 0.31	1.79 ± 0.08	3345.7	159.9
020921.1-522922	32.34	-52.48964	0.12 ⁴	0209.3-5228	26.41 ± 0.92	1.81 ± 0.02	2596.5	3385.9
020946.7+262530	32.44471	26.42522	0.68 ¹	0209.8+2626	4.46 ± 1.23	2.36 ± 0.23	1697.4	20.6
021205.7-255758	33.02392	-25.96619	0.38 ⁵	0212.2-2559	1.35 ± 0.29	1.82 ± 0.14	3083.0	56.5
021216.9-022155	33.07033	-2.36547	0.25 ¹	0212.2-0219	4.46 ± 0.89	2.05 ± 0.16	1970.6	60.5
021230.5-350330	33.12708	-35.05836	0.393 ²	0212.4-3502	5.94 ± 0.70	2.08 ± 0.10	2166.6	161.8
021252.1+224452	33.22004	22.74783	0.459 ¹	0212.9+2244	19.78 ± 1.81	2.06 ± 0.07	1698.4	320.2
021358.7-695137	33.49454	-69.86028	0.34 ⁵	0213.8-6949	0.16 ± 0.033	1.59 ± 0.13	9080.6	76.9
021409.8-473235	33.54092	-47.54311	0.28 ⁵	new	0.288 ± 0.087	1.94 ± 0.23	5000.0	21.5
021417.9+514451	33.57475	51.74775	0.049 ¹	0214.3+5145	2.72 ± 0.27	1.82 ± 0.07	4074.6	276.8
021515.2-161738	33.8135	-16.29394	0.283 ¹	new	0.063 ± 0.028	1.71 ± 0.32	10000.0	15.8
021517.9+755453	33.82458	75.91472	0.15 ⁵	0215.3+7555	0.115 ± 0.028	1.58 ± 0.14	11224.3	43.2
021552.3-402343	33.968	-40.39542	0.24 ⁴	new	0.695 ± 0.229	2.28 ± 0.34	3000.0	14.9
021632.1+231450	34.13367	23.24728	0.288 ¹	0216.5+2313	1.98 ± 0.28	1.83 ± 0.10	3736.9	142.0
021650.8-663642	34.21187	-66.61181	0.673 ³	0216.8-6635	24.94 ± 1.66	2.02 ± 0.05	1576.2	657.7
021900.0+244520	34.75167	24.75572	–	0219.0+2443	2.49 ± 0.30	1.92 ± 0.09	3674.8	191.3
021905.5-172512	34.77287	-17.42025	0.128 ¹	0219.1-1724	4.38 ± 0.63	2.07 ± 0.12	2426.7	110.8
022048.5-084250	35.20188	-8.71397	0.525 ²	0220.8-0841	0.308 ± 0.078	1.72 ± 0.16	6195.6	43.6
022105.0+063939	35.27075	6.66106	0.27 ⁵	new	0.063 ± 0.028	1.64 ± 0.26	10000.0	10.9
022304.5+682154	35.76883	68.36522	0.23 ⁵	0223.0+6821	2.98 ± 0.32	2.04 ± 0.08	3919.8	166.4
022314.2-111738	35.80933	-11.29397	0.2 ³	0223.1-1117	2.02 ± 0.28	1.88 ± 0.10	3466.0	144.7
022540.8-561812	36.41992	-56.30339	0.32 ⁵	new	0.048 ± 0.025	1.60 ± 0.34	10000.0	13.0
022638.9-444122	36.66196	-44.68958	0.68 ³	0226.5-4441	2.63 ± 0.31	1.94 ± 0.09	3424.3	221.0
022716.6+020200	36.819	2.03336	0.45 ¹	0227.3+0201	12.71 ± 0.98	1.98 ± 0.06	2207.4	484.1
023109.3-575506	37.78863	-57.91833	0.032 ¹	0231.2-5754	3.32 ± 0.36	2.05 ± 0.09	2918.0	184.2
023241.1-112020	38.17462	-11.33894	0.209 ¹	0232.5-1118	0.515 ± 0.123	1.84 ± 0.17	4825.9	43.1
023248.6+201717	38.2025	20.28814	0.139 ¹	0232.8+2018	0.739 ± 0.109	1.72 ± 0.10	6348.9	147.5
023341.0+065611	38.42079	6.93642	0.31 ⁵	0233.5+0654	59.63 ± 7.62	2.30 ± 0.10	989.04	177.2
023410.3-062825	38.54283	-6.47383	0.7 ³	0234.3-0628	2.20 ± 0.33	2.00 ± 0.12	3131.3	93.1
023430.1+804337	38.62754	80.72703	0.5 ⁵	0233.9+8041	0.120 ± 0.020	1.51 ± 0.09	8983.2	40.8
023536.7-293843	38.90283	-29.64528	0.35 ⁴	0235.6-2939	0.653 ± 0.133	1.92 ± 0.15	4685.4	57.0
023734.0-360328	39.39183	-36.05789	0.411 ¹	0237.6-3602	1.78 ± 0.24	1.86 ± 0.09	3718.0	147.4
023800.6-390504	39.50262	-39.08464	0.21 ⁵	0238.1-3905	5.88 ± 0.60	1.92 ± 0.08	2333.1	260.4
023832.5-311657	39.63529	-31.28275	0.2329 ¹	0238.4-3116	11.25 ± 0.65	1.76 ± 0.04	2774.9	1179.2
023853.9+255407	39.7245	25.90194	0.38 ⁵	0238.7+2555	0.609 ± 0.213	1.71 ± 0.20	4178.7	36.7
023927.2+132738	39.86342	13.46067	0.5 ⁵	0239.5+1326	2.32 ± 0.61	2.31 ± 0.22	2482.2	21.0
024115.5-304140	40.31454	-30.69447	0.3 ⁴	new	0.544 ± 0.248	1.89 ± 0.29	3000.0	10.3
024121.8+654311	40.34063	65.71992	0.18 ⁵	0241.3+6543	9.07 ± 0.65	2.08 ± 0.05	3101.3	406.4
024151.4-160333	40.46404	-16.05925	0.37 ⁵	0241.9-1603	1.43 ± 0.25	1.78 ± 0.12	3554.6	102.4

Continued on next page

Table 4 – continued from previous page

2BIGB Jname	R.A.(deg)	Dec.(deg)	z	4FGL J	N₀ (10⁻¹⁵)	Γ	E₀ (GeV)	TS
024302.9+004627	40.76217	0.77422	0.409 ¹	new	1.12 ± 0.32	1.87±0.19	3000.0	30.6
024440.3-581954	41.16779	-58.33181	0.26 ¹	0244.6-5819	3.62 ± 0.27	1.74±0.05	3789.6	629.2
024641.8-334342	41.67425	-33.72839	0.65 ⁵	0246.6-3348	0.127 ± 0.044	1.79±0.25	7327.9	19.1
024751.7-225002	41.96525	-22.83392	0.55 ⁵	new	0.312 ± 0.104	1.94±0.26	5000.0	21.5
024800.7+223119	42.00312	22.52219	0.54 ⁵	0248.0+2232	1.19 ± 0.27	1.93±0.16	3769.3	37.4
025038.0+171208	42.65813	17.20247	1.1 ¹	0250.6+1712	1.77 ± 0.19	1.81±0.08	5057.5	232.1
025047.6+562935	42.69821	56.49322	0.27 ⁵	0250.7+5630	2.89 ± 0.35	2.05±0.09	3981.0	120.5
025111.5-183112	42.798	-18.52019	0.5 ⁵	0251.1-1830	0.461 ± 0.083	1.63±0.11	6462.7	97.6
025707.9+335730	44.28279	33.95839	0.29 ⁵	0257.0+3358	2.21 ± 0.44	2.14±0.17	2725.8	48.0
025857.5+055243	44.73979	5.87886	–	0259.0+0552	16.08 ± 1.37	2.02±0.06	2067.9	388.8
025933.4-170538	44.88921	-17.09392	0.44 ⁵	0259.5-1705	0.631 ± 0.143	1.91±0.16	4682.1	51.4
030103.7+344101	45.26558	34.68367	0.246 ¹	new	2.15 ± 0.41	2.15±0.17	3000.0	49.8
030326.4-240711	45.86	-24.11978	0.266 ¹	0303.4-2407	463.0 ± 11.4	1.92±0.01	954.3	10126.1
030330.2+055430	45.87575	5.90842	0.196 ¹	0303.3+0555	0.065 ± 0.021	1.64±0.23	13787.6	28.3
030416.3-283218	46.06804	-28.53836	0.4 ²	0304.4-2833	0.429 ± 0.084	1.69±0.13	6034.5	75.0
030433.9-005404	46.14142	-0.90119	0.511 ¹	0304.5-0054	1.52 ± 0.28	2.02±0.15	3524.2	63.4
030515.1-160816	46.31283	-16.13794	0.31 ⁵	0305.1-1608	1.06 ± 0.15	1.76±0.10	4963.6	148.1
030544.2+403510	46.43396	40.58625	0.24 ⁵	new	0.057 ± 0.030	1.51±0.31	10000.0	14.5
030816.8-285105	47.07017	-28.85158	0.29 ⁵	0308.1-2852	1.32 ± 0.33	2.00±0.19	2756.5	31.0
030926.0-395927	47.35854	-39.99106	0.24 ⁵	0309.4-4000	0.830 ± 0.190	1.97±0.20	3514.8	38.0
031034.7-501631	47.64458	-50.27528	0.26 ⁵	0310.6-5017	1.84 ± 0.19	1.87±0.08	4290.2	280.8
031103.3-440228	47.76358	-44.04111	0.35 ⁵	0311.5-4402	1.18 ± 0.31	2.13±0.30	2716.2	24.7
031234.1-322317	48.14229	-32.38806	0.067 ¹	0312.4-3221	1.14 ± 0.28	2.08±0.19	2791.6	28.3
031235.7-222117	48.14875	-22.35478	0.28 ⁵	0312.5-2221	3.13 ± 0.34	1.79±0.07	3201.8	254.8
031250.3+361519	48.20954	36.25544	0.071 ¹	0312.9+3614	2.10 ± 0.27	1.84±0.09	3960.7	164.8
031423.1+061956	48.59962	6.33239	0.62 ²	0314.3+0620	1.50 ± 0.24	1.74±0.11	4408.2	113.8
031527.1-264400	48.86304	-26.73347	0.42 ⁵	0315.4-2643	0.783 ± 0.179	1.86±0.16	3967.9	51.9
031612.7+090443	49.05304	9.07867	0.372 ²	0316.2+0905	35.57 ± 1.91	1.95±0.04	2038.4	1118.9
031614.3-643731	49.05963	-64.62539	–	0316.2-6437	3.79 ± 0.28	1.84±0.05	3672.6	578.9
031614.9-260757	49.06221	-26.13256	0.443 ¹	0316.2-2608	9.69 ± 0.80	1.88±0.06	2282.9	484.0
031633.7-221612	49.14062	-22.27022	0.228 ¹	new	0.597 ± 0.227	1.81±0.22	3000.0	17.3
031746.1+201106	49.44417	20.18525	0.29 ⁵	new	0.076 ± 0.032	1.59±0.26	10000.0	18.0
031855.1+190816	49.73129	19.13792	0.43 ⁵	new	1.02 ± 0.35	1.72±0.18	3000.0	22.4
031916.7+190420	49.81975	19.07242	0.43 ⁵	new	0.959 ± 0.374	1.77±0.19	3000.0	14.3
031951.8+184534	49.96583	18.75961	0.19 ¹	0319.8+1845	1.36 ± 0.09	1.63±0.04	5977.7	286.4
032009.2-704533	50.03833	-70.75917	0.37 ⁵	0319.4-7045	0.502 ± 0.101	1.76±0.14	4922.6	64.9
032038.0+112452	50.15846	11.41453	0.35 ⁵	new	0.760 ± 0.187	2.09±0.19	5000.0	30.7
032056.4+042448	50.23492	4.41344	0.46 ⁵	new	25.40 ± 7.04	2.72±0.33	1000.0	19.1
032160.0+233611	50.49983	23.60311	–	0322.0+2335	23.13 ± 1.27	1.93±0.04	2311.7	1029.7
032343.6-011146	50.93171	-1.19614	0.44 ³	0323.7-0111	9.61 ± 0.68	1.92±0.05	2793.4	580.8
032523.5-563544	51.34804	-56.59572	0.06 ¹	0325.5-5635	8.70 ± 0.60	1.92±0.05	2554.4	654.0
032541.1-164616	51.42121	-16.77133	0.291 ¹	0325.6-1646	13.14 ± 0.72	1.90±0.04	2795.3	1107.3
032613.9+022514	51.55808	2.42075	0.147 ¹	0326.2+0225	7.55 ± 0.62	1.85±0.06	2979.3	482.6
032647.3-340447	51.69729	-34.07994	0.51 ⁵	0326.7-3404	3.51 ± 0.58	2.05±0.13	2191.8	81.9
032852.7-571605	52.21954	-57.26819	0.48 ³	0328.8-5715	0.130 ± 0.033	1.66±0.18	8744.1	43.8
033050.0-240611	52.7085	-24.10328	0.43 ⁵	0330.7-2408	0.982 ± 0.208	1.83±0.15	3613.5	61.2
033118.5-615528	52.827	-61.92464	0.21 ⁵	0331.3-6156	17.99 ± 1.11	2.02±0.05	1949.8	715.4
033202.3-703948	53.00979	-70.66358	0.24 ⁵	new	0.064 ± 0.023	1.43±0.22	10000.0	33.8
033223.8+822645	53.09904	82.44586	–	0333.1+8227	3.48 ± 0.55	1.89±0.10	2328.0	121.9
033349.0+291631	53.45417	29.27542	–	0333.7+2916	31.07 ± 1.73	1.95±0.04	1985.6	1007.2
033356.7+653656	53.48642	65.61558	0.16 ⁵	0333.9+6537	7.30 ± 0.37	1.98±0.04	4253.2	947.0
033415.4-372543	53.56425	-37.42861	0.39 ³	0334.2-3725	304.17 ± 9.58	2.07±0.02	949.7	4900.6
033513.9-445943	53.80783	-44.9955	–	0335.1-4459	7.69 ± 0.74	1.93±0.07	2142.1	323.4
033623.8-034738	54.09913	-3.79406	0.162 ¹	0336.5-0348	0.319 ± 0.092	1.42±0.15	6396.0	69.9
033812.5-244350	54.55221	-24.73056	0.251 ¹	0338.1-2443	0.191 ± 0.065	1.63±0.22	6797.3	37.0
033829.3+130215	54.62196	13.03764	–	0338.5+1302	14.15 ± 0.78	1.73±0.03	3142.3	1211.6

Continued on next page

Table 4 – continued from previous page

2BIGB Jname	R.A.(deg)	Dec.(deg)	z	4FGL J	$N_0 (10^{-15})$	Γ	$E_0 (\text{GeV})$	TS
033832.0-570448	54.63342	-57.08022	0.3 ⁵	0338.7-5706	0.098 ± 0.037	1.95±0.25	7814.7	16.0
033851.1-532425	54.71629	-53.40703	0.37 ⁵	new	0.735 ± 0.255	2.27±0.32	3000.0	14.6
033859.6-284619	54.74833	-28.77219	0.27 ⁵	0338.9-2848	7.08 ± 0.63	1.91±0.07	2492.0	390.0
033913.7-173600	54.80708	-17.60022	0.066 ¹	0339.2-1736	10.76 ± 0.81	1.93±0.06	2554.8	520.3
034254.2-370737	55.72575	-37.12706	0.201 ¹	new	0.423 ± 0.181	1.62±0.21	3000.0	16.9
034424.9+343017	56.10388	34.50497	–	0344.4+3432	0.306 ± 0.080	1.94±0.20	6668.3	28.1
034819.9+603508	57.08275	60.58572	–	0348.2+6035	0.338 ± 0.057	1.85±0.13	9198.6	78.6
034923.2-115927	57.34658	-11.99089	0.188 ¹	0349.4-1159	1.41 ± 0.17	1.67±0.08	4907.3	244.5
034957.8+064126	57.49096	6.69061	0.26 ⁵	0350.0+0640	0.048 ± 0.016	1.37±0.23	17167.7	40.1
035028.0-514454	57.61792	-51.74842	0.32 ⁵	0350.4-5144	0.867 ± 0.145	1.85±0.12	4211.8	98.2
035051.3-281632	57.71383	-28.27578	0.47 ⁵	0350.8-2814	0.273 ± 0.090	1.68±0.20	6653.3	33.0
035154.5-370344	57.97725	-37.06231	0.165 ¹	new	0.388 ± 0.167	1.53±0.20	3000.0	18.7
035257.5-683117	58.23946	-68.52142	0.087 ¹	0353.0-6831	0.420 ± 0.053	1.80±0.09	8753.5	208.6
035305.0-362308	58.27096	-36.38567	0.31 ⁵	0352.9-3623	0.371 ± 0.071	1.55±0.11	6484.7	84.4
035308.5+825631	58.28525	82.94203	0.069 ²	0353.7+8257	0.196 ± 0.035	1.76±0.12	9108.8	82.3
035309.5+565430	58.28975	56.90853	–	0353.0+5654	2.73 ± 0.35	2.23±0.11	3752.9	99.8
035513.3-184308	58.80533	-18.71903	0.28 ⁵	0355.1-1841	0.783 ± 0.223	1.76±0.17	3406.5	30.2
035610.9-132906	59.04538	-13.485	0.35 ⁵	0356.1-1329	1.350 ± 0.32	1.98±0.18	2999.9	35.9
035726.1-031759	59.35871	-3.29983	0.3 ⁵	0357.2-0319	0.178 ± 0.046	1.85±0.15	9871.7	37.2
035733.0-680932	59.38733	-68.15911	0.089 ¹	new	0.083 ± 0.026	1.76±0.23	10000.0	25.5
035856.0-305447	59.73375	-30.91328	0.65 ²	0359.0-3053	2.88 ± 0.41	1.93±0.11	2750.6	141.4
035923.5-023501	59.84783	-2.58383	0.34 ⁵	0359.4-0236	0.205 ± 0.057	1.74±0.18	8742.2	28.5
040111.0-535458	60.29667	-53.91625	0.59 ⁵	0401.0-5353	0.111 ± 0.026	1.73±0.16	11028.	61.5
040128.7+815311	60.36967	81.88664	0.215 ¹	new	0.067 ± 0.022	1.74±0.19	10000.0	18.4
040254.4+643510	60.72679	64.58611	0.31 ⁵	0402.9+6433	2.42 ± 0.49	2.50±0.32	2942.2	36.3
040324.6-242947	60.85237	-24.49639	0.357 ¹	0403.5-2437	22.35 ± 4.54	2.26±0.15	1039.8	64.7
040928.1+320246	62.36879	32.04611	0.28 ⁵	0409.4+3201	1.71 ± 0.32	1.90±0.13	3486.0	70.1
041238.5-392629	63.16021	-39.44153	0.5 ⁵	new	0.230 ± 0.091	1.66±0.24	5000.0	23.7
041458.1-533943	63.74217	-53.66219	–	0414.8-5338	0.207 ± 0.036	1.71±0.12	10526.6	113.1
041652.5+010523	64.21867	1.08997	0.287 ¹	0416.9+0105	4.63 ± 0.45	1.79±0.07	3493.3	365.5
042011.0-601505	65.04592	-60.25153	0.33 ⁵	0420.3-6016	2.27 ± 0.40	1.85±0.12	2530.5	95.7
042013.4+401121	65.05596	40.18922	0.14 ⁵	0420.2+4012	1.10 ± 0.19	1.82±0.12	5076.1	73.0
042132.9-062903	65.38717	-6.48431	0.39 ¹	new	1.38 ± 0.54	1.99±0.23	3000.0	21.0
042218.3+195055	65.57642	19.84861	0.516 ¹	0422.3+1951	3.74 ± 0.51	1.97±0.10	3334.0	119.2
042525.4+632001	66.35563	63.33386	0.27 ⁵	0425.3+6319	0.933 ± 0.108	1.80±0.08	6829.4	199.7
042733.4-183010	66.88896	-18.50286	0.22 ⁵	new	0.067 ± 0.027	1.53±0.24	10000.0	21.0
042900.2-323641	67.25071	-32.61144	0.34 ⁴	0429.3-3238	1.40 ± 0.32	1.89±0.15	2800.3	39.4
042958.9-305935	67.49554	-30.99311	0.21 ⁵	0429.9-3101	5.25 ± 0.54	1.91±0.08	2534.9	258.1
043046.4+030337	67.69325	3.06047	0.43 ⁵	new	0.065 ± 0.036	1.69±0.41	10000.0	9.65
043145.1+740326	67.93775	74.05739	–	0431.8+7403	5.41 ± 0.48	1.91±0.06	2753.7	359.4
043307.5+322840	68.28142	32.47797	–	0433.1+3227	0.892 ± 0.143	1.84±0.12	5871.0	101.0
043332.9-104232	68.38704	-10.709	0.29 ⁵	new	1.37 ± 0.35	2.38±0.22	3000.0	24.9
043344.1-572613	68.43388	-57.437	–	0433.7-5725	7.15 ± 0.63	1.97±0.07	2221.1	359.8
043441.0+092348	68.67075	9.39683	0.21 ⁵	0434.7+0922	9.35 ± 0.84	1.94±0.06	2632.0	332.8
043517.8-262122	68.824	-26.35619	0.31 ⁴	0435.4-2623	9.38 ± 3.04	2.14±0.20	1143.1	29.4
043837.1-732921	69.65446	-73.48933	0.15 ⁵	0438.0-7329	1.42 ± 0.17	1.88±0.09	4354.2	174.1
043932.0-320052	69.88417	-32.01453	0.4 ⁵	0439.4-3202	2.36 ± 0.30	1.88±0.09	3358.5	169.3
044018.6-245933	70.07762	-24.99267	0.6 ²	0440.2-2458	0.481 ± 0.072	1.64±0.10	7277.5	159.0
044050.4+275046	70.20987	27.84636	0.2 ⁵	0440.8+2749	9.35 ± 0.86	2.03±0.07	2747.5	294.9
044127.5+150455	70.36446	15.08211	0.109 ¹	0441.5+1505	2.14 ± 0.37	2.09±0.13	3990.5	76.3
044240.7+614039	70.66938	61.67769	0.18 ⁵	0442.7+6142	1.78 ± 0.21	1.99±0.10	4580.7	159.4
044328.4-415156	70.86833	-41.86558	0.3 ⁴	0443.4-4152	1.08 ± 0.20	1.82±0.13	3635.0	76.2
044837.6-163243	72.15671	-16.54531	0.35 ²	0448.6-1632	12.73 ± 0.89	1.88±0.05	2379.5	640.1
044924.7-435008	72.35288	-43.83581	0.19 ³	0449.4-4350	379.41 ± 5.51	1.86±0.01	1604.8	35037.1
045107.1-232533	72.78125	-23.42608	0.36 ⁵	new	0.823 ± 0.374	2.56±0.44	3000.0	10.1
045148.6+572141	72.95267	57.36158	0.31 ⁵	0451.8+5721	0.310 ± 0.065	1.92±0.15	7606.6	45.5

Continued on next page

Table 4 – continued from previous page

2BIGB Jname	R.A.(deg)	Dec.(deg)	z	4FGL J	N₀ (10⁻¹⁵)	Γ	E₀ (GeV)	TS
045215.0+210303	73.06375	21.05106	0.31 ⁵	new	0.634 ± 0.326	1.62±0.22	3000.0	13.3
045804.9+115143	74.52033	11.86197	0.2 ⁵	0458.0+1152	0.247 ± 72.3	1.56±0.01	7495.6	44.7
045937.0-541707	74.90413	-54.28539	0.5 ⁵	0459.7-5413	2.52 ± 0.57	1.98±0.16	2136.8	49.5
050021.5+523801	75.0895	52.63375	0.15 ⁵	0500.2+5237	1.48 ± 0.14	1.93±0.08	6063.1	247.9
050043.1+190317	75.18292	19.05481	0.25 ⁵	new	0.325 ± 0.145	1.80±0.27	5000.0	11.0
050130.0+020400	75.375	2.06681	0.58 ⁵	new	0.269 ± 0.122	1.63±0.26	5000.0	18.3
050141.2+304825	75.4215	30.80711	0.31 ⁵	0501.7+3048	0.817 ± 0.136	1.83±0.12	5648.4	71.7
050240.7-120429	75.66971	-12.07486	0.45 ⁵	new	0.247 ± 0.105	1.92±0.26	5000.0	9.58
050305.8+653401	75.77429	65.56697	0.25 ⁵	0502.9+6533	0.261 ± 0.064	1.61±0.16	6935.5	57.6
050335.0-111506	75.89754	-11.25172	0.4 ³	0503.5-1116	0.899 ± 0.151	1.87±0.11	5150.7	92.9
050339.6+451659	75.91487	45.28317	0.25 ⁵	0503.6+4518	3.02 ± 0.35	1.94±0.09	4180.8	155.0
050419.1-095632	76.08129	-9.94244	0.32 ⁴	new	0.978 ± 0.325	2.18±0.25	3000.0	16.8
050534.8+041554	76.39483	4.26514	0.424 ¹	0505.6+0415	2.91 ± 0.30	1.86±0.08	4545.4	300.0
050558.8+611335	76.49496	61.22664	0.27 ⁵	0506.0+6113	4.64 ± 0.36	1.97±0.06	3682.4	383.9
050601.7-382055	76.50696	-38.34875	0.182 ¹	0505.8-3817	11.85 ± 1.93	1.94±0.10	1363.0	140.8
050639.1-085801	76.66625	-8.96717	0.28 ⁵	0506.7-0857	6.97 ± 0.92	2.10±0.11	2193.2	131.6
050643.0-234419	76.67933	-23.73872	0.45 ⁴	new	11.05 ± 5.30	2.32±0.37	1000.0	11.8
050650.1+032358	76.70892	3.39964	0.32 ⁵	0506.9+0323	1.888 ± 0.31	1.90±0.12	3719.5	100.1
050657.8-543503	76.74083	-54.58442	0.26 ³	0506.9-5435	2.91 ± 0.23	1.61±0.05	4069.4	679.5
050727.3-334635	76.86363	-33.7765	0.39 ²	0507.4-3346	0.677 ± 0.102	1.65±0.09	5836.5	143.0
050756.2+673724	76.984	67.62342	0.34 ²	0507.9+6737	4.65 ± 0.17	1.53±0.02	6321.6	3341.2
050938.2-040045	77.40904	-4.01267	0.304 ¹	0509.6-0402	1.63 ± 0.30	1.94±0.14	3623.9	62.8
050957.3-641741	77.48867	-64.29489	–	0509.9-6417	2.72 ± 0.29	1.81±0.07	3363.9	264.7
051533.2-012355	78.88829	-1.39867	0.25 ⁵	0515.5-0125	1.50 ± 0.28	2.01±0.13	3774.7	54.6
051631.0+735108	79.13004	73.85239	0.251 ¹	0516.4+7350	2.99 ± 0.25	1.94±0.06	3639.7	334.2
052042.0+653351	80.17492	65.56436	0.4 ⁵	new	0.231 ± 0.089	1.87±0.27	5000.0	15.7
052133.7-295748	80.39025	-29.96342	0.45 ⁵	new	0.667 ± 0.254	1.93±0.29	3000.0	12.2
052146.0+211251	80.4415	21.21428	0.108 ¹	0521.7+2112	427.69 ± 6.89	1.95±0.01	1555.2	14959.2
052439.8-261554	81.16567	-26.26525	0.26 ⁴	new	0.340 ± 0.110	2.02±0.29	5000.0	19.7
052542.4-601340	81.42675	-60.22783	0.45 ⁵	0525.6-6013	2.64 ± 0.21	1.77±0.06	4237.8	518.3
052645.4-151900	81.68933	-15.31681	0.21 ⁵	0526.7-1519	6.07 ± 0.65	1.89±0.07	2591.1	218.1
052846.1-592003	82.19192	-59.33433	1.13 ²	0528.7-5920	5.36 ± 0.69	1.99±0.10	2155.1	155.4
052902.6+093435	82.26067	9.5765	0.3 ⁵	0529.1+0935	1.88 ± 0.29	2.03±0.13	4198.4	86.3
053626.9-254748	84.11204	-25.79672	–	0536.5-2548	2.05 ± 0.36	1.97±0.13	2885.7	72.8
053629.1-334302	84.12108	-33.71736	0.34 ³	0536.4-3343	2.01 ± 0.15	1.70±0.05	6837.5	746.2
053645.3-255841	84.18892	-25.97819	0.32 ⁵	new	0.110 ± 0.089	1.46±0.34	5000.0	9.49
053749.0-571830	84.454	-57.30836	1.18 ²	0537.7-5717	6.97 ± 0.68	2.01±0.08	2260.2	243.5
053810.4-390842	84.54317	-39.14514	0.27 ⁴	0538.2-3910	1.44 ± 0.24	1.89±0.12	3483.0	82.7
054030.0+582338	85.12504	58.394	–	0540.5+5823	4.28 ± 0.35	1.86±0.06	3667.2	436.4
054106.9-485410	85.27883	-48.90286	0.6 ⁵	0541.1-4854	1.09 ± 0.21	1.93±0.14	3583.5	58.6
054357.0-553207	85.98837	-55.53542	0.273 ¹	0543.9-5531	29.09 ± 1.13	1.76±0.02	2301.7	2909.4
054656.8-220457	86.73654	-22.08258	0.28 ¹	0546.9-2206	0.283 ± 0.082	1.95±0.21	5926.7	29.1
054903.0-215001	87.26417	-21.83369	0.35 ⁵	new	0.280 ± 0.100	1.88±0.27	5000.0	20.1
054906.9+325803	87.27862	32.96769	0.25 ⁵	0549.0+3258	0.728 ± 0.146	1.83±0.13	5802.5	58.8
055026.6-435703	87.61075	-43.95089	0.4 ⁵	0550.5-4356	0.843 ± 0.134	1.81±0.11	4802.6	112.6
055040.6-321616	87.66904	-32.27122	0.069 ¹	0550.5-3216	2.31 ± 0.29	1.82±0.09	3467.0	183.6
055333.1-203418	88.388	-20.57192	0.38 ³	0553.5-2034	11.93 ± 0.84	2.02±0.05	2426.2	542.9
055411.1-275729	88.54625	-27.95828	0.231 ¹	new	0.075 ± 0.028	1.58±0.26	10000.0	21.1
055716.8-061706	89.32012	-6.28519	0.29 ⁵	0557.3-0615	0.608 ± 0.122	2.14±0.16	6378.2	53.3
055806.4-383831	89.52675	-38.64211	0.302 ¹	0558.0-3837	5.88 ± 0.44	1.85±0.05	3173.3	561.1
055941.0+304228	89.92079	30.70789	0.3 ⁵	0559.6+3044	0.221 ± 0.054	1.58±0.13	9294.8	49.6
055959.3+640958	89.99717	64.16628	0.32 ⁵	0559.9+6409	1.74 ± 0.34	1.98±0.14	2879.3	59.2
060015.0+124343	90.0625	12.72867	0.12 ⁵	0600.3+1244	0.388 ± 0.058	1.53±0.09	11246.8	152.4
060200.4+531600	90.50183	53.26669	0.052 ¹	0602.0+5315	6.96 ± 0.48	1.98±0.05	3118.4	539.3
060251.3-401845	90.71371	-40.31258	–	0602.8-4019	25.47 ± 1.38	1.92±0.04	2031.7	1195.7
060408.1-481725	91.03587	-48.29033	0.23 ⁴	0604.1-4816	0.986 ± 0.142	1.74±0.10	5014.9	165.0

Continued on next page

Table 4 – continued from previous page

2BIGB Jname	R.A.(deg)	Dec.(deg)	z	4FGL J	$N_0 (10^{-15})$	Γ	$E_0 (\text{GeV})$	TS
060433.8-403754	91.14083	-40.63186	0.28 ⁵	new	0.271 ± 0.110	1.92 ± 0.28	5000.0	12.0
060635.7-472954	91.64892	-47.49856	0.037 ¹	0606.5-4730	4.32 ± 0.57	1.97 ± 0.10	2471.7	136.7
060714.4-251859	91.80992	-25.31653	0.275 ¹	0607.2-2518	1.79 ± 0.34	1.87 ± 0.13	2929.1	69.8
060915.1-024754	92.31275	-2.79847	0.23 ⁵	0609.2-0247	6.94 ± 0.59	1.84 ± 0.06	3378.1	408.1
061104.1+682956	92.76717	68.49906	0.5 ⁵	new	0.049 ± 0.020	1.48 ± 0.25	10000.0	16.9
061106.6+432357	92.77746	43.39925	0.28 ⁵	0611.1+4325	2.04 ± 0.24	1.86 ± 0.08	4127.7	171.9
061610.3-173305	94.04287	-17.55153	0.55 ⁴	new	0.964 ± 0.402	1.75 ± 0.22	3000.0	19.3
061702.8+434033	94.26146	43.67606	0.26 ⁵	0616.9+4340	0.058 ± 0.020	1.64 ± 0.23	12380.4	21.0
061740.9-171557	94.4205	-17.26597	–	0617.7-1715	15.29 ± 1.12	1.89 ± 0.05	2341.5	596.1
061949.6+573549	94.95654	57.59694	0.45 ⁵	new	0.674 ± 0.276	2.05 ± 0.29	3000.0	11.7
062040.0+264331	95.16687	26.72553	0.14 ⁵	0620.7+2643	0.138 ± 0.028	1.37 ± 0.12	15250.4	102.5
062046.1-503350	95.19221	-50.56414	0.25 ⁵	0620.7-5034	0.143 ± 0.051	2.14 ± 0.25	8173.1	40.4
062149.7-341149	95.45704	-34.19706	0.529 ¹	0621.7-3411	0.739 ± 0.216	2.09 ± 0.23	3913.1	22.5
062337.9-525756	95.90779	-52.96556	0.29 ⁴	0623.9-5259	4.03 ± 1.11	1.92 ± 0.17	1805.5	44.5
062445.1-323055	96.18771	-32.51542	0.252 ¹	new	0.915 ± 0.289	1.97 ± 0.20	3000.0	19.2
062626.3-171046	96.6095	-17.17961	0.7 ³	0626.4-1712	3.67 ± 1.11	1.96 ± 0.19	2045.2	32.7
062636.7-425806	96.65296	-42.96833	0.27 ⁵	0626.4-4259	1.54 ± 0.21	1.84 ± 0.09	4043.8	134.1
062753.4-151957	96.97237	-15.33253	0.29 ⁵	new	0.063 ± 0.034	1.60 ± 0.33	10000.0	11.8
063015.1-201236	97.56275	-20.21011	0.22 ⁵	new	0.379 ± 0.247	1.71 ± 0.34	5000.0	20.5
063059.5-240646	97.748	-24.11281	1.239 ³	0630.9-2406	136.68 ± 3.36	1.84 ± 0.01	1725.0	7739.2
063359.1+584035	98.49879	58.67661	0.29 ⁵	0633.9+5840	0.318 ± 0.086	2.00 ± 0.20	5175.8	28.0
064007.2-125315	100.02992	-12.8875	0.11 ⁵	0640.0-1253	0.476 ± 0.061	1.61 ± 0.08	11216.	206.8
064050.3+243319	100.20975	24.55533	0.27 ⁵	0640.8+2432	0.317 ± 0.083	1.77 ± 0.16	6554.2	32.3
064435.1+603851	101.14879	60.64753	0.33 ⁵	0644.6+6039	3.62 ± 0.45	1.98 ± 0.09	2660.6	159.8
064443.7-285116	101.18225	-28.85458	0.35 ⁴	0644.6-2853	1.24 ± 0.18	1.89 ± 0.11	4628.9	99.4
064710.0-513547	101.79183	-51.59661	0.22 ⁵	0647.0-5138	0.595 ± 0.118	1.67 ± 0.13	5189.1	80.9
064814.0+160656	102.05821	16.11569	0.35 ⁵	0648.1+1605	0.404 ± 0.114	1.79 ± 0.19	6116.6	34.3
064847.6+151624	102.19854	15.27356	0.179 ¹	0648.7+1516	4.87 ± 0.29	1.66 ± 0.04	5206.4	1135.4
064850.5-694522	102.21038	-69.75628	0.28 ⁵	new	0.522 ± 0.262	1.75 ± 0.27	3000.0	17.2
064933.6-313920	102.39	-31.65564	–	0649.5-3139	0.977 ± 0.118	1.64 ± 0.08	6550.6	233.4
065010.3-514421	102.54304	-51.73942	0.31 ⁵	0650.2-5144	0.420 ± 0.074	1.78 ± 0.12	6719.3	91.5
065035.3+205555	102.64721	20.93219	0.3 ⁵	0650.6+2055	1.71 ± 0.18	1.68 ± 0.07	5243.5	287.4
065046.5+250259	102.69367	25.04986	0.203 ²	0650.7+2503	79.215 ± 2.17	1.72 ± 0.01	2063.2	6426.8
065105.0+401338	102.77254	40.22725	0.18 ⁵	0651.0+4013	13.90 ± 1.19	2.11 ± 0.07	1932.6	312.4
065200.6-480859	103.00237	-48.14981	0.4 ⁵	0652.1-4813	1.95 ± 0.40	1.98 ± 0.15	2770.2	57.1
065610.7+423702	104.04442	42.61744	0.059 ¹	0656.3+4235	0.770 ± 0.133	2.02 ± 0.13	5740.3	90.0
065635.6+421524	104.14821	42.25686	0.45 ⁵	0656.5+4218	0.924 ± 0.248	1.89 ± 0.17	3717.5	40.5
065845.0+063711	104.68758	6.61986	0.23 ⁵	0658.6+0636	2.32 ± 0.50	1.70 ± 0.11	3031.0	80.6
065932.9-674350	104.88717	-67.73058	0.43 ⁵	0659.6-6742	0.165 ± 0.043	1.59 ± 0.16	8608.3	54.0
070014.3+130424	105.05963	13.07344	0.21 ⁵	0700.2+1304	4.73 ± 0.59	1.92 ± 0.09	2841.6	157.4
070132.2+250953	105.384	25.16492	0.33 ⁵	0701.5+2511	0.619 ± 0.168	1.64 ± 0.17	4666.0	62.7
070315.9+680831	105.81625	68.142	0.27 ⁵	0703.2+6809	0.257 ± 0.077	1.84 ± 0.20	5079.9	25.8
070610.8+024449	106.54508	2.747	0.22 ⁵	0706.1+0246	0.118 ± 0.031	1.47 ± 0.15	14197.2	52.8
070631.7+374436	106.63204	37.74342	–	0706.5+3744	12.07 ± 0.63	1.88 ± 0.04	2876.0	1179.3
070858.3+224135	107.24283	22.69317	–	0709.1+2241	32.93 ± 1.95	2.07 ± 0.05	1750.9	748.0
070912.5-152703	107.30213	-15.45097	0.1 ⁵	0709.2-1527	0.756 ± 0.121	1.72 ± 0.10	7399.8	100.0
070947.1-300905	107.44962	-30.15158	–	0709.7-3009	1.64 ± 0.28	1.88 ± 0.12	3772.7	81.1
071030.1+590820	107.62521	59.13903	0.12 ¹	0710.4+5908	2.03 ± 0.15	1.68 ± 0.05	5221.1	695.2
071218.9+571948	108.07871	57.33014	0.095 ²	0712.4+5724	20.93 ± 2.17	2.58 ± 0.13	1337.9	145.1
071223.6+331333	108.09825	33.22603	0.41 ⁵	0712.5+3311	0.641 ± 0.189	1.91 ± 0.19	3716.5	21.9
071745.1-552022	109.43775	-55.33944	–	0717.7-5519	0.895 ± 0.096	1.90 ± 0.07	4609.9	77.8
071908.1-705403	109.78587	-70.90097	0.33 ⁵	0719.1-7055	0.688 ± 0.157	2.01 ± 0.16	4251.3	36.0
072113.1-022055	110.30792	-2.34861	0.38 ⁵	0721.3-0222	0.914 ± 0.209	1.85 ± 0.16	4469.2	49.3
072259.7-073134	110.74867	-7.52631	0.17 ⁵	0723.0-0732	5.07 ± 0.66	2.08 ± 0.11	2983.2	121.7
072314.0+584120	110.8085	58.68908	0.26 ⁵	0723.4+5841	0.065 ± 0.019	1.52 ± 0.20	11255.8	29.9
072348.3+205130	110.95142	20.85856	0.21 ⁵	0723.7+2050	2.94 ± 0.52	1.70 ± 0.10	2774.5	142.3

Continued on next page

Table 4 – continued from previous page

2BIGB Jname	R.A.(deg)	Dec.(deg)	z	4FGL J	N₀ (10⁻¹⁵)	Γ	E₀ (GeV)	TS
072529.5-050336	111.37304	-5.06014	0.1 ⁵	0725.5-0504	0.404 ± 0.099	2.10±0.20	6606.1	34.4
072547.9-054832	111.4495	-5.809	–	0725.7-0549	1.69 ± 0.25	1.91±0.11	4439.9	105.9
072659.5+373423	111.74804	37.57308	0.35 ⁴	0727.1+3734	0.279 ± 0.073	1.85±0.19	6067.6	35.2
073026.1+330722	112.60858	33.12303	0.11 ¹	0730.4+3308	3.91 ± 0.44	1.92±0.08	2918.6	194.1
073049.5-660218	112.70633	-66.03858	0.106 ¹	0730.7-6602	1.27 ± 0.14	1.72±0.07	5271.4	250.7
073152.7+280433	112.96967	28.07586	0.248 ¹	0731.9+2805	1.59 ± 0.39	1.94±0.17	2716.6	32.6
073326.8+515355	113.36163	51.89886	0.09 ⁵	0733.4+5152	1.05 ± 0.14	1.73±0.09	4748.6	162.0
073329.6+351542	113.37321	35.26189	0.177 ¹	new	9.947 ± 4.04	2.20±0.24	1000.0	15.7
073706.0-824840	114.27513	-82.81117	0.23 ⁵	0737.3-8247	4.41 ± 0.38	1.88±0.06	3075.8	312.0
073927.4-672136	114.86412	-67.36011	0.53 ⁵	0739.8-6722	2.25 ± 0.33	2.09±0.13	3233.9	91.8
074221.1-813136	115.58808	-81.52672	0.43 ⁵	new	0.350 ± 0.109	1.79±0.18	5000.0	24.3
074405.4+743358	116.02237	74.56617	0.314 ¹	0744.1+7434	2.00 ± 0.18	1.83±0.07	4327.0	421.5
074419.1-621100	116.08254	-62.18344	0.38 ⁵	new	0.065 ± 0.027	1.35±0.24	10000.0	24.7
074627.0-022549	116.61258	-2.43036	–	0746.3-0225	2.53 ± 0.28	1.75±0.07	4115.2	243.9
074642.0-475455	116.67629	-47.91528	–	0746.6-4754	17.66 ± 0.99	1.98±0.04	2458.8	858.1
074710.0-073724	116.79179	-7.62358	0.32 ⁵	0747.2-0736	1.12 ± 0.25	2.03±0.18	4037.1	46.7
074716.2+851208	116.81767	85.20244	0.28 ⁵	0748.3+8511	0.75 ± 0.097	1.69±0.08	5192.8	160.5
074722.2+090548	116.84238	9.09667	0.28 ⁵	0747.5+0905	5.58 ± 0.76	2.06±0.11	2276.6	133.8
074724.7-492633	116.85308	-49.44253	–	0747.5-4927	11.90 ± 1.64	2.10±0.10	1818.6	154.5
074914.0+231316	117.30838	23.22131	0.175 ¹	0749.2+2314	0.422 ± 0.103	2.07±0.21	6218.3	52.2
074929.6+745144	117.37317	74.86242	0.607 ²	0749.7+7450	1.61 ± 0.27	2.19±0.15	3032.1	75.1
075936.1+132117	119.90058	13.35494	0.3 ⁴	0759.6+1321	1.69 ± 0.21	1.85±0.09	4319.9	179.0
080015.5+561107	120.06471	56.18547	0.38 ⁵	0800.3+5611	2.24 ± 0.37	1.99±0.13	2644.2	80.9
080056.5+073235	120.23562	7.54308	0.44 ⁵	0800.9+0733	1.18 ± 0.22	1.92±0.13	3413.8	51.9
080102.1+644449	120.25892	64.74711	0.2 ²	0801.1+6444	3.09 ± 0.40	1.91±0.09	2618.4	158.9
080204.1+100637	120.52004	10.11047	0.57 ³	0802.0+1006	4.39 ± 0.56	2.05±0.10	2598.1	141.9
080215.9-094210	120.56625	-9.70303	–	0802.3-0942	5.49 ± 0.53	1.89±0.07	3103.9	313.9
080312.0-033600	120.80042	-3.60022	0.365 ¹	0803.2-0337	26.96 ± 1.73	2.01±0.05	1830.8	699.4
080323.0+481617	120.84592	48.27158	0.501 ¹	new	0.113 ± 0.067	1.62±0.32	5000.0	9.30
080457.7-062426	121.24058	-6.40725	0.27 ⁴	0804.9-0624	2.04 ± 0.26	1.82±0.09	4362.9	178.9
080526.6+753424	121.36096	75.57358	0.12 ¹	0805.4+7534	22.01 ± 0.83	1.83±0.02	2334.5	2664.5
080625.9+593107	121.608	59.51861	0.3 ²	0806.5+5930	2.64 ± 0.35	1.85±0.09	2961.7	201.2
080938.1+345537	122.41212	34.92703	0.083 ¹	0809.6+3455	1.33 ± 0.21	1.83±0.12	3852.5	119.3
080949.2+521858	122.45496	52.31619	0.137 ¹	0809.8+5218	186.28 ± 4.59	1.84±0.01	1296.9	8962.0
081003.3-752723	122.51367	-75.45656	0.47 ³	new	1.29 ± 0.56	1.83±0.21	5000.0	32.0
081012.0-703047	122.55017	-70.51308	–	new	0.066 ± 0.032	1.47±0.31	10000.0	20.6
081201.9+023733	123.00775	2.62583	0.2 ⁵	0812.0+0237	2.79 ± 0.29	1.83±0.08	4189.2	304.8
081231.3+282056	123.13025	28.34897	0.47 ¹	0812.6+2821	0.885 ± 0.217	1.90±0.19	3664.5	50.1
081240.8+650911	123.17017	65.15308	0.23 ⁵	0812.8+6507	1.96 ± 0.29	1.92±0.11	3190.2	119.3
081338.1-035716	123.40862	-3.95464	0.33 ⁵	0813.7-0356	0.512 ± 0.106	1.73±0.13	6054.8	63.9
081421.3+294021	123.58858	29.67256	0.32 ⁴	0814.4+2941	0.773 ± 0.189	1.83±0.16	4081.8	51.9
081539.8+655004	123.91592	65.83461	0.47 ⁵	0815.5+6554	0.128 ± 0.026	1.74±0.13	7184.4	22.5
081627.2-131152	124.11333	-13.19792	0.37 ³	0816.4-1311	35.78 ± 1.72	1.83±0.03	2070.2	1743.8
081751.0+324340	124.46246	32.728	0.32 ⁴	0817.8+3243	1.78 ± 0.345	2.05±0.15	3220.1	70.6
081917.6-075626	124.82325	-7.94056	0.37 ⁴	0819.4-0756	0.617 ± 0.109	1.76±0.13	6346.3	98.6
081941.8+053023	124.92433	5.50639	0.37 ⁵	new	7.64 ± 4.07	1.94±0.26	1000.0	18.8
082021.1-280159	125.09125	-28.03308	–	0820.1-2801	0.041 ± 0.010	1.54±0.15	25099.2	43.8
082030.8-031413	125.12846	-3.23717	0.45 ⁵	new	0.308 ± 0.124	1.73±0.27	5000.0	14.0
082051.2+235345	125.21329	23.89589	0.402 ¹	0820.9+2353	4.39 ± 0.85	1.99±0.14	2056.7	71.8
082314.6-632930	125.81079	-63.49172	0.23 ⁴	0823.1-6330	0.215 ± 0.053	1.69±0.16	8130.8	48.2
082320.5+112551	125.83562	11.43092	0.44 ¹	new	0.444 ± 0.247	1.80±0.32	3000.0	9.28
082627.9-640415	126.61608	-64.07094	0.24 ⁵	0826.4-6404	1.65 ± 0.17	1.76±0.07	5091.4	280.5
082706.2-070845	126.77567	-7.14608	0.247 ²	0827.0-0708	2.15 ± 0.24	1.77±0.08	4361.7	255.3
082801.1+231217	127.00479	23.20492	0.5 ⁴	0828.0+2307	0.611 ± 0.130	1.94±0.17	4870.5	50.0
082814.2+415351	127.05925	41.89769	0.225 ¹	0828.3+4152	0.448 ± 0.138	1.81±0.21	4303.7	34.1
082904.8+175415	127.27012	17.90442	0.089 ¹	0829.0+1755	9.85 ± 1.50	2.18±0.12	1706.9	101.6

Continued on next page

Table 4 – continued from previous page

2BIGB Jname	R.A.(deg)	Dec.(deg)	z	4FGL J	$N_0 (10^{-15})$	Γ	$E_0 (\text{GeV})$	TS
083010.9+523027	127.5455	52.50756	0.205 ¹	0830.0+5231	0.474 ± 0.122	1.65±0.15	4829.1	67.5
083015.1-094455	127.56308	-9.74883	0.5 ⁵	new	1.58 ± 0.37	1.85±0.15	3000.0	53.1
083133.1+174630	127.88771	17.77519	0.3 ⁴	0831.5+1747	1.17 ± 0.19	1.95±0.13	4390.9	101.3
083251.5+330011	128.21442	33.00306	0.671 ¹	new	0.316 ± 0.100	1.61±0.18	5000.0	27.4
083724.6+145820	129.35262	14.97239	0.278 ¹	0837.3+1458	0.609 ± 0.132	1.77±0.15	4918.5	55.7
083955.1+121702	129.97963	12.28414	0.336 ¹	new	0.065 ± 0.030	1.61±0.28	10000.0	12.7
084121.6-355505	130.34012	-35.91831	–	0841.3-3554	13.04 ± 0.16	1.83±0.01	3261.2	1034.8
084225.1+025252	130.60629	2.88131	0.425 ¹	0842.5+0251	0.902 ± 0.226	1.83±0.16	3671.7	45.1
084310.0+503410	130.79254	50.56953	0.439 ¹	new	0.036 ± 0.019	1.29±0.29	10000.0	19.5
084701.6-233701	131.75654	-23.61714	0.061 ¹	0847.0-2336	19.72 ± 1.10	1.98±0.04	2451.5	920.7
084712.9+113350	131.80388	11.56394	0.198 ¹	0847.2+1134	1.63 ± 0.17	1.67±0.07	5198.5	332.1
084839.7+050618	132.16529	5.105	–	0848.7+0508	0.054 ± 0.016	1.56±0.20	19270.6	43.2
085036.2+345522	132.65079	34.92297	0.145 ¹	0850.5+3455	5.98 ± 0.71	1.98±0.09	2204.3	175.7
085310.1-365820	133.29379	-36.97239	–	0853.1-3657	10.47 ± 0.15	1.99±0.01	3108.7	519.8
085409.9+440830	133.54117	44.14175	0.23 ⁴	0854.3+4408	2.87 ± 0.33	1.79±0.08	2973.7	221.2
085410.2+275421	133.54233	27.90597	0.494 ¹	0854.0+2753	0.051 ± 0.017	1.51±0.23	14143.4	29.4
085749.1+013530	134.45754	1.59172	0.281 ¹	new	22.98 ± 5.89	2.76±0.35	1000.0	24.8
085802.9-313038	134.51208	-31.51064	0.34 ⁵	0858.0-3130	0.837 ± 0.142	1.73±0.11	5870.0	104.8
085910.3+834500	134.79279	83.75006	0.33 ¹	new	0.119 ± 0.049	1.39±0.19	5000.0	21.7
085920.6+004712	134.83567	0.78669	0.57 ²	new	0.405 ± 0.130	2.08±0.26	5000.0	21.2
085930.6+621730	134.87762	62.29178	0.38 ⁴	0859.4+6218	10.51 ± 2.30	2.06±0.14	1236.3	72.1
090038.7+674223	135.16121	67.70647	–	0901.2+6742	86.42 ± 12.8	2.66±0.13	738.8	121.9
090133.8+671316	135.39088	67.22136	0.55 ⁵	0901.5+6711	0.512 ± 0.101	2.09±0.17	5081.6	57.4
090535.0+135806	136.39575	13.96844	0.34 ³	0905.6+1358	15.16 ± 0.91	1.82±0.04	2498.9	997.7
090802.2-095937	137.00921	-9.99369	0.054 ¹	new	0.072 ± 0.038	1.58±0.37	10000.0	20.8
090809.1-072709	137.03808	-7.4525	0.22 ⁵	new	0.624 ± 0.282	1.75±0.23	3000.0	14.3
090858.7-211854	137.24442	-21.31517	0.33 ⁵	new	0.909 ± 0.248	1.74±0.14	3000.0	20.8
090900.6+231112	137.25262	23.18692	0.223 ¹	0908.9+2311	2.18 ± 0.23	1.73±0.07	4620.6	329.2
090953.3+310603	137.472	31.10086	0.272 ¹	0909.7+3104	0.854 ± 0.211	1.91±0.18	3554.9	41.1
091003.9-181612	137.51612	-18.27006	0.45 ⁵	0910.1-1816	1.035 ± 0.28	2.01±0.18	3361.6	23.0
091037.0+332924	137.65429	33.49011	0.35 ²	0910.6+3329	19.62 ± 0.96	1.95±0.04	2610.3	1754.1
091211.2+275927	138.04675	27.99108	0.56 ³	0912.2+2800	0.198 ± 0.048	1.57±0.17	8101.2	54.2
091230.1+155527	138.12754	15.92439	0.212 ¹	0912.5+1556	0.978 ± 0.136	2.05±0.10	5611.8	160.7
091300.2-210321	138.25092	-21.05583	0.198 ¹	0912.9-2102	8.04 ± 0.52	1.81±0.04	3484.5	801.5
091322.4+813305	138.34321	81.55139	0.639 ²	0913.3+8133	0.136 ± 0.037	1.50±0.16	7431.3	53.7
091408.3-015945	138.53442	-1.99586	0.49 ⁵	0914.1-0202	7.02 ± 2.72	2.16±0.28	1356.6	26.0
091429.1+684508	138.62379	68.75242	0.45 ⁵	0914.5+6845	0.451 ± 0.084	1.90±0.14	5351.4	62.6
091552.4+293324	138.96833	29.55667	0.19 ³	0915.9+2933	97.54 ± 3.74	1.90±0.02	1345.5	3051.3
091651.9+523828	139.21642	52.64119	0.19 ¹	0916.7+5238	0.777 ± 0.139	1.88±0.13	4042.9	79.8
091714.1-034314	139.31087	-3.72061	0.308 ¹	0917.3-0342	0.307 ± 0.069	1.69±0.16	7377.6	65.1
091926.2-220042	139.85929	-22.01186	0.45 ⁵	new	0.396 ± 0.095	1.89±0.21	5000.0	21.2
092057.5-225721	140.23946	-22.95597	0.32 ⁴	0920.9-2256	0.508 ± 0.110	1.79±0.14	5572.5	54.9
092252.0+755403	140.71671	75.90089	0.4 ⁵	new	0.359 ± 0.155	1.71±0.23	3000.0	13.7
092401.0+053345	141.00437	5.56258	0.57 ¹	0924.0+0534	1.95 ± 0.42	1.90±0.16	3011.8	64.1
092542.9+595816	141.42871	59.97117	0.7 ³	0925.7+5959	0.708 ± 0.118	1.81±0.11	4518.3	92.2
092837.4+404845	142.156	40.81258	0.55 ³	0928.5+4048	2.06 ± 0.34	2.03±0.14	2746.9	86.2
093037.6+495025	142.65654	49.84044	0.187 ¹	0930.5+4951	0.356 ± 0.067	1.76±0.14	7112.3	77.3
093239.4+104235	143.16404	10.70981	0.361 ¹	0932.7+1041	1.15 ± 0.23	1.93±0.15	3620.8	54.0
093430.2-172121	143.62579	-17.35583	0.25 ¹	0934.5-1720	0.502 ± 0.150	1.89±0.21	5013.1	27.9
093514.8-173658	143.81158	-17.61633	0.29 ⁵	0935.3-1736	1.42 ± 0.19	1.91±0.10	5081.4	168.5
093623.1-211039	144.09633	-21.17769	0.53 ³	0936.3-2111	1.94 ± 0.26	1.86±0.10	3768.4	132.2
093754.7-143350	144.478	-14.56397	0.27 ⁵	0937.9-1434	1.63 ± 0.23	1.92±0.11	3997.8	120.9
094022.4+614826	145.0935	61.80733	0.21 ¹	0940.4+6148	1.48 ± 0.22	1.78±0.10	3677.1	161.5
094223.3+284414	145.59704	28.73731	0.366 ¹	0942.3+2842	0.768 ± 0.160	1.87±0.16	4209.3	52.1
094432.3+573535	146.13467	57.59331	0.717 ²	new	0.681 ± 0.252	2.02±0.27	3000.0	16.8
094502.0-044833	146.25846	-4.80939	0.43 ⁵	new	0.921 ± 0.304	1.91±0.21	3000.0	19.7

Continued on next page

Table 4 – continued from previous page

2BIGB Jname	R.A.(deg)	Dec.(deg)	z	4FGL J	N₀ (10⁻¹⁵)	Γ	E₀ (GeV)	TS
094620.2+010451	146.58425	1.08103	0.577 ¹	0946.2+0104	0.565 ± 0.112	1.87±0.15	6186.1	68.2
094709.5-254100	146.78967	-25.68333	–	0947.1-2541	19.29 ± 1.16	1.89±0.04	2210.8	872.1
094934.0+480826	147.39146	48.14075	0.728 ¹	new	0.041 ± 0.024	1.85±0.61	10000.0	10.2
095127.8+010210	147.86596	1.03619	0.5 ²	new	0.610 ± 0.378	1.69±0.32	3000.0	17.0
095202.3-171443	148.00938	-17.24542	0.45 ⁵	new	0.622 ± 0.301	1.86±0.32	3000.0	13.5
095214.7+393615	148.06133	39.60436	0.58 ⁴	0952.1+3932	0.242 ± 0.061	1.85±0.19	6457.2	41.2
095224.1+750213	148.10058	75.03708	0.181 ¹	0952.2+7503	0.048 ± 0.010	1.58±0.14	17090.0	75.1
095249.6+071330	148.20654	7.22503	0.31 ⁵	0952.8+0712	1.75 ± 0.34	2.01±0.15	3045.7	55.9
095302.7-084018	148.26125	-8.67172	0.37 ³	0953.0-0840	57.48 ± 2.05	1.86±0.02	1946.8	3069.2
095304.3-765802	148.26812	-76.96722	0.25 ⁵	0953.4-7659	0.602 ± 0.093	1.86±0.12	6582.4	104.4
095409.9+491459	148.54108	49.24986	0.41 ²	0954.2+4913	0.398 ± 0.055	1.56±0.09	7683.6	202.1
095419.6-251958	148.58183	-25.33289	0.32 ⁵	0954.2-2520	0.773 ± 0.135	1.92±0.14	5213.0	84.3
095507.1+355100	148.78292	35.85025	0.557 ²	0955.1+3551	0.405 ± 0.104	1.96±0.21	4649.5	34.5
095628.0-095719	149.11754	-9.95531	0.161 ¹	0956.5-0958	0.239 ± 0.077	1.60±0.19	6609.2	29.3
095806.0-031740	149.52496	-3.2945	0.43 ⁴	0958.0-0319	0.079 ± 0.024	1.61±0.19	12405.5	34.7
095813.0-675242	149.55417	-67.8785	0.21 ⁵	0958.1-6753	0.574 ± 0.164	1.87±0.21	4348.8	28.8
095849.8+703959	149.70758	70.6665	0.31 ⁵	0958.8+7039	0.220 ± 0.059	1.79±0.20	5969.7	31.4
095929.9+212321	149.87454	21.38917	0.36 ¹	0959.4+2120	5.55 ± 1.03	1.98±0.13	1967.9	92.5
100234.0+221615	150.64337	22.27083	0.4 ⁴	1002.5+2215	0.979 ± 0.161	1.81±0.12	4796.1	104.1
100326.6+020455	150.86092	2.08214	0.48 ⁴	1003.4+0205	1.13 ± 0.27	1.81±0.15	3334.0	46.0
100342.9-213809	150.92858	-21.63592	0.17 ⁵	1003.6-2137	0.155 ± 0.051	1.53±0.21	8484.6	34.9
100612.2+644011	151.55092	64.66989	0.39 ⁴	1006.5+6440	0.928 ± 0.184	1.85±0.13	3594.5	73.4
100656.5+345445	151.73529	34.91256	0.612 ¹	1007.0+3455	1.39 ± 0.19	1.79±0.10	3949.0	158.2
100811.4+470521	152.04763	47.08933	0.343 ¹	new	0.061 ± 0.021	1.37±0.20	10000.0	25.5
101016.0-311908	152.56658	-31.31897	0.14 ¹	1010.2-3119	2.05 ± 0.17	1.79±0.06	5864.5	499.2
101244.3+422957	153.1845	42.49917	0.365 ¹	1012.7+4228	1.36 ± 0.17	1.63±0.07	4272.1	226.7
101504.1+492600	153.76721	49.43356	0.2 ³	1015.0+4926	623.8 ± 10.0	1.85±0.01	1006.1	27125.8
101616.8+410812	154.07008	41.13681	0.27 ¹	new	0.071 ± 0.026	1.59±0.22	10000.0	27.7
101620.7-424722	154.08613	-42.78961	0.25 ⁵	1016.1-4247	1.05 ± 0.14	1.83±0.09	5560.4	144.1
101706.7+520247	154.27783	52.04644	0.379 ¹	1017.3+5204	0.508 ± 0.125	1.84±0.16	3934.1	37.5
101717.1-154933	154.32462	-15.826	0.53 ⁵	new	0.628 ± 0.308	1.90±0.31	3000.0	11.8
101724.4+253956	154.35158	25.66556	0.417 ¹	new	0.096 ± 0.030	1.40±0.19	10000.0	40.6
102100.4+162554	155.25146	16.43167	0.556 ²	1021.1+1626	0.876 ± 0.239	1.93±0.20	3394.1	31.3
102243.7-011302	155.68221	-1.21728	0.22 ⁴	1022.7-0112	9.24 ± 0.72	1.91±0.06	2712.7	500.1
102339.8+300057	155.91567	30.01608	0.433 ¹	1023.8+3002	0.839 ± 0.164	1.85±0.15	4228.1	71.4
102356.2-433601	155.98404	-43.60042	0.32 ³	1023.8-4335	11.87 ± 0.71	1.77±0.04	2893.2	1005.6
102432.4-454426	156.13487	-45.74081	0.37 ⁵	1024.5-4543	0.986 ± 0.171	1.93±0.13	4659.9	77.1
102523.0+040229	156.34596	4.0415	0.208 ¹	new	0.977 ± 0.317	2.14±0.29	3000.0	16.1
102634.4-854314	156.64317	-85.72061	–	1027.0-8542	6.09 ± 0.36	1.83±0.04	3577.1	893.0
102658.6-174858	156.74404	-17.81633	0.114 ²	1026.9-1749	23.11 ± 1.29	1.89±0.04	2186.9	1012.2
102703.0+060933	156.76417	6.15942	0.449 ¹	1026.9+0608	0.217 ± 97.9	1.60±0.03	8861.5	64.0
102724.9+631752	156.85383	63.29803	0.58 ³	1027.6+6317	3.98 ± 0.35	1.93±0.07	2921.9	399.0
103040.4-203036	157.66833	-20.51008	0.28 ⁵	1030.6-2028	3.43 ± 0.35	1.82±0.07	3621.6	287.0
103118.5+505335	157.82721	50.89331	0.16 ⁴	1031.3+5053	9.10 ± 0.45	1.74±0.03	3123.1	1600.9
103137.9-260716	157.90787	-26.12128	0.25 ⁵	new	0.337 ± 0.123	1.74±0.22	5000.0	22.7
103317.9+422236	158.32479	42.37675	0.211 ¹	1033.5+4221	0.163 ± 0.055	1.61±0.21	5963.4	22.7
103332.2-503528	158.38396	-50.59133	0.24 ⁵	1033.5-5035	6.54 ± 0.52	1.76±0.05	3274.7	471.9
103346.4+370824	158.44333	37.14025	0.448 ¹	1033.7+3708	19.29 ± 2.77	2.05±0.09	1341.4	201.6
103438.5-464403	158.66038	-46.73431	0.33 ⁵	1034.7-4645	1.03 ± 0.32	1.77±0.17	3262.6	31.0
103656.0-195424	159.23313	-19.90669	0.3 ⁵	new	0.441 ± 0.145	2.19±0.29	5000.0	26.9
103744.3+571155	159.43458	57.19881	0.33 ³	1037.7+5711	229.07 ± 5.18	1.90±0.01	1179.4	10701.0
104029.0+094753	160.12075	9.79831	0.304 ¹	new	0.981 ± 0.324	1.99±0.26	3000.0	20.2
104058.4+134150	160.24325	13.69739	0.7 ³	1041.0+1342	0.650 ± 0.126	1.72±0.12	5217.5	76.2
104108.6-120331	160.28575	-12.05861	0.31 ⁵	1041.1-1201	4.75 ± 1.11	2.01±0.16	1859.9	46.6
104149.2+390119	160.45483	39.02211	0.21 ¹	1041.7+3902	1.59 ± 0.29	1.96±0.14	2984.2	69.5
104203.0-412929	160.5125	-41.49164	0.25 ⁵	1042.1-4128	1.55 ± 0.22	1.84±0.10	4003.2	122.1

Continued on next page

Table 4 – continued from previous page

2BIGB Jname	R.A.(deg)	Dec.(deg)	z	4FGL J	$N_0 (10^{-15})$	Γ	$E_0 (\text{GeV})$	TS
104303.8+005420	160.76604	0.90569	0.4 ⁴	1042.9+0054	0.437 ± 0.086	1.73±0.13	6893.4	67.1
104516.3+275133	161.31788	27.85928	0.45 ⁴	new	1.17 ± 0.29	1.96±0.19	3000.0	35.3
104651.5-253545	161.7145	-25.59603	0.25 ¹	1046.8-2534	0.591 ± 0.100	1.78±0.11	6269.3	93.5
104705.9+673758	161.77458	67.63278	0.5 ⁵	1047.2+6740	0.687 ± 0.151	1.88±0.16	3599.3	49.4
104745.8+543741	161.94088	54.62814	0.54 ²	new	0.051 ± 0.021	1.56±0.26	10000.0	16.1
104756.9-373730	161.98725	-37.62522	–	1047.9-3738	0.884 ± 0.156	1.86±0.13	4692.0	75.2
104810.9+855958	162.0455	85.99961	0.23 ⁵	new	1.05 ± 0.29	2.21±0.29	3000.0	20.6
104857.1+500945	162.24004	50.16256	0.403 ¹	1049.7+5011	12.68 ± 1.74	2.47±0.15	1359.3	88.3
104938.8+274213	162.41163	27.70361	0.144 ¹	1049.8+2741	1.17 ± 0.29	1.86±0.17	3002.4	39.9
105125.4+394325	162.85567	39.72381	0.497 ¹	1051.4+3942	0.699 ± 0.108	1.72±0.10	5416.0	123.0
105224.5+081409	163.10221	8.23597	0.223 ¹	1052.3+0818	20.58 ± 6.53	2.45±0.27	944.5	22.5
105344.1+492956	163.43388	49.49892	0.14 ¹	1053.7+4930	5.48 ± 0.47	1.89±0.06	2647.2	396.1
105437.9+202740	163.65779	20.46119	0.225 ¹	new	11.19 ± 4.53	2.45±0.32	1000.0	13.1
105451.5+162607	163.7145	16.43544	0.505 ¹	new	0.550 ± 0.252	1.61±0.21	3000.0	19.2
105534.4-012616	163.89317	-1.43781	0.33 ⁴	1055.5-0125	3.02 ± 0.40	1.79±0.09	3344.3	169.1
105606.1+025213	164.02754	2.87044	0.236 ¹	new	0.096 ± 0.033	1.48±0.22	10000.0	28.1
105707.4+551032	164.281	55.17558	0.7 ³	1057.2+5510	0.539 ± 0.097	1.77±0.12	4933.5	84.8
105750.8-275410	164.4615	-27.90303	0.091 ¹	1057.8-2754	7.57 ± 0.68	1.85±0.06	2622.1	392.4
105837.7+562811	164.65717	56.46978	0.143 ¹	1058.6+5627	244.83 ± 6.33	1.95±0.02	1055.2	8102.3
110021.1+401928	165.08775	40.32444	0.225 ²	1100.3+4020	2.19 ± 0.23	1.87±0.08	3939.8	274.4
110124.7+410847	165.353	41.14647	0.38 ⁴	1101.4+4108	1.17 ± 0.14	1.77±0.09	4698.9	208.4
110253.0-014906	165.72092	-1.81856	0.56 ⁵	1102.8-0148	0.050 ± 0.021	1.42±0.23	11947.3	16.8
110337.6-232931	165.90675	-23.49194	0.186 ¹	1103.6-2329	1.47 ± 0.15	1.67±0.07	5733.0	302.7
110357.3+261118	165.98871	26.18858	0.712 ²	1104.0+2611	2.51 ± 0.53	1.94±0.15	2331.3	62.0
110427.3+381231	166.11383	38.20886	0.03 ¹	1104.4+3812	1577.3 ± 12.0	1.77±0.01	1286.4	144108.0
110748.1+150210	166.95025	15.03628	0.25 ²	1107.8+1501	10.49 ± 0.84	1.96±0.06	2308.8	445.5
110916.2+241120	167.31738	24.18889	0.35 ²	1109.3+2411	5.04 ± 0.58	1.85±0.08	2527.3	228.9
110938.5+373611	167.41046	37.60325	0.398 ¹	1109.6+3735	0.594 ± 0.106	1.76±0.13	6056.8	78.0
111037.1+713356	167.65667	71.56572	–	1110.2+7135	2.23 ± 0.20	1.90±0.07	3505.8	254.3
111130.9+345203	167.87871	34.86764	0.68 ³	new	0.086 ± 0.034	1.88±0.28	10000.0	16.5
111158.1+485701	167.99542	48.95039	0.44 ⁴	1111.8+4858	0.253 ± 0.083	1.84±0.24	4602.6	22.5
111207.9+260803	168.03308	26.13439	0.45 ¹	new	0.335 ± 0.098	2.13±0.23	5000.0	24.7
111224.6+175121	168.1025	17.85603	0.42 ¹	1112.4+1751	4.09 ± 1.40	1.82±0.18	1586.1	53.9
111706.3+201407	169.27608	20.23542	0.138 ¹	1117.0+2013	34.38 ± 1.68	1.93±0.04	1844.1	1499.3
111709.8+585921	169.29063	58.98917	0.081 ¹	new	0.517 ± 0.174	1.65±0.17	3000.0	32.4
111715.2-533813	169.3135	-53.637	–	1117.2-5337	7.30 ± 0.58	1.91±0.05	2982.3	372.8
111717.5+000633	169.32308	0.10931	0.451 ¹	new	0.785 ± 0.150	1.76±0.13	5000.0	74.3
111757.2+535554	169.4885	53.93192	0.44 ³	1118.0+5356	15.91 ± 0.87	1.89±0.04	2116.4	1172.6
111939.6-304720	169.91492	-30.78911	0.412 ¹	1119.6-3047	0.083 ± 0.025	1.57±0.23	11621.0	35.5
112048.1+421212	170.20025	42.2035	0.35 ³	1120.8+4212	7.18 ± 0.31	1.61±0.03	4307.4	2448.7
112318.1-323218	170.82521	-32.53847	0.34 ²	1123.1-3233	0.988 ± 0.228	2.08±0.21	3699.7	36.2
112349.2+722959	170.95487	72.49989	0.38 ⁵	1123.8+7230	0.125 ± 0.029	1.67±0.14	8772.3	50.8
112405.3+204553	171.02229	20.76489	0.54 ³	1124.0+2045	0.890 ± 0.173	1.94±0.16	4331.3	62.2
112453.8+493409	171.22429	49.56939	0.36 ⁴	1124.9+4934	5.41 ± 0.43	1.79±0.05	2767.1	527.1
112503.6+214300	171.26517	21.71667	0.36 ⁴	1124.9+2143	1.50 ± 0.36	1.94±0.18	2820.0	38.3
112508.6-210105	171.28596	-21.01828	0.24 ⁵	1125.1-2101	5.57 ± 0.54	1.93±0.07	2950.9	268.4
112552.0-074220	171.46658	-7.70581	0.279 ¹	1125.9-0742	1.88 ± 0.27	1.92±0.11	3937.1	129.1
112912.5-101349	172.30221	-10.23042	–	1129.2-1014	1.47 ± 0.48	1.92±0.21	2534.5	20.0
113032.1-780105	172.63358	-78.01817	0.23 ⁵	1130.5-7801	1.20 ± 0.12	1.61±0.06	6043.5	329.8
113046.1-313807	172.69225	-31.63542	0.151 ¹	1130.5-3137	0.021 ± 78.5	1.47±0.23	24721.7	27.2
113105.3-094406	172.77196	-9.73511	0.33 ⁵	1131.1-0944	1.89 ± 0.41	1.86±0.15	2948.6	65.6
113209.3-473853	173.03858	-47.64814	0.21 ⁵	1132.2-4736	4.30 ± 0.55	2.01±0.09	2762.0	128.9
113444.7-172901	173.68625	-17.48383	0.571 ¹	1134.8-1729	0.134 ± 0.035	1.56±0.16	10521.5	47.9
113626.4+700927	174.11008	70.15753	0.045 ¹	1136.4+7009	13.85 ± 0.48	1.78±0.02	2679.2	2192.7
113630.0+673704	174.12542	67.61789	0.1342 ¹	1136.4+6736	3.06 ± 0.19	1.72±0.04	3928.9	752.8
113650.0+255052	174.20879	25.84786	0.155 ¹	1136.8+2550	1.28 ± 0.19	1.86±0.11	4148.8	120.4

Continued on next page

Table 4 – continued from previous page

2BIGB Jname	R.A.(deg)	Dec.(deg)	z	4FGL J	N₀ (10⁻¹⁵)	Γ	E₀ (GeV)	TS
113755.6-171042	174.48175	-17.17836	0.61 ¹	1137.9-1708	1.12 ± 0.16	1.67±0.09	4974.5	153.4
113900.8+553035	174.75321	55.50989	0.63 ⁴	new	0.049 ± 0.019	1.53±0.25	10000.0	17.7
114023.5+152809	175.09783	15.46942	0.24 ¹	1140.5+1528	0.208 ± 0.047	1.69±0.15	9341.9	60.5
114118.7+680429	175.32775	68.07489	0.57 ⁵	1141.4+6805	1.28 ± 0.15	1.74±0.08	4209.3	195.0
114141.1-140754	175.42417	-14.13183	0.32 ⁵	1141.5-1408	4.53 ± 0.87	1.87±0.12	2157.0	90.5
114352.7+155821	175.96946	15.97275	0.67 ²	new	0.302 ± 0.113	1.88±0.28	5000.0	18.5
114535.1-034001	176.39633	-3.66708	0.167 ¹	new	1.06 ± 0.31	1.92±0.22	3000.0	26.7
114600.8-063854	176.50354	-6.64858	0.37 ⁵	1146.0-0638	0.951 ± 0.136	1.69±0.09	5578.3	153.5
114930.4+243926	177.37646	24.65744	0.402 ¹	1149.4+2441	4.69 ± 2.21	1.44±0.22	4876.3	37.6
115017.0+101652	177.57088	10.28136	0.284 ¹	new	0.306 ± 0.128	1.76±0.25	5000.0	19.2
115034.8+415440	177.64483	41.91111	0.32 ³	1150.6+4154	50.95 ± 1.95	1.80±0.02	1726.4	3185.8
115124.7+585917	177.85271	58.98819	0.3 ³	1151.5+5859	6.02 ± 0.35	1.90±0.04	3445.5	1007.8
115257.6+241345	178.24017	24.22928	0.175 ¹	new	0.271 ± 0.103	1.96±0.26	5000.0	14.8
115404.6-001009	178.519	-0.16933	0.254 ¹	1154.0-0010	1.84 ± 0.22	1.74±0.08	4465.4	231.0
115514.9-111122	178.81192	-11.18958	0.47 ⁵	1155.2-1111	0.634 ± 0.164	1.89±0.19	4675.2	39.3
115520.5-341719	178.8355	-34.28883	–	1155.5-3418	1.20 ± 0.15	1.84±0.09	5336.6	184.1
115633.2-225004	179.13842	-22.8345	–	1156.6-2248	3.93 ± 0.53	2.05±0.11	2852.7	130.1
115803.7-033337	179.51562	-3.56044	0.37 ⁵	new	0.142 ± 0.093	1.44±0.31	5000.0	9.46
115853.0+081943	179.72167	8.32869	0.29 ¹	1158.9+0818	1.12 ± 0.22	1.89±0.15	3679.1	56.4
115912.6-143154	179.80263	-14.53189	0.48 ⁵	1158.8-1430	0.413 ± 0.096	1.78±0.18	6672.9	56.2
120055.1-143039	180.22963	-14.51103	0.48 ⁵	1200.8-1429	2.29 ± 0.39	2.13±0.14	3248.2	75.7
120317.9-392620	180.82454	-39.43914	0.28 ⁵	1203.4-3925	1.53 ± 0.17	1.79±0.08	5128.8	222.8
120412.1+114555	181.0505	11.76539	0.296 ¹	1204.0+1146	1.89 ± 0.27	1.85±0.10	3887.6	141.4
120416.7-071009	181.06942	-7.16917	0.184 ¹	1204.2-0709	10.83 ± 0.79	1.88±0.05	2647.1	589.9
120543.3+582933	181.43029	58.49267	0.4 ²	new	0.692 ± 0.211	1.87±0.21	3000.0	24.7
120711.5-174605	181.79787	-17.76831	0.7 ³	new	0.336 ± 41.3	1.85±0.01	5000.0	15.8
120804.3+301549	182.01804	30.26386	0.33 ⁴	1208.1+3017	0.305 ± 0.082	1.87±0.20	5648.8	33.5
120837.1+612106	182.15471	61.35178	0.275 ¹	1208.4+6121	0.992 ± 0.164	1.88±0.13	3789.3	97.2
120905.2-462948	182.27163	-46.49678	–	1209.0-4630	2.99 ± 0.83	2.23±0.23	2126.4	22.9
121038.3-252713	182.65971	-25.45383	0.47 ⁵	new	0.644 ± 0.326	1.81±0.28	3000.0	12.2
121134.2+390054	182.89258	39.01497	0.602 ²	1211.6+3901	1.13 ± 0.34	1.78±0.17	2583.1	36.6
121158.6+224233	182.99425	22.70922	0.453 ¹	1212.0+2242	2.08 ± 0.46	1.92±0.16	2521.7	50.3
121300.8+512935	183.25342	51.49325	0.796 ²	1213.0+5129	10.94 ± 1.21	2.08±0.09	1648.8	228.8
121323.1-261807	183.34637	-26.30214	0.278 ¹	1213.3-2618	1.23 ± 0.17	1.75±0.10	4982.2	158.4
121511.0+073204	183.79575	7.53464	0.137 ¹	1215.1+0731	0.958 ± 0.141	1.70±0.10	5267.9	145.9
121603.3-024304	184.01362	-2.71792	0.359 ²	1216.1-0242	1.093 ± 0.24	2.07±0.18	3713.9	42.0
121606.2+092909	184.02588	9.486	0.094 ¹	1216.1+0930	5.54 ± 0.79	1.99±0.10	2183.7	123.4
121618.4+205957	184.07646	20.99917	0.607 ¹	new	0.043 ± 0.024	1.43±0.33	10000.0	11.3
121945.0+044622	184.93738	4.77289	0.28 ⁴	1219.7+0444	2.37 ± 0.39	2.05±0.14	3144.9	86.2
121945.7-031423	184.94046	-3.23994	0.299 ¹	1219.7-0313	5.88 ± 0.65	1.86±0.08	2690.5	249.9
122014.5-245948	185.06054	-24.99683	0.48 ⁵	1220.1-2458	0.714 ± 0.136	2.07±0.16	5467.7	73.7
122019.1-371414	185.08254	-37.23728	0.28 ⁵	1220.2-3713	4.01 ± 0.51	1.98±0.10	2792.4	151.6
122107.8+474228	185.28242	47.70792	0.21 ¹	new	0.099 ± 0.062	1.42±0.30	5000.0	12.5
122122.0+301037	185.34146	30.177	0.18 ¹	1221.3+3010	19.234 ± 0.563	1.70±0.02	4441.7	5315.1
122211.0+354058	185.54754	35.68289	0.57 ³	new	0.713 ± 0.256	1.89±0.26	3000.0	20.5
122307.2+110038	185.78017	11.01058	0.5 ⁴	1223.0+1100	2.38 ± 0.42	1.86±0.12	2863.2	80.0
122327.5+082030	185.86458	8.34181	–	1223.5+0818	1.46 ± 0.27	1.90±0.13	3446.2	68.9
122337.0-303250	185.90421	-30.54725	0.26 ⁵	1223.6-3032	0.458 ± 0.094	1.70±0.14	6380.1	72.5
122353.0+465048	185.97092	46.84689	0.25 ¹	new	0.946 ± 0.236	2.23±0.23	3000.0	28.0
122358.1+795328	185.99192	79.89117	0.29 ⁵	1223.9+7954	0.390 ± 0.073	1.88±0.15	5732.7	71.3
122401.0+223939	186.00421	22.66092	0.482 ¹	1224.1+2239	0.059 ± 0.024	1.85±0.29	13133.1	26.7
122424.2+243623	186.10083	24.60656	0.218 ¹	1224.4+2436	20.52 ± 1.02	1.97±0.04	2355.4	1300.2
122525.3-155317	186.35538	-15.88806	0.34 ⁵	new	0.059 ± 0.026	1.48±0.25	10000.0	13.9
122536.8-344721	186.40342	-34.78942	0.31 ⁵	1225.3-3446	0.629 ± 0.147	1.97±0.18	4569.9	36.3
122644.2+063853	186.68425	6.64808	0.583 ¹	1226.7+0637	0.525 ± 0.097	1.71±0.12	6054.6	94.7
123014.1+251807	187.55867	25.30197	0.135 ²	1230.2+2517	665.4 ± 17.7	2.14±0.02	816.4	7663.2

Continued on next page

Table 4 – continued from previous page

2BIGB Jname	R.A.(deg)	Dec.(deg)	z	4FGL J	$N_0 (10^{-15})$	Γ	$E_0 (\text{GeV})$	TS
123123.1+142124	187.84962	14.35678	0.256 ¹	1231.5+1421	1.60 ± 0.23	1.81 ± 0.10	4195.7	153.3
123131.4+641418	187.88083	64.23842	0.163 ¹	1231.6+6415	2.49 ± 0.27	1.84 ± 0.08	3165.6	254.5
123143.6+284749	187.9315	28.79714	0.236 ¹	1231.7+2847	68.24 ± 2.59	1.98 ± 0.03	1580.7	2603.0
123205.0-105600	188.02071	-10.9335	0.19 ⁵	new	0.204 ± 0.171	1.01 ± 0.35	10000.0	10.1
123235.9-372056	188.14979	-37.34914	0.25 ⁵	1232.5-3720	3.79 ± 0.42	1.87 ± 0.08	3216.8	231.8
123305.1+170133	188.27138	17.02592	0.24 ⁴	1233.1+1703	1.09 ± 0.22	1.90 ± 0.14	3736.1	47.7
123402.4+281502	188.50987	28.25056	0.424 ¹	new	0.664 ± 0.294	1.82 ± 0.28	3000.0	13.8
123444.2-043622	188.68425	-4.60622	–	1234.7-0434	2.18 ± 0.39	2.25 ± 0.18	3099.3	55.0
123623.0+390000	189.09588	39.00025	0.389 ¹	1236.3+3858	2.31 ± 0.33	1.93 ± 0.12	2894.0	127.6
123705.6+302005	189.27338	30.33475	0.33 ²	new	0.059 ± 0.023	1.38 ± 0.21	10000.0	23.8
123739.1+625842	189.41283	62.97858	0.297 ¹	1237.8+6256	0.516 ± 0.121	1.73 ± 0.15	4103.1	50.6
123922.6+413251	189.84433	41.54756	0.16 ²	new	0.544 ± 0.245	1.70 ± 0.25	3000.0	24.9
124021.0-714857	190.08837	-71.81603	0.21 ⁵	1240.4-7148	3.61 ± 0.28	1.86 ± 0.06	4432.1	454.6
124141.0+344030	190.4225	34.67522	0.54 ¹	1241.5+3439	0.953 ± 0.203	1.84 ± 0.15	3655.9	55.4
124148.3+063601	190.45113	6.60033	0.51 ³	1241.9+0636	0.437 ± 0.130	1.69 ± 0.18	4616.7	30.2
124149.4-145558	190.45583	-14.93289	0.44 ³	1241.8-1456	2.27 ± 0.28	1.83 ± 0.08	3897.8	166.7
124232.3+763417	190.63475	76.57158	0.48 ⁵	new	0.252 ± 0.066	1.78 ± 0.17	5000.0	29.3
124312.7+362744	190.80308	36.46222	0.31 ³	1243.2+3627	66.73 ± 2.34	1.76 ± 0.02	1636.7	4245.3
124700.7+442318	191.75308	44.38856	0.6 ²	1247.0+4421	1.54 ± 0.19	1.72 ± 0.08	3837.8	198.1
124919.3-280834	192.33046	-28.14289	0.15 ⁵	1249.2-2809	10.45 ± 1.21	2.00 ± 0.08	1987.2	215.8
124946.7+370747	192.44475	37.12994	0.286 ²	1249.8+3707	2.13 ± 0.22	1.80 ± 0.07	3903.4	264.6
125015.5+315559	192.56471	31.93317	0.6 ³	new	0.195 ± 0.078	1.51 ± 0.20	5000.0	19.1
125117.9+103907	192.8245	10.65197	0.245 ¹	1251.2+1039	4.331 ± 0.79	2.13 ± 0.15	2113.5	58.1
125341.3-393159	193.42192	-39.53314	0.179 ¹	1253.5-3934	0.142 ± 0.042	1.57 ± 0.17	8640.2	32.4
125347.0+032630	193.44583	3.44178	0.066 ¹	1253.8+0327	15.55 ± 1.14	1.96 ± 0.06	2168.1	524.8
125359.3+624257	193.49725	62.716	0.3 ⁴	1253.8+6242	7.24 ± 0.52	2.01 ± 0.06	2443.7	517.5
125433.3+221103	193.63863	22.18439	0.42 ³	1254.5+2210	18.89 ± 1.69	2.04 ± 0.07	1650.2	372.1
125616.0-114637	194.06646	-11.77703	0.058 ¹	1256.2-1146	13.88 ± 0.99	1.97 ± 0.05	2342.3	587.2
125639.4+060907	194.16396	6.15217	0.423 ¹	new	0.255 ± 0.106	1.59 ± 0.22	5000.0	21.1
125708.4+264925	194.28487	26.82381	0.375 ¹	new	10.56 ± 5.34	2.45 ± 0.54	1000.0	13.1
125731.9+241240	194.38304	24.21119	0.14 ¹	1257.6+2413	0.158 ± 0.075	2.05 ± 0.41	7301.8	24.8
125820.8+612045	194.58671	61.34597	0.224 ¹	1258.3+6121	1.49 ± 0.23	2.07 ± 0.12	3090.3	86.2
125821.5+212351	194.58942	21.39753	0.5 ⁵	new	0.375 ± 0.267	1.70 ± 0.36	3000.0	9.62
125822.1+062827	194.59504	6.47422	0.542 ¹	new	0.317 ± 0.109	1.91 ± 0.24	5000.0	17.7
125848.0-044745	194.70017	-4.79583	0.586 ¹	1258.7-0452	0.510 ± 0.129	1.74 ± 0.16	5768.0	32.5
125949.1-374858	194.9575	-37.81614	0.23 ⁵	1259.8-3749	12.04 ± 1.07	2.04 ± 0.07	2147.6	292.9
130008.5+175537	195.03546	17.92711	0.55 ⁴	1300.0+1753	61.07 ± 15.8	2.64 ± 0.24	712.0	37.0
130145.7+405624	195.44021	40.94017	0.649 ³	1301.6+4056	1.76 ± 0.32	1.97 ± 0.14	2759.3	65.3
130421.0-435310	196.0875	-43.88617	–	1304.3-4353	58.54 ± 2.16	1.88 ± 0.02	1884.1	2549.8
130531.3+385522	196.38029	38.92281	0.376 ¹	new	8.705 ± 3.35	2.11 ± 0.22	1000.0	23.2
130631.0+192244	196.62912	19.37889	0.314 ¹	new	0.715 ± 0.282	2.07 ± 0.38	3000.0	12.7
130713.4-034431	196.80575	-3.74194	0.27 ⁵	new	0.847 ± 0.322	2.00 ± 0.26	3000.0	13.2
130738.0-425938	196.90825	-42.99414	–	1307.6-4259	23.82 ± 1.06	1.90 ± 0.03	2525.4	1588.5
131012.2-115749	197.55075	-11.96372	0.14 ¹	1310.2-1158	6.51 ± 0.72	1.97 ± 0.08	2469.1	221.3
131106.5+003510	197.77696	0.58611	0.418 ²	1311.0+0034	2.19 ± 0.34	2.06 ± 0.14	3802.3	119.0
131146.0+395317	197.94183	39.88819	0.159 ²	1311.8+3954	0.363 ± 0.088	2.00 ± 0.19	5333.0	43.1
131234.7-185901	198.14458	-18.98372	0.48 ⁴	1312.6-1900	1.27 ± 0.37	1.80 ± 0.18	3149.4	41.8
131248.8-235047	198.20321	-23.84647	–	1312.8-2350	2.71 ± 0.24	1.86 ± 0.06	4741.0	351.0
131330.1+020105	198.37558	2.01828	0.356 ¹	new	22.82 ± 5.90	2.85 ± 0.36	1000.0	21.4
131440.6-090148	198.66929	-9.03006	0.43 ⁵	new	0.496 ± 0.129	1.85 ± 0.18	5000.0	34.6
131503.4-423649	198.76413	-42.61381	0.105 ¹	1315.0-4236	0.711 ± 0.073	1.62 ± 0.07	7598.8	204.6
131532.6+113331	198.88592	11.55883	0.36 ⁴	1315.5+1135	0.866 ± 0.133	1.78 ± 0.10	5488.2	116.9
131553.0-073302	198.97071	-7.55056	–	1315.9-0732	6.97 ± 0.64	1.99 ± 0.07	2700.8	295.8
131639.8+205514	199.16604	20.92081	0.255 ¹	new	0.265 ± 0.095	2.06 ± 0.29	5000.0	14.6
131654.6+301454	199.22737	30.24839	0.55 ⁴	1316.5+3013	0.849 ± 0.260	1.90 ± 0.22	2910.3	22.7
131921.3+775822	199.83858	77.97283	0.21 ⁵	1319.8+7759	6.41 ± 0.59	2.00 ± 0.07	2184.6	301.3

Continued on next page

Table 4 – continued from previous page

2BIGB Jname	R.A.(deg)	Dec.(deg)	z	4FGL J	N₀ (10⁻¹⁵)	Γ	E₀ (GeV)	TS
131931.7+140533	199.88225	14.09256	0.573 ¹	1319.5+1404	1.36 ± 0.25	2.00±0.14	3533.4	55.4
132301.0+043951	200.75421	4.66431	0.224 ¹	1322.9+0437	0.892 ± 0.204	1.92±0.16	3733.9	43.8
132358.4+140559	200.99321	14.09986	0.32 ⁴	1323.9+1405	4.83 ± 0.45	1.82±0.06	3150.8	340.7
132531.8+662103	201.38242	66.35083	0.21 ¹	new	0.634 ± 0.210	2.04±0.27	3000.0	19.9
132541.9-022810	201.42454	-2.46944	0.8 ²	1325.6-0227	1.53 ± 0.35	1.96±0.16	3003.4	43.2
132615.0+293330	201.56242	29.55856	0.431 ¹	new	11.98 ± 4.96	2.09±0.23	1000.0	28.7
132617.1+122958	201.57375	12.49967	0.204 ¹	1326.1+1232	0.488 ± 0.143	1.91±0.20	4460.5	22.1
132833.5+114520	202.13979	11.75572	0.49 ²	new	0.387 ± 0.119	1.64±0.18	5000.0	35.0
132840.6-472749	202.16921	-47.46367	–	1328.5-4727	2.55 ± 0.25	1.92±0.07	5151.8	327.5
133021.5+444120	202.58971	44.68897	0.31 ⁴	1330.3+4441	9.54 ± 1.12	2.08±0.09	1693.9	181.8
133025.1+700138	202.60754	70.02742	0.23 ⁵	1330.2+7002	4.76 ± 0.43	1.94±0.07	2484.1	312.9
133102.9+565541	202.76213	56.92822	0.27 ¹	1331.0+5653	0.491 ± 0.098	1.74±0.14	4875.0	76.3
133326.0+623541	203.35821	62.59494	0.48 ⁴	new	0.046 ± 0.021	1.40±0.27	10000.0	23.3
133529.8-295038	203.874	-29.84414	0.51 ²	1335.3-2949	4.74 ± 0.64	2.08±0.11	2471.2	119.9
133612.1+231958	204.0505	23.33303	0.267 ¹	1336.2+2320	1.64 ± 0.31	2.00±0.16	2983.2	57.4
133806.4-093114	204.52646	-9.52072	–	new	0.543 ± 0.249	1.68±0.22	3000.0	16.6
134029.8+441004	205.12421	44.16778	0.54 ¹	1340.5+4409	0.250 ± 0.049	1.71±0.14	8069.2	83.2
134042.0-041006	205.17508	-4.16856	0.25 ⁵	1340.8-0409	5.82 ± 0.78	2.05±0.11	2278.0	111.2
134105.0+395945	205.27125	39.99597	0.172 ¹	1341.2+3958	2.24 ± 0.34	1.80±0.10	2946.9	148.5
134240.3+093911	205.668	9.65319	0.43 ⁴	1342.6+0944	6.43 ± 0.91	2.18±0.13	2040.6	95.3
134706.9-295842	206.77867	-29.97844	–	1347.1-2959	5.22 ± 0.54	1.94±0.08	2845.5	236.8
134853.0+075647	207.22254	7.94658	0.25 ¹	new	0.540 ± 0.124	2.04±0.18	5000.0	42.2
135117.5-153016	207.82271	-15.50444	0.25 ⁵	1351.4-1529	2.86 ± 0.45	2.07±0.13	2984.9	80.0
135120.9+111453	207.83688	11.24808	0.51 ³	1351.3+1115	9.00 ± 0.62	1.84±0.05	2849.3	661.5
135328.0+560056	208.36687	56.01581	0.404 ¹	1353.4+5600	0.291 ± 0.068	1.86±0.18	5839.9	51.8
135340.2-663957	208.41758	-66.666	–	1353.6-6640	5.71 ± 0.36	1.90±0.05	4293.8	631.3
135345.2-393710	208.43821	-39.61964	0.37 ⁵	1353.7-3936	0.052 ± 0.020	1.51±0.23	12585.1	18.0
140022.1-400823	210.092	-40.13989	0.27 ⁵	1400.2-4010	0.998 ± 0.254	1.86±0.17	3601.6	37.5
140027.1-293936	210.11288	-29.66011	0.48 ⁵	new	0.787 ± 0.308	2.20±0.31	3000.0	10.3
140121.1+520928	210.33808	52.15803	0.482 ¹	new	0.323 ± 0.171	1.62±0.26	3000.0	17.8
140350.3+243304	210.95954	24.55133	0.34 ¹	new	0.068 ± 0.027	1.51±0.23	10000.0	20.3
140449.6+655431	211.20671	65.90875	0.363 ¹	1404.8+6554	4.60 ± 0.35	1.90±0.06	2907.2	513.1
140450.9+040202	211.21208	4.03394	0.37 ³	1404.8+0402	11.29 ± 1.10	1.94±0.07	2069.7	312.9
140519.6+305351	211.33179	30.89767	0.34 ¹	new	0.262 ± 0.086	1.98±0.28	5000.0	18.4
140609.6-250809	211.54	-25.13589	–	1406.1-2508	7.96 ± 0.97	2.02±0.09	2128.9	164.9
140630.0-393509	211.62508	-39.58592	0.37 ⁴	1406.6-3934	0.092 ± 0.02	1.48±0.15	13123.0	46.1
140635.8-005548	211.64933	-0.93022	0.255 ¹	new	1.11 ± 0.33	2.49±0.28	3000.0	19.4
140642.7+530833	211.67808	53.14275	0.458 ¹	new	5.36 ± 3.22	2.13±0.33	1000.0	11.7
140659.2+164207	211.74662	16.70217	0.54 ³	1406.9+1643	0.983 ± 0.153	1.80±0.11	4800.3	106.2
140923.1+593940	212.34792	59.66125	0.496 ¹	new	0.502 ± 0.187	2.26±0.32	3000.0	10.1
141003.9+051557	212.51633	5.26606	0.544 ¹	new	0.056 ± 0.026	1.37±0.26	10000.0	19.1
141029.6+282055	212.62317	28.34881	0.521 ¹	1410.4+2820	6.48 ± 0.95	2.05±0.12	1838.6	106.2
141030.8+610012	212.62846	61.00353	0.384 ¹	new	0.439 ± 0.181	1.60±0.22	3000.0	24.0
141046.0+740511	212.69167	74.08644	–	1410.7+7405	3.55 ± 0.30	1.82±0.06	3338.3	457.9
141133.0-072253	212.88879	-7.38144	0.32 ⁵	1411.5-0723	1.12 ± 0.22	1.88±0.14	3942.8	56.8
141140.6+340424	212.919	34.0735	0.421 ¹	new	0.495 ± 0.221	1.97±0.32	3000.0	11.3
141208.2+383521	213.03429	38.58922	0.45 ⁴	1412.0+3836	0.620 ± 0.125	1.82±0.15	4436.7	59.5
141612.2-241813	214.05071	-24.30372	0.136 ¹	1416.1-2417	1.26 ± 0.21	1.85±0.11	4273.2	88.0
141756.7+254325	214.48612	25.72386	0.24 ¹	1417.9+2543	0.310 ± 0.045	1.41±0.09	10403.	209.9
141826.3-023334	214.60971	-2.55944	0.356 ³	1418.4-0233	69.28 ± 2.39	1.78±0.02	1835.9	3765.2
141828.1+354249	214.61917	35.71367	0.47 ⁵	1418.4+3543	369.00 ± 14.0	2.17±0.03	792.2	3420.6
141900.0+773229	214.75129	77.54147	0.27 ³	1418.9+7731	3.09 ± 0.28	1.81±0.06	3143.0	356.3
141927.5+044513	214.86454	4.75381	0.7 ³	1419.3+0444	0.783 ± 0.162	1.74±0.13	4501.1	65.3
142238.9+580155	215.66196	58.03211	0.638 ¹	1422.6+5801	0.882 ± 0.118	1.75±0.09	4741.7	165.4
142412.4-175008	216.05146	-17.83569	0.082 ¹	1424.1-1750	1.56 ± 0.27	1.94±0.13	3799.5	68.8
142421.2+370552	216.08833	37.09803	0.29 ¹	new	0.045 ± 0.023	1.37±0.28	10000.0	17.2

Continued on next page

Table 4 – continued from previous page

2BIGB Jname	R.A.(deg)	Dec.(deg)	z	4FGL J	$N_0 (10^{-15})$	Γ	$E_0 (\text{GeV})$	TS
142422.9+343356	216.09546	34.56575	0.576 ¹	new	0.267 ± 0.085	1.64±0.19	5000.0	30.0
142526.2-011825	216.35908	-1.30717	0.4 ⁴	1425.4-0119	0.327 ± 0.081	1.75±0.15	6225.8	37.2
142710.5+054130	216.79383	5.69181	0.36 ⁴	new	0.857 ± 0.298	1.85±0.22	3000.0	16.9
142725.9-182303	216.85804	-18.38436	0.36 ⁵	1427.4-1823	2.93 ± 0.41	1.92±0.10	3204.2	126.9
142745.9+390832	216.94125	39.14225	0.165 ¹	new	0.374 ± 0.182	1.84±0.31	3000.0	10.2
142829.9+743002	217.12454	74.50061	0.31 ⁵	1428.8+7429	0.104 ± 0.027	1.95±0.19	9121.8	39.5
142832.6+424021	217.13592	42.6725	0.129 ¹	1428.5+4240	2.57 ± 0.17	1.63±0.04	5015.0	898.4
142904.1+120410	217.26917	12.0695	0.7 ³	new	0.876 ± 0.298	2.34±0.32	3000.0	13.8
143211.6+764355	218.04842	76.73219	0.53 ⁵	1432.8+7648	5.88 ± 1.34	1.98±0.14	1435.9	64.1
143342.8-730438	218.42817	-73.07725	0.23 ⁵	new	0.932 ± 0.294	1.92±0.21	3000.0	24.4
143441.5+664026	218.67275	66.67403	0.35 ⁵	1434.8+6640	0.246 ± 0.050	1.59±0.13	6578.8	84.0
143657.8+563925	219.24067	56.65708	0.381 ²	1436.9+5638	6.77 ± 0.46	1.87±0.05	2727.4	686.0
143825.6+120418	219.60658	12.07189	0.848 ¹	new	1.10 ± 0.32	2.03±0.23	3000.0	25.1
143917.5+393242	219.82283	39.54522	0.344 ¹	1439.3+3932	10.18 ± 0.72	2.01±0.06	2276.0	536.9
143950.9-395518	219.96192	-39.92189	–	1439.9-3953	2.98 ± 0.46	2.02±0.13	3077.9	93.9
143959.5-234141	219.99775	-23.69472	0.25 ⁵	1440.0-2343	4.27 ± 0.52	1.97±0.10	2910.1	152.2
144037.8-384655	220.15763	-38.78194	0.27 ⁴	1440.6-3846	1.71 ± 0.15	1.68±0.06	6238.7	443.6
144052.9+061016	220.22054	6.17114	0.396 ²	1440.9+0609	7.66 ± 0.73	2.09±0.08	2758.3	338.7
144128.0-193552	220.3665	-19.59789	–	1441.4-1934	0.860 ± 0.147	1.75±0.11	5129.2	87.1
144236.0-462301	220.65167	-46.38383	0.103 ¹	1442.6-4623	4.82 ± 0.57	1.96±0.08	2926.1	161.0
144248.2+120040	220.701	12.01119	0.16 ¹	1442.7+1200	3.37 ± 0.31	1.78±0.06	3856.1	370.6
144334.0+251558	220.89337	25.26614	0.529 ¹	1443.6+2515	0.738 ± 0.144	1.62±0.11	13738.0	15.3
144357.2-390840	220.98833	-39.14444	0.065 ¹	1443.9-3908	82.146 ± 2.28	1.84±0.02	2013.7	5407.4
144506.2-032612	221.276	-3.43681	0.31 ³	1445.0-0326	3.83 ± 0.34	1.73±0.06	4007.4	381.0
144644.8-182925	221.68679	-18.49031	–	1446.8-1830	0.697 ± 0.185	1.94±0.20	4395.1	25.6
144656.8-265658	221.73683	-26.9495	0.32 ⁵	1447.0-2657	0.532 ± 0.117	1.93±0.15	5374.9	45.8
144800.6+360831	222.00246	36.142	0.28 ³	1448.0+3608	32.89 ± 1.34	1.83±0.03	2009.7	2543.6
144941.9-091000	222.42454	-9.16678	0.21 ⁵	1449.7-0910	1.00 ± 0.29	1.73±0.16	3293.4	30.4
145127.7+635419	222.8655	63.90536	0.65 ¹	1451.4+6355	1.14 ± 0.12	1.78±0.07	4866.3	286.3
145224.5-414951	223.10225	-41.83083	0.26 ⁵	1452.0-4148	0.283 ± 0.072	1.98±0.19	7360.0	32.0
145427.1+512433	223.613	51.40936	0.39 ³	1454.4+5124	162.89 ± 3.84	2.08±0.02	1446.2	8064.1
145543.7-760052	223.93204	-76.0145	–	1455.8-7601	0.860 ± 0.138	1.97±0.12	4910.8	85.2
145603.6+504826	224.01508	50.80725	0.479 ²	1456.0+5051	0.517 ± 0.141	1.81±0.20	4459.5	42.8
145741.8-464210	224.42408	-46.70281	0.16 ⁵	1457.8-4642	0.252 ± 0.063	1.75±0.16	7965.2	33.1
145820.8+412101	224.58658	41.35053	0.17 ¹	new	0.689 ± 0.219	2.00±0.21	3000.0	15.6
150316.6+165117	225.819	16.85489	0.39 ⁴	1503.3+1651	0.713 ± 0.174	2.04±0.20	4163.6	34.6
150340.7-154114	225.91946	-15.68722	0.38 ³	1503.7-1540	6.03 ± 0.42	1.81±0.05	3867.5	599.9
150425.6-004742	226.10687	-0.795	0.35 ⁵	new	0.819 ± 0.352	1.92±0.25	3000.0	9.48
150525.0-824231	226.35587	-82.70864	0.39 ⁵	1505.5-8241	0.809 ± 0.106	1.77±0.08	4326.9	78.2
150637.1-054004	226.65463	-5.66797	0.518 ¹	1506.4-0540	0.081 ± 0.023	1.66±0.18	14091.6	30.5
150644.5+081400	226.68525	8.23353	0.376 ²	1506.6+0813	8.61 ± 0.60	1.74±0.04	2992.1	769.3
150716.4+172103	226.81842	17.35092	0.565 ¹	1507.2+1721	1.92 ± 0.24	1.89±0.09	3967.2	158.8
150842.7+270909	227.17787	27.1525	0.27 ¹	1508.8+2708	2.11 ± 0.36	1.91±0.13	3018.4	88.9
150947.9+555617	227.44979	55.93814	0.2 ⁴	1509.7+5556	2.21 ± 0.21	1.88±0.07	3682.1	303.2
151041.1+333504	227.67133	33.58464	0.114 ¹	new	0.406 ± 0.211	1.30±0.57	10000.0	13.6
151148.6-051346	227.95237	-5.22967	–	1511.8-0513	4.64 ± 0.41	1.86±0.06	3969.6	401.7
151212.7-225508	228.05312	-22.919	0.315 ¹	1512.1-2255	4.82 ± 0.51	1.94±0.08	3174.6	208.1
151324.2-075451	228.35075	-7.91431	0.04 ¹	new	0.452 ± 0.162	1.75±0.22	5000.0	23.8
151433.7+190319	228.64062	19.05544	0.36 ⁴	new	19.80 ± 6.034	2.76±0.34	1000.0	20.7
151444.0-772254	228.68342	-77.38172	–	1514.4-7719	0.052 ± 0.017	1.69±0.20	12837.4	20.7
151556.2+242620	228.98404	24.43892	0.228 ¹	new	0.452 ± 0.218	1.47±0.20	3000.0	26.1
151618.7-152344	229.078	-15.39561	0.33 ⁵	new	0.463 ± 0.146	1.84±0.21	5000.0	23.0
151641.6+291810	229.17329	29.30278	0.13 ¹	1516.8+2918	29.69 ± 5.91	2.58±0.20	959.3	54.6
151747.6+652523	229.44829	65.42314	0.702 ¹	1517.7+6525	8.99 ± 0.45	1.81±0.03	2941.8	1363.1
151803.6-273131	229.51496	-27.52531	0.14 ⁵	1518.0-2731	30.33 ± 1.39	2.04±0.04	2334.8	1272.1
151826.7+075222	229.61113	7.87292	0.41 ¹	1518.4+0750	0.139 ± 0.042	1.71±0.21	8623.9	25.0

Continued on next page

Table 4 – continued from previous page

2BIGB Jname	R.A.(deg)	Dec.(deg)	z	4FGL J	N₀ (10⁻¹⁵)	Γ	E₀ (GeV)	TS
151838.9+404500	229.66204	40.75006	0.065 ¹	1518.6+4044	2.13 ± 0.28	1.86±0.09	3188.4	165.5
151845.7+061356	229.6905	6.23225	0.102 ¹	1518.6+0614	0.355 ± 0.114	1.74±0.24	5381.4	29.9
152048.9-034851	230.20371	-3.81433	–	1520.8-0348	8.59 ± 0.58	1.81±0.04	3290.7	659.3
152213.9-074818	230.55788	-7.80517	0.4 ⁵	new	0.862 ± 0.353	1.96±0.24	3000.0	10.5
152603.2-083146	231.51321	-8.52958	0.35 ⁵	1526.1-0831	2.31 ± 0.30	1.97±0.10	3788.3	125.4
152646.7-153026	231.6945	-15.50731	0.21 ⁴	1526.7-1529	1.49 ± 0.26	2.02±0.14	3963.2	62.3
152810.8-673056	232.04512	-67.51564	–	1528.4-6729	1.14 ± 0.04	1.97±0.03	4469.1	79.5
152835.8+200420	232.149	20.07236	0.52 ⁵	1528.4+2004	0.632 ± 0.158	2.09±0.20	4458.8	32.4
152913.6+381217	232.3065	38.20486	0.27 ⁴	1529.2+3812	1.21 ± 0.24	2.08±0.17	3212.7	48.3
153202.2+301628	233.00929	30.27469	0.065 ¹	1532.0+3016	4.81 ± 0.44	1.90±0.07	2951.9	334.9
153311.3+185429	233.29688	18.90808	0.305 ¹	1533.2+1855	1.22 ± 0.16	1.75±0.10	4963.3	166.8
153324.3+341640	233.35113	34.27789	0.41 ³	1533.2+3416	4.44 ± 0.42	1.86±0.07	2816.2	321.5
153447.0+371554	233.69667	37.26519	0.143 ¹	1534.8+3716	2.28 ± 0.30	2.05±0.12	3305.7	147.5
153500.8+532037	233.75333	53.34369	0.59 ³	1535.0+5320	0.871 ± 0.124	1.70±0.09	4614.7	139.4
153529.7-313346	233.87371	-31.56286	0.27 ⁵	1535.3-3135	0.284 ± 0.091	1.74±0.21	6143.6	24.9
153646.8+013800	234.19483	1.63336	0.311 ¹	new	1.37 ± 0.42	2.39±0.31	3000.0	17.0
153941.0-112835	234.92167	-11.47644	0.22 ⁵	1539.7-1127	1.92 ± 0.25	1.81±0.09	4629.9	155.4
154015.1+815505	235.06625	81.91822	–	1540.1+8155	3.66 ± 0.22	1.69±0.04	4052.7	980.5
154150.1+141437	235.45871	14.24378	0.223 ¹	1541.7+1413	1.08 ± 0.20	1.92±0.14	4186.7	68.0
154203.1-291509	235.51287	-29.25256	0.49 ³	1541.9-2915	3.11 ± 0.34	1.87±0.08	3765.4	213.6
154433.2+322148	236.13829	32.3635	0.32 ⁴	new	0.203 ± 0.157	2.48±0.43	5000.0	10.1
154439.4-112804	236.16404	-11.46803	–	1544.5-1126	546.30 ± 43.5	2.76±0.08	631.73	394.8
154458.9-664146	236.24533	-66.69636	0.23 ⁵	1545.0-6642	0.642 ± 0.082	1.79±0.09	7448.8	174.8
154546.6-233928	236.44408	-23.65789	0.121 ¹	1545.8-2336	0.350 ± 0.078	1.78±0.16	7783.1	50.5
154604.3+081913	236.51775	8.32042	0.35 ³	1546.0+0819	6.33 ± 0.55	1.82±0.06	2910.6	394.0
154625.0-285723	236.60417	-28.95661	0.4 ⁴	new	0.434 ± 0.135	2.01±0.22	5000.0	18.7
154712.1-280221	236.80054	-28.03931	0.28 ⁴	1547.3-2802	2.16 ± 0.37	1.82±0.12	3564.1	93.8
154849.8-225102	237.20733	-22.85069	0.192 ¹	1548.8-2250	5.26 ± 0.36	1.75±0.04	4446.4	659.2
154902.0+482158	237.25837	48.36611	0.63 ⁴	new	0.077 ± 0.022	1.75±0.20	10000.0	30.7
154918.7+423500	237.32779	42.5835	0.49 ⁴	1549.3+4234	2.65 ± 0.62	2.06±0.18	2020.4	42.4
154946.0-304501	237.44292	-30.75031	–	1549.8-3044	0.877 ± 0.146	1.87±0.12	5330.6	89.4
154952.0-065907	237.46683	-6.9855	0.29 ⁵	1549.8-0659	11.39 ± 0.80	1.90±0.05	2844.9	573.0
155053.3-082246	237.722	-8.37967	0.27 ⁵	1550.8-0822	0.648 ± 0.120	1.85±0.14	6050.7	68.7
155333.6-311830	238.38983	-31.30858	0.21 ³	1553.5-3118	24.78 ± 1.34	1.98±0.04	2235.7	928.1
155432.6-121325	238.63575	-12.22364	0.33 ⁵	1554.4-1215	1.02 ± 0.24	1.68±0.13	4008.2	38.8
155543.0+111124	238.92937	11.19011	0.36 ²	1555.7+1111	338.94 ± 4.35	1.67±0.01	1846.7	36422.2
160005.4-252439	240.02233	-25.41103	0.26 ⁵	1559.8-2525	5.87 ± 1.04	2.42±0.19	2108.1	45.9
160218.1+305109	240.57533	30.85264	0.47 ³	1602.2+3051	2.96 ± 0.51	2.27±0.16	2349.3	62.0
160339.5+500955	240.91458	50.16536	0.4 ⁴	1603.8+5009	1.30 ± 0.18	1.89±0.10	3826.4	116.0
160519.1+542059	241.32942	54.34997	0.212 ¹	1605.5+5423	1.28 ± 0.22	1.83±0.11	3172.1	87.5
160618.0+134532	241.57667	13.75908	0.29 ¹	new	1.24 ± 0.42	1.75±0.20	3000.0	33.5
160620.9+563017	241.58696	56.50486	0.45 ¹	1606.3+5629	0.298 ± 0.054	1.78±0.13	7033.1	91.1
160740.7+254113	241.91938	25.68708	0.534 ¹	new	0.310 ± 0.105	1.99±0.27	5000.0	17.5
161004.1+671026	242.51688	67.17397	0.27 ⁴	new	0.436 ± 0.254	1.95±0.46	3000.0	11.4
161046.4-664901	242.6935	-66.817	0.11 ⁵	1610.7-6648	31.82 ± 0.94	1.77±0.02	2870.3	4199.5
161204.9-043815	243.02029	-4.63761	0.7 ³	new	1.19 ± 0.42	2.40±0.34	3000.0	10.6
161327.2-190836	243.36321	-19.14342	0.31 ⁵	1613.3-1907	1.20 ± 0.31	2.19±0.25	3982.8	21.3
161444.0-085120	243.68329	-8.85572	0.5 ⁵	new	0.156 ± 0.047	1.58±0.20	10000.0	33.1
161608.4+224107	244.03517	22.68528	0.33 ¹	new	0.638 ± 0.348	1.89±0.34	3000.0	13.6
162115.2-003140	245.31338	-0.52783	0.414 ²	new	1.51 ± 0.45	1.91±0.20	3000.0	26.4
162259.3+440142	245.74692	44.02858	0.38 ⁴	new	0.460 ± 0.188	1.92±0.25	3000.0	11.0
162330.6+085724	245.87733	8.95675	0.533 ¹	1623.4+0858	1.15 ± 0.28	1.99±0.20	3410.3	37.1
162625.9+351341	246.60775	35.22819	0.498 ¹	1626.3+3514	0.472 ± 0.091	1.61±0.12	5404.5	92.3
162646.0+630048	246.69187	63.0135	0.2 ⁵	1626.5+6257	0.655 ± 0.171	1.73±0.15	3332.8	44.3
162713.0+314956	246.80408	31.83228	0.58 ¹	1627.3+3148	0.627 ± 0.130	1.87±0.15	4787.0	58.4
162839.0+252756	247.16262	25.46558	0.22 ¹	new	0.055 ± 0.025	1.87±0.28	10000.0	10.3

Continued on next page

Table 4 – continued from previous page

2BIGB Jname	R.A.(deg)	Dec.(deg)	z	4FGL J	$N_0 (10^{-15})$	Γ	$E_0 (\text{GeV})$	TS
163043.1+522138	247.67975	52.36075	–	1630.7+5221	45.40 ± 1.85	2.05 ± 0.03	1613.3	1881.7
163124.7+421702	247.85296	42.284	0.47 ¹	new	0.437 ± 0.211	1.92 ± 0.28	3000.0	10.0
163146.7+414632	247.94467	41.77575	0.58 ⁵	1631.8+4144	0.321 ± 0.070	1.72 ± 0.15	5946.3	57.7
163213.8+580052	248.05767	58.01456	0.32 ⁵	1632.4+5800	0.292 ± 0.081	1.85 ± 0.20	4839.0	30.8
163658.4-124836	249.24342	-12.81014	0.24 ¹	new	0.370 ± 0.165	1.68 ± 0.23	5000.0	14.7
163709.5+432600	249.28958	43.43336	0.343 ¹	new	0.073 ± 0.028	1.91 ± 0.28	10000.0	26.4
163716.7+131438	249.31971	13.24414	0.559 ²	1637.1+1316	4.24 ± 1.12	2.04 ± 0.17	1863.6	37.3
163726.6+454749	249.361	45.79703	0.192 ¹	1637.6+4548	0.277 ± 0.093	2.21 ± 0.28	5309.5	32.0
163751.0-344915	249.4625	-34.82094	–	1637.8-3449	12.53 ± 0.79	1.90 ± 0.04	3159.1	644.7
163801.6+732615	249.50683	73.43772	–	1637.7+7326	0.484 ± 0.124	1.79 ± 0.16	3970.5	41.0
163808.8+004222	249.53683	0.70625	0.35 ⁵	1638.0+0042	0.161 ± 0.041	1.67 ± 0.17	10407.6	39.4
164011.0+062826	250.04604	6.47414	0.31 ⁵	1640.2+0629	0.670 ± 0.186	1.70 ± 0.17	4635.8	55.5
164014.9+685234	250.06225	68.87614	0.26 ⁵	1640.3+6850	2.24 ± 0.31	1.99 ± 0.10	2875.8	122.1
164220.3+221143	250.58467	22.1955	0.592 ¹	1642.4+2211	0.945 ± 0.224	2.16 ± 0.21	3679.7	36.7
164328.9-064619	250.8705	-6.77208	0.082 ¹	1643.5-0646	2.82 ± 0.47	2.22 ± 0.15	3477.9	62.8
164339.5+331647	250.91442	33.27994	0.42 ⁵	1643.7+3317	0.075 ± 0.020	1.47 ± 0.17	12290.1	40.2
164420.0+454644	251.08333	45.77892	0.225 ¹	1644.2+4546	0.527 ± 0.115	1.86 ± 0.16	4335.9	55.2
164651.8-132848	251.71575	-13.48006	0.35 ⁵	1646.7-1330	0.478 ± 0.124	1.77 ± 0.17	6466.1	32.4
165140.0+721824	252.91646	72.30689	0.24 ⁵	1651.6+7219	2.31 ± 0.27	1.84 ± 0.08	3245.2	230.9
165249.9+402310	253.208	40.38617	0.31 ³	1652.7+4024	0.996 ± 0.146	1.91 ± 0.11	5283.6	103.8
165352.2+394536	253.46758	39.76014	0.03 ¹	1653.8+3945	365.72 ± 5.33	1.77 ± 0.01	1477.7	32177.7
165517.9-224045	253.82479	-22.67931	0.4 ⁴	new	0.786 ± 0.249	2.35 ± 0.31	5000.0	27.8
165655.1-201056	254.22975	-20.18228	0.23 ⁴	1656.9-2010	6.10 ± 0.52	1.88 ± 0.06	3570.2	334.4
170238.5+311543	255.66058	31.26214	0.32 ⁴	1702.6+3114	2.34 ± 0.24	1.86 ± 0.08	3829.2	262.9
170409.6+123421	256.03992	12.57269	0.4 ²	1704.2+1234	32.22 ± 5.25	2.27 ± 0.12	1113.2	97.5
170433.8-052840	256.14096	-5.47797	0.35 ⁵	1704.5-0527	7.22 ± 0.59	1.99 ± 0.06	3491.2	341.9
170534.8+604215	256.39508	60.70436	0.28 ¹	new	0.044 ± 0.019	1.63 ± 0.27	10000.0	12.5
171108.7+024404	257.78621	2.73467	0.46 ⁵	new	0.423 ± 0.137	1.94 ± 0.21	5000.0	16.1
171248.8+293116	258.20321	29.52133	0.42 ³	1712.7+2932	2.03 ± 0.24	1.82 ± 0.09	3916.0	195.4
171405.4-202752	258.52267	-20.46456	0.09 ⁵	1714.0-2029	0.263 ± 0.039	1.57 ± 0.10	13307.8	110.1
171553.3+884415	258.97208	88.73758	0.48 ⁵	1713.7+8844	0.235 ± 0.062	1.73 ± 0.15	6004.9	32.0
171921.5+120721	259.83958	12.12275	0.34 ⁵	1719.3+1205	0.634 ± 0.092	1.87 ± 0.11	7478.6	122.4
172504.3+115215	261.26808	11.87097	0.18 ³	1725.0+1152	71.89 ± 2.12	1.86 ± 0.02	2220.6	4695.5
172818.6+501310	262.07762	50.21958	0.055 ¹	1728.3+5013	14.17 ± 0.52	1.66 ± 0.02	3005.0	2747.4
173044.8+380454	262.68663	38.08192	0.22 ⁵	new	0.464 ± 0.118	1.79 ± 0.17	5000.0	40.9
173329.0+451950	263.37067	45.33069	0.317 ¹	new	0.571 ± 0.248	1.98 ± 0.26	3000.0	13.0
173605.3+203301	264.02188	20.55031	–	1736.0+2033	3.76 ± 0.38	1.88 ± 0.07	3407.3	259.3
173842.5+382102	264.67696	38.35072	0.31 ⁵	new	0.055 ± 0.026	1.59 ± 0.31	10000.0	17.7
174357.5+375310	265.98975	37.88628	0.5 ⁵	new	0.768 ± 0.261	2.20 ± 0.27	3000.0	12.7
174357.8+193509	265.991	19.58592	0.08 ¹	1744.0+1935	10.06 ± 0.73	1.93 ± 0.05	2710.3	512.6
174419.8+185218	266.0825	18.87167	0.39 ⁵	1744.4+1851	0.182 ± 0.057	1.77 ± 0.22	7827.2	21.8
174459.5-172639	266.24804	-17.44419	–	1744.9-1727	11.55 ± 0.70	1.94 ± 0.04	3756.7	687.2
174537.8+395130	266.40733	39.85853	0.267 ¹	1745.6+3950	1.91 ± 0.42	1.96 ± 0.15	2588.1	51.1
174702.5+493801	266.76046	49.63378	0.46 ¹	1747.2+4937	0.368 ± 0.116	1.63 ± 0.17	4253.6	29.8
174837.6-085440	267.15679	-8.91131	0.33 ⁵	1748.5-0854	0.638 ± 0.191	1.75 ± 0.19	5737.2	32.6
175615.1+552218	269.06625	55.37167	0.657 ³	1756.3+5522	2.87 ± 0.26	1.81 ± 0.07	3558.4	348.0
175713.1+703337	269.30446	70.5605	0.407 ¹	1757.0+7032	0.321 ± 0.058	1.80 ± 0.13	7827.6	81.6
175949.2+703719	269.955	70.62194	–	1800.1+7037	1.66 ± 0.30	2.04 ± 0.13	3282.2	71.3
180002.0+281045	270.0085	28.17936	0.44 ⁵	1800.1+2812	0.478 ± 0.095	1.76 ± 0.14	5688.0	69.6
180354.3+654825	270.97633	65.80697	0.085 ²	new	0.246 ± 0.112	2.42 ± 0.43	5000.0	20.9
180732.2+642926	271.88408	64.49064	0.239 ¹	1807.2+6429	2.108 ± 0.31	1.98 ± 0.11	2833.5	102.8
180845.7+241905	272.19037	24.31825	0.45 ⁵	1808.8+2419	2.36 ± 0.39	2.40 ± 0.17	3084.5	61.1
180849.7+352042	272.20704	35.34519	0.22 ⁵	1808.8+3522	3.30 ± 0.62	2.30 ± 0.16	2482.3	59.9
180925.4+204131	272.35592	20.69197	0.28 ³	1809.3+2042	4.81 ± 0.59	1.96 ± 0.09	2724.9	168.7
181118.0+034113	272.82508	3.68711	–	1811.3+0340	14.29 ± 0.94	1.88 ± 0.04	2824.9	649.4
181335.0+314417	273.39667	31.73822	0.117 ¹	1813.5+3144	21.06 ± 1.38	2.16 ± 0.05	2381.9	929.8

Continued on next page

Table 4 – continued from previous page

2BIGB Jname	R.A.(deg)	Dec.(deg)	z	4FGL J	N₀ (10⁻¹⁵)	Γ	E₀ (GeV)	TS
181403.4+382810	273.51429	38.4695	0.35 ⁵	1814.0+3828	3.23 ± 0.62	2.31±0.19	2195.3	45.9
182021.0+362343	275.08742	36.39531	0.33 ⁵	1820.3+3624	0.866 ± 0.129	1.73±0.10	5099.2	136.6
182338.6-345412	275.91083	-34.90336	–	1823.6-3453	24.00 ± 1.21	1.73±0.03	2592.6	1513.1
182419.0+430949	276.07929	43.16375	0.487 ¹	1824.5+4311	0.707 ± 0.115	1.84±0.11	5235.9	99.4
182833.5-592054	277.13979	-59.34853	–	new	0.581 ± 0.291	1.72±0.26	3000.0	15.6
182854.7-241735	277.22796	-24.29308	0.05 ⁵	1829.0-2417	10.72 ± 1.11	2.13±0.08	2664.3	172.8
182924.3+540259	277.35121	54.04989	–	1829.3+5402	3.50 ± 0.28	1.89±0.06	3481.3	420.5
183201.0+382137	278.00408	38.36028	0.22 ⁵	1831.9+3820	1.75 ± 0.30	2.19±0.14	3114.9	63.4
183806.7-600032	279.52808	-60.00892	0.18 ⁵	1838.0-5959	1.73 ± 0.25	1.91±0.11	3854.7	115.0
183820.6-602522	279.586	-60.42289	0.121 ¹	1838.4-6023	0.334 ± 0.080	1.75±0.16	6577.3	50.5
183849.1+480234	279.70479	48.04289	0.3 ²	1838.8+4802	32.07 ± 0.98	1.83±0.02	2551.8	4025.6
184120.0+590608	280.33462	59.10225	0.53 ¹	new	1.62 ± 0.59	2.58±0.32	3000.0	13.4
184121.7+290940	280.34054	29.16133	0.18 ⁵	1841.3+2909	0.799 ± 0.098	1.73±0.08	7363.2	197.1
184147.0+321839	280.446	32.31086	0.24 ⁵	1841.8+3218	3.62 ± 0.34	1.87±0.07	3641.7	315.2
184229.8-584157	280.62429	-58.69931	0.33 ⁵	1842.4-5840	0.425 ± 0.066	1.58±0.10	7897.2	144.7
184425.4+154645	281.10567	15.77939	0.11 ⁵	1844.4+1547	36.00 ± 1.81	2.03±0.04	2324.6	1161.3
184445.7-324641	281.19021	-32.77819	–	1844.8-3248	0.848 ± 0.197	1.92±0.14	4713.2	32.0
184822.6+653657	282.09396	65.61597	0.364 ¹	1848.5+6537	0.263 ± 0.054	1.73±0.15	6785.4	64.9
184847.1+424539	282.19633	42.76097	0.4 ⁵	1848.9+4247	2.13 ± 0.30	2.04±0.11	3270.0	104.1
184919.5-164724	282.33108	-16.79	0.16 ⁵	1849.2-1647	2.11 ± 0.25	1.84±0.09	4991.4	166.4
185024.0+263153	282.60013	26.53156	0.22 ⁵	1850.5+2631	0.349 ± 0.071	1.60±0.13	7765.8	85.9
185352.1+671355	283.46692	67.23197	0.212 ¹	1853.8+6714	0.574 ± 0.170	2.18±0.22	4071.5	18.9
185813.4+432451	284.55596	43.41442	0.17 ⁵	1858.3+4321	8.682 ± 1.55	2.16±0.14	1596.0	74.6
190411.8+362658	286.04933	36.44964	0.13 ⁵	1904.1+3627	3.48 ± 0.31	1.82±0.06	3853.1	382.6
191052.1+285624	287.71721	28.94008	0.3 ⁵	1910.8+2856	0.935 ± 0.147	1.75±0.10	5479.1	112.6
191129.7-190824	287.87392	-19.14022	0.16 ⁵	1911.4-1908	2.53 ± 0.26	1.84±0.08	4743.2	242.6
191251.2-124919	288.21313	-12.82194	–	1912.7-1250	1.88 ± 0.33	2.14±0.15	4180.3	57.0
191401.9+443832	288.50783	44.64228	0.28 ⁵	1913.9+4439	3.18 ± 0.37	1.91±0.08	3102.8	176.5
191803.6+033031	289.515	3.50864	0.23 ⁵	1918.0+0331	0.424 ± 0.083	1.63±0.12	9022.0	70.2
191809.6+375313	289.54017	37.88697	–	1918.1+3752	2.95 ± 0.40	2.12±0.11	3088.3	97.4
192157.6+581701	290.49017	58.28367	0.4 ⁵	new	0.621 ± 0.220	1.76±0.19	3000.0	19.0
192242.3-745356	290.67625	-74.89906	0.36 ⁵	1922.5-7453	3.75 ± 0.41	1.86±0.08	2975.9	236.6
192325.4-250209	290.85583	-25.03583	0.65 ⁴	1923.4-2503	0.131 ± 0.044	1.70±0.21	9214.1	18.2
192502.2+281542	291.25937	28.26169	0.16 ⁵	1925.0+2815	3.91 ± 0.41	1.92±0.08	3720.1	244.7
192519.1+370535	291.32946	37.09322	0.26 ⁵	new	0.562 ± 0.135	2.04±0.18	5000.0	31.2
192649.9+615442	291.70787	61.91178	–	1926.8+6154	16.46 ± 0.77	1.85±0.03	2802.2	1933.5
193109.3+093716	292.78858	9.62128	–	1931.1+0937	25.17 ± 1.10	1.81±0.03	3309.6	2045.4
193320.3+072621	293.3345	7.43933	0.17 ⁵	1933.3+0726	4.18 ± 0.28	1.85±0.05	5235.0	612.9
193412.8-241920	293.55321	-24.32233	0.23 ⁵	1934.3-2419	0.871 ± 0.168	1.75±0.12	4783.2	63.3
193419.6+600139	293.58175	60.02764	–	1934.2+6002	2.24 ± 0.27	1.89±0.09	3288.4	156.1
193656.0-471950	294.23375	-47.33056	0.265 ¹	1936.9-4720	3.06 ± 0.25	1.68±0.05	4397.4	499.3
194247.5+103327	295.69783	10.5575	–	1942.7+1033	23.25 ± 0.88	1.85±0.02	3437.8	2304.3
194333.8-053353	295.89083	-5.56492	0.5 ⁵	new	0.709 ± 0.192	1.80±0.18	5000.0	27.2
194356.2+211822	295.98433	21.30636	0.22 ⁵	1944.0+2117	0.322 ± 0.042	1.41±0.07	15712.	200.2
194422.4-452331	296.09333	-45.39217	0.21 ⁵	1944.4-4523	0.549 ± 0.085	1.52±0.09	7020.6	163.8
194455.2-214319	296.22983	-21.722	0.28 ⁴	1944.9-2143	7.99 ± 0.52	1.85±0.05	3443.7	688.1
194934.2+090653	297.3925	9.11489	–	1949.5+0906	3.83 ± 0.43	1.91±0.08	3677.5	202.0
195500.7-160338	298.75271	-16.06064	0.23 ⁴	1955.1-1604	10.52 ± 1.00	2.04±0.08	2485.3	282.2
195502.8-564028	298.76187	-56.67461	0.2 ⁵	1954.9-5640	3.16 ± 0.34	1.89±0.08	3384.1	222.6
195547.9+021512	298.94942	2.25356	–	1955.7+0214	0.832 ± 0.130	1.87±0.12	6514.6	116.1
195800.5+243806	299.502	24.635	–	1958.1+2438	1.96 ± 0.27	2.07±0.10	5326.7	87.7
195812.7+694325	299.55279	69.72364	0.28 ⁵	new	0.073 ± 0.027	1.73±0.23	10000.0	15.1
195814.1-301111	299.56212	-30.18656	0.119 ¹	1958.3-3010	4.90 ± 0.33	1.78±0.05	4453.9	637.6
195945.7-472519	299.94025	-47.422	–	1959.7-4725	15.00 ± 0.80	1.80±0.03	2606.6	1153.5
195959.8+650854	299.99929	65.14853	0.047 ¹	2000.0+6508	257.95 ± 3.57	1.79±0.01	1732.8	26776.7
200112.9+435252	300.30362	43.88136	–	2001.2+4353	67.97 ± 2.11	1.90±0.02	2029.6	2634.3
200204.2-573645	300.51742	-57.61258	0.26 ⁵	2001.9-5737	5.49 ± 0.67	2.18±0.11	2299.0	123.4

Continued on next page

Table 4 – continued from previous page

2BIGB Jname	R.A.(deg)	Dec.(deg)	z	4FGL J	$N_0 (10^{-15})$	Γ	$E_0 (\text{GeV})$	TS
200227.3-711936	300.61363	-71.32672	0.21 ⁵	2002.4-7119	0.461 \pm 0.067	1.69 \pm 0.10	7304.2	145.1
200245.4+630233	300.68908	63.04258	–	2002.6+6302	0.089 \pm 0.024	1.39 \pm 0.15	10770.7	49.1
200506.0+700439	301.27487	70.07764	–	2005.1+7003	2.71 \pm 0.23	1.81 \pm 0.06	4402.4	368.9
200925.4-484953	302.35579	-48.83153	0.071 ¹	2009.4-4849	43.15 \pm 1.28	1.82 \pm 0.02	2397.8	4119.3
201213.7-523251	303.05713	-52.54753	0.37 ⁵	2012.1-5234	0.245 \pm 0.059	1.74 \pm 0.16	7529.7	43.0
201428.6-004722	303.61933	-0.78967	0.231 ¹	2014.3-0047	3.29 \pm 0.37	1.93 \pm 0.09	3754.2	189.2
201431.1+064852	303.6295	6.81458	0.341 ¹	2014.5+0648	1.93 \pm 0.25	1.83 \pm 0.09	4697.1	176.5
201503.1+162227	303.76587	16.37422	0.25 ⁵	2015.0+1621	15.26 \pm 2.41	2.21 \pm 0.12	1619.2	93.5
201525.0-143203	303.85425	-14.53442	0.31 ⁵	2015.3-1432	1.06 \pm 0.50	1.68 \pm 0.23	2567.5	22.7
201619.6+495324	304.08146	49.89014	–	2016.3+4953	0.188 \pm 0.039	1.72 \pm 0.13	10489.3	56.7
202143.9-722611	305.43275	-72.43661	0.29 ⁵	2022.0-7224	0.560 \pm 0.103	1.78 \pm 0.12	5157.5	78.6
202429.4-084804	306.12238	-8.80125	–	2024.4-0847	6.11 \pm 0.58	1.94 \pm 0.07	3057.8	305.3
202630.8+764448	306.62829	76.74675	0.29 ⁵	2026.1+7645	0.141 \pm 0.023	1.60 \pm 0.10	13567.5	120.3
202658.4+334308	306.74346	33.719	0.24 ⁵	2027.0+3343	0.076 \pm 0.014	1.99 \pm 0.13	21708.3	40.3
203024.0-503413	307.60017	-50.57028	0.53 ⁵	new	0.546 \pm 96.9	1.80 \pm 0.01	5000.0	50.8
203027.1-143917	307.61629	-14.65475	0.43 ⁵	2030.5-1439	1.34 \pm 0.30	1.72 \pm 0.14	3481.2	64.2
203031.7+223439	307.632	22.57761	–	2030.5+2235	0.327 \pm 0.083	1.73 \pm 0.16	6582.2	36.0
203057.1+193612	307.738	19.60358	0.27 ⁵	2030.9+1935	8.43 \pm 0.66	1.83 \pm 0.05	2878.9	473.8
203117.6+002745	307.82338	0.46253	0.48 ⁵	new	21.32 \pm 6.43	3.11 \pm 0.46	1000.0	12.4
203451.1-420038	308.71283	-42.01061	0.29 ⁵	2034.8-4200	3.71 \pm 0.44	1.92 \pm 0.09	3016.2	176.4
203649.5-332830	309.20621	-33.47514	0.23 ¹	2036.9-3329	0.560 \pm 0.083	1.61 \pm 0.10	7721.2	136.6
203923.5+521950	309.84796	52.33058	0.053 ¹	2039.5+5218	1.14 \pm 0.13	1.80 \pm 0.08	6468.0	191.8
204006.6-462018	310.02758	-46.33833	0.31 ⁵	2040.1-4621	0.871 \pm 0.142	1.73 \pm 0.11	4985.5	91.6
204008.3-711459	310.03446	-71.24997	0.161 ¹	2040.2-7115	1.85 \pm 0.17	1.71 \pm 0.06	4760.1	390.7
204150.2-373339	310.45929	-37.56106	0.098 ¹	2041.9-3735	3.09 \pm 0.46	1.95 \pm 0.11	2928.3	102.2
204201.9-731913	310.508	-73.32042	0.31 ⁵	2041.8-7319	1.64 \pm 0.25	1.82 \pm 0.11	3519.9	128.7
204206.0+242652	310.52517	24.44786	0.104 ¹	2042.1+2427	1.83 \pm 0.17	1.85 \pm 0.07	5656.1	316.6
204921.7-003926	312.34058	-0.65733	0.25 ¹	2049.7-0036	0.017 \pm 0.010	1.14 \pm 0.35	22467.9	24.3
205242.5+081040	313.17725	8.17786	0.53 ⁵	2052.5+0810	0.039 \pm 0.012	1.40 \pm 0.20	18832.6	37.5
205350.7+292314	313.46133	29.38736	0.23 ⁵	2053.8+2922	4.40 \pm 0.33	1.71 \pm 0.05	4449.5	571.1
205456.8+001537	313.73687	0.26053	0.151 ¹	2054.8+0015	1.30 \pm 0.09	1.64 \pm 0.04	4357.6	109.8
205528.2-002117	313.86758	-0.35472	0.44 ¹	2055.4-0020	1.62 \pm 0.22	1.83 \pm 0.10	4676.4	160.0
205642.7+494005	314.17787	49.66819	0.15 ⁵	2056.7+4939	4.61 \pm 0.25	1.78 \pm 0.03	6410.9	953.1
205846.7-144304	314.69475	-14.71803	0.078 ¹	2058.8-1442	0.854 \pm 0.218	1.83 \pm 0.18	3836.9	39.4
210123.9+091324	315.34942	9.22356	0.29 ⁵	2101.3+0912	1.58 \pm 0.42	1.82 \pm 0.16	2977.4	46.9
210338.4-623225	315.90992	-62.5405	–	2103.8-6233	122.68 \pm 4.60	2.11 \pm 0.03	1187.0	2442.4
210415.9+211808	316.06633	21.30228	0.36 ⁵	new	1.32 \pm 0.23	1.91 \pm 0.14	5000.0	122.3
210421.9-021238	316.09138	-2.21081	0.45 ³	2104.3-0212	0.496 \pm 0.085	1.67 \pm 0.11	7223.5	115.5
210721.2-145418	316.83821	-14.90511	0.34 ⁴	new	1.43 \pm 0.37	2.27 \pm 0.26	3000.0	24.7
210844.7-025034	317.18637	-2.84278	0.15 ¹	2108.7-0250	6.20 \pm 0.85	2.05 \pm 0.11	2251.5	130.9
210936.1+395513	317.40058	39.92042	–	2109.6+3954	0.196 \pm 0.035	1.54 \pm 0.10	13253.6	81.9
211011.2-861847	317.54658	-86.31322	0.31 ⁵	2109.8-8618	0.429 \pm 0.067	1.75 \pm 0.10	7141.1	123.7
211243.0+081835	318.17917	8.30978	0.27 ⁵	2112.7+0819	2.98 \pm 0.31	1.95 \pm 0.08	4041.2	253.1
211522.0+121802	318.84167	12.30072	0.28 ⁵	2115.2+1218	2.88 \pm 0.38	1.98 \pm 0.11	3291.5	131.9
211614.5+333920	319.06054	33.65569	0.12 ⁵	2116.2+3339	99.53 \pm 2.94	1.92 \pm 0.02	1714.6	4134.6
211754.1-324328	319.47879	-32.7245	0.215 ¹	2117.8-3243	2.92 \pm 0.48	2.04 \pm 0.15	3084.4	83.2
212743.0+361305	321.92929	36.21825	0.876 ³	2127.7+3612	19.69 \pm 1.23	1.96 \pm 0.04	2221.6	688.0
212840.0-194152	322.1665	-19.698	0.24 ⁵	new	0.601 \pm 0.250	1.75 \pm 0.22	3000.0	13.5
213004.8-563222	322.51987	-56.53947	–	new	1.13 \pm 0.35	1.98 \pm 0.24	3000.0	24.9
213103.2-274657	322.7635	-27.78275	0.38 ³	2131.0-2746	10.89 \pm 0.78	1.79 \pm 0.05	2510.6	704.6
213135.0-091523	322.89754	-9.25653	0.449 ¹	2131.5-0916	9.47 \pm 0.81	1.92 \pm 0.06	2508.0	391.4
213151.5-251558	322.96475	-25.26625	0.86 ³	2131.7-2515	2.76 \pm 0.33	1.85 \pm 0.09	3493.4	190.1
213314.4+252859	323.30983	25.48306	0.294 ¹	2133.1+2529	2.02 \pm 0.37	1.85 \pm 0.12	3321.2	97.5
213349.2+664704	323.455	66.78453	–	2133.9+6646	6.87 \pm 0.54	2.03 \pm 0.06	3169.5	341.1
213448.2-164205	323.70092	-16.70156	0.85 ⁵	new	0.862 \pm 0.327	1.96 \pm 0.24	3000.0	12.6
213821.1+355823	324.58804	35.97322	0.25 ⁵	2138.3+3556	0.565 \pm 0.137	1.90 \pm 0.18	5116.9	36.7

Continued on next page

Table 4 – continued from previous page

2BIGB Jname	R.A.(deg)	Dec.(deg)	z	4FGL J	N₀ (10⁻¹⁵)	Γ	E₀ (GeV)	TS
213852.7-205347	324.71979	-20.89661	0.29 ¹	2138.8-2055	0.594 ± 0.120	1.81±0.15	5258.9	66.7
214226.5+365949	325.61037	36.99714	0.24 ⁵	2142.4+3659	1.72 ± 0.27	1.84±0.11	3917.5	110.1
214239.8-202819	325.66575	-20.47197	0.53 ⁵	2142.5-2029	1.07 ± 0.25	1.94±0.18	3520.1	48.1
214247.6+195810	325.69842	19.96969	0.38 ⁵	2142.8+1958	0.407 ± 0.080	1.74±0.13	6472.5	54.4
214429.6-563849	326.12321	-56.64694	0.48 ⁵	new	0.070 ± 0.015	1.70±0.13	10000.0	15.6
214442.1-181800	326.17538	-18.30011	0.23 ⁵	new	0.328 ± 0.082	1.84±0.18	5000.0	22.3
214530.2+100605	326.37579	10.10153	0.37 ⁴	2145.5+1006	0.134 ± 0.037	1.70±0.18	9846.4	34.5
214552.3+071927	326.46788	7.32425	0.237 ¹	2145.7+0718	2.01 ± 0.43	1.90±0.15	2970.2	69.2
214637.0-134400	326.65396	-13.73344	0.42 ³	2146.5-1344	16.34 ± 0.80	1.74±0.03	2897.8	1620.2
215015.5-141049	327.56463	-14.18053	0.22 ¹	2150.1-1410	1.92 ± 0.25	1.71±0.09	4219.8	187.4
215051.7+111916	327.71546	11.32131	0.495 ¹	2150.8+1118	1.42 ± 0.52	1.83±0.19	2361.4	13.8
215123.2+415633	327.84675	41.94275	0.1 ⁵	2151.4+4156	3.29 ± 0.39	1.96±0.08	3464.3	162.6
215214.0-120541	328.05879	-12.09478	0.121 ¹	2152.0-1205	2.04 ± 0.37	2.25±0.16	3261.9	62.0
215305.3-004230	328.27217	-0.70844	0.341 ¹	2153.1-0041	0.374 ± 0.071	1.79±0.14	8245.7	89.1
215601.6+181837	329.00683	18.31033	0.36 ³	2156.0+1818	1.82 ± 0.20	1.74±0.07	4923.4	272.4
215852.0-301332	329.71687	-30.22556	0.117 ¹	2158.8-3013	1283.1 ± 13.8	1.86±0.01	1136.4	59940.3
215910.9-284116	329.7955	-28.68789	0.271 ¹	2159.1-2840	2.64 ± 0.282	1.87±0.08	3975.5	234.2
215936.1-461953	329.90058	-46.33164	0.4 ⁵	2159.6-4620	0.480 ± 0.082	1.67±0.12	6445.5	96.0
220107.3-590640	330.28054	-59.11128	0.21 ⁵	new	0.302 ± 0.091	2.06±0.20	5000.0	19.5
220123.8+294934	330.34925	29.82628	0.24 ⁵	new	0.886 ± 0.312	1.96±0.23	3000.0	13.4
220155.8-170700	330.48263	-17.11675	0.169 ¹	new	0.105 ± 0.087	1.12±0.31	5000.0	33.6
220704.1+222231	331.76713	22.37542	0.558 ¹	2207.1+2222	0.231 ± 0.092	1.76±0.23	5594.6	13.4
220941.7-045110	332.42371	-4.85286	0.255 ⁵	2209.7-0451	1.87 ± 0.26	1.91±0.10	4071.9	126.8
221029.7+362159	332.62367	36.36661	0.37 ⁵	new	1.07 ± 0.34	2.38±0.30	3000.0	14.1
221058.5+320341	332.74392	32.06142	0.32 ⁵	2210.8+3203	0.020 ± 77.5	1.35±0.21	23882.1	26.1
221108.3-000302	332.78471	-0.05064	0.362 ¹	2211.0-0003	0.957 ± 0.170	1.88±0.13	4921.2	80.9
221109.9-002327	332.79112	-0.39097	0.448 ¹	new	1.19 ± 0.42	2.17±0.24	3000.0	14.0
221330.4-475425	333.37646	-47.907	–	2213.5-4754	0.693 ± 0.137	1.77±0.14	4521.5	67.7
221405.0+393857	333.52104	39.64936	–	new	0.705 ± 0.324	1.81±0.25	3000.0	12.7
221659.5-672800	334.24812	-67.46672	0.27 ⁵	new	0.310 ± 0.089	1.90±0.19	5000.0	24.6
221728.4-310620	334.36854	-31.10567	0.46 ¹	new	0.044 ± 0.026	1.39±0.34	10000.0	14.3
222028.7+281355	335.11967	28.23214	0.15 ⁵	2220.5+2813	2.57 ± 0.41	1.95±0.11	2975.4	81.9
222129.3-522527	335.37208	-52.42433	0.34 ³	2221.5-5225	13.51 ± 0.85	1.78±0.04	2254.5	912.4
222329.6+010226	335.87321	1.04075	0.51 ³	2223.3+0102	0.767 ± 0.188	1.74±0.16	4169.9	45.3
222425.0+035458	336.10404	3.91617	0.35 ⁵	2224.5+0353	0.877 ± 0.220	1.98±0.19	3903.3	31.9
222636.5+021037	336.65188	2.17706	0.35 ⁵	2226.6+0210	0.188 ± 0.064	1.57±0.20	7376.1	30.3
223248.8-202226	338.20333	-20.37394	0.31 ⁵	2232.6-2023	0.966 ± 0.282	1.57±0.14	3194.9	57.3
223301.1+133601	338.25463	13.60053	0.214 ¹	2232.8+1334	0.262 ± 0.107	1.60±0.21	5067.1	21.1
223626.3+370713	339.10975	37.12042	0.2 ⁵	2236.6+3706	0.204 ± 0.059	1.75±0.20	7366.3	33.5
223704.8+184055	339.27012	18.68208	0.5 ⁴	2236.9+1839	0.252 ± 0.092	1.79±0.22	5424.6	15.5
223812.7-394018	339.55304	-39.67192	0.25 ¹	new	0.261 ± 0.093	1.92±0.25	5000.0	16.8
223928.8-243944	339.87008	-24.66228	0.115 ¹	new	0.061 ± 0.028	1.42±0.26	10000.0	22.9
224017.1-524113	340.07379	-52.68717	0.25 ⁵	2240.3-5241	1.00 ± 0.17	2.16±0.14	6321.5	120.2
224046.9+132602	340.19537	13.43411	0.66 ¹	new	0.086 ± 0.031	1.76±0.20	10000.0	19.3
224123.5+294247	340.34812	29.71317	0.48 ⁵	2241.3+2943	0.295 ± 0.059	1.90±0.15	8666.2	90.7
224340.0-123059	340.91792	-12.51647	0.226 ¹	2243.7-1231	3.901 ± 0.53	1.93±0.10	2933.5	152.9
224354.7+202103	340.97808	20.35106	–	2243.9+2021	158.08 ± 4.27	1.87±0.02	1485.7	6488.2
224436.7+250343	341.15275	25.06197	0.36 ⁴	2244.6+2502	7.47 ± 1.33	2.20±0.15	1718.5	65.5
224448.1-000619	341.20038	-0.10542	0.7 ³	2244.9-0007	3.06 ± 0.98	2.20±0.24	1990.8	18.9
224531.9-173358	341.38271	-17.56636	0.43 ⁵	2245.5-1734	0.148 ± 0.051	1.72±0.21	7144.5	20.3
224642.1-520640	341.67533	-52.11119	0.0979 ¹	2246.7-5207	0.227 ± 0.043	1.60±0.12	9127.4	95.1
224753.2+441315	341.97175	44.22097	–	2247.8+4413	1.40 ± 0.13	1.71±0.06	6147.0	347.0
224833.3+322334	342.13892	32.39278	0.45 ⁵	new	1.02 ± 0.33	2.14±0.26	3000.0	14.8
224910.7-130002	342.29471	-13.00078	0.35 ⁴	2249.4-1300	790.5 ± 12.0	2.42±0.01	1155.9	15006.6
224938.5-594422	342.41029	-59.73969	0.29 ⁵	2249.7-5944	3.12 ± 0.45	2.27±0.14	2498.9	91.5
225005.7+382437	342.52392	38.41033	0.119 ¹	2250.0+3825	2.36 ± 0.19	1.69±0.05	5333.2	515.6

Continued on next page

Table 4 – continued from previous page

2BIGB Jname	R.A.(deg)	Dec.(deg)	z	4FGL J	$N_0 (10^{-15})$	Γ	$E_0 (\text{GeV})$	TS
225147.5-320612	342.94804	-32.10356	0.246 ¹	2251.7-3208	0.245 ± 0.059	1.77 ± 0.18	7155.9	52.2
225354.2+140436	343.476	14.07692	0.327 ¹	2253.7+1405	1.49 ± 0.37	1.89 ± 0.16	3283.4	49.4
225613.3-330338	344.05546	-33.06064	0.243 ¹	new	1.60 ± 0.44	1.99 ± 0.17	3000.0	51.6
225636.1-554709	344.15021	-55.78603	0.2 ⁵	new	0.050 ± 0.020	1.62 ± 0.27	10000.0	16.3
225819.0-552537	344.579	-55.42703	0.479 ¹	2258.4-5524	12.40 ± 1.42	2.13 ± 0.09	1547.3	207.0
230012.4+405225	345.05154	40.87364	0.34 ⁵	2300.1+4053	0.129 ± 0.038	1.38 ± 0.16	9726.6	44.1
230436.7+370507	346.15296	37.08542	–	2304.6+3704	3.88 ± 0.30	1.82 ± 0.06	4067.3	473.9
230635.0-110348	346.64583	-11.06342	0.45 ⁵	2306.6-1105	4.67 ± 1.36	2.01 ± 0.19	1714.3	44.7
230722.1-120517	346.84208	-12.08822	0.32 ⁴	2307.4-1206	0.623 ± 0.162	1.94 ± 0.20	4404.5	33.7
230848.7+542611	347.20308	54.43644	–	new	0.255 ± 0.047	1.71 ± 0.12	10000.0	66.9
230940.8-363248	347.42013	-36.54683	–	2309.7-3632	9.55 ± 0.93	2.02 ± 0.08	2021.6	268.5
231023.4+311949	347.59738	31.33033	0.48 ⁵	new	0.156 ± 0.082	1.66 ± 0.28	5000.0	9.14
231347.9-692331	348.44946	-69.39194	0.53 ⁵	2313.4-6922	0.187 ± 0.051	1.62 ± 0.16	6606.8	41.9
231357.3+144423	348.48892	14.73981	0.162 ¹	2314.0+1445	4.38 ± 0.44	1.79 ± 0.07	3319.5	320.5
231732.0-453359	349.38321	-45.56656	0.59 ³	2317.4-4533	14.06 ± 1.09	2.07 ± 0.07	1921.2	438.5
231905.1-420648	349.77462	-42.11344	0.054 ¹	2319.1-4207	5.42 ± 0.65	1.97 ± 0.09	2283.2	181.3
231943.5+161149	349.93117	16.19711	–	2319.7+1609	0.538 ± 0.117	1.88 ± 0.16	5291.1	50.4
232039.8-630918	350.16583	-63.155	0.2 ¹	2321.0-6308	0.569 ± 0.127	1.93 ± 0.16	4246.3	45.4
232137.0-161928	350.40408	-16.32453	–	2321.5-1619	2.33 ± 0.26	1.87 ± 0.08	3959.8	241.3
232240.4-422042	350.66833	-42.34517	0.09 ¹	new	0.189 ± 0.089	1.57 ± 0.25	5000.0	17.6
232244.0+343613	350.68342	34.60383	0.094 ¹	2322.7+3436	3.54 ± 0.38	1.89 ± 0.08	3304.6	236.2
232254.4-491630	350.72671	-49.27503	0.38 ³	2322.8-4916	7.88 ± 0.58	1.90 ± 0.05	2853.9	597.9
232352.1+421058	350.96696	42.18292	0.059 ²	2323.8+4210	26.81 ± 1.05	1.90 ± 0.03	2471.7	2147.1
232444.6-404049	351.18604	-40.68036	0.24 ³	2324.7-4041	12.07 ± 0.66	1.79 ± 0.04	3032.8	1392.5
232520.3-201212	351.33438	-20.20353	0.31 ⁵	2325.2-2010	0.982 ± 0.216	1.77 ± 0.15	3711.5	59.4
232538.0+164642	351.40879	16.77856	0.25 ⁵	2325.6+1644	2.40 ± 0.39	1.98 ± 0.12	2995.8	84.4
232914.3+375414	352.30942	37.90403	0.21 ⁵	2329.2+3755	5.46 ± 0.44	1.83 ± 0.06	3372.7	477.5
232938.2+610114	352.40933	61.02056	–	2329.7+6101	5.04 ± 0.49	2.07 ± 0.08	3623.6	206.2
233014.2-294550	352.559	-29.76392	0.297 ¹	2330.3-2948	2.75 ± 0.57	2.12 ± 0.17	2220.4	44.0
233016.2-233641	352.56733	-23.61144	0.32 ⁵	2330.3-2332	4.06 ± 0.842	2.22 ± 0.18	1978.0	41.7
233113.0-030130	352.80404	-3.02511	0.35 ⁴	2331.5-0258	1.12 ± 0.21	2.01 ± 0.16	4160.6	60.0
233252.2-052142	353.21746	-5.36183	0.4 ⁵	new	0.227 ± 0.091	1.73 ± 0.24	5000.0	13.7
233553.0-581015	353.97079	-58.17097	0.35 ⁵	new	0.045 ± 0.021	1.98 ± 0.44	10000.0	10.9
233920.9-740435	354.83704	-74.07664	0.4 ⁵	2339.2-7403	4.39 ± 0.36	1.98 ± 0.07	3050.4	375.9
234042.9+385511	355.17858	38.91994	0.35 ⁵	2340.5+3854	1.01 ± 0.20	1.89 ± 0.14	3964.3	49.1
234054.2+801516	355.22596	80.25444	0.274 ¹	2340.8+8015	20.28 ± 0.87	1.89 ± 0.03	2911.8	2451.2
234333.6+343950	355.88992	34.66411	0.36 ¹	2343.6+3438	1.74 ± 0.21	1.70 ± 0.08	4300.1	205.8
234704.8+514217	356.77012	51.70497	0.044 ¹	2347.0+5141	63.10 ± 1.95	1.82 ± 0.02	1938.2	4198.4
234753.3+543630	356.97208	54.60842	0.4 ⁵	2347.9+5436	0.93 ± 0.09	1.71 ± 0.07	6913.5	262.6
235018.0-055927	357.57513	-5.99103	0.515 ¹	new	0.349 ± 0.111	1.81 ± 0.21	5000.0	22.3
235034.0-300604	357.64292	-30.10119	0.23 ¹	2350.6-3005	7.51 ± 0.73	2.07 ± 0.08	2325.4	259.0
235116.1-760015	357.81721	-76.00431	0.25 ⁵	2351.3-7559	5.00 ± 0.43	1.98 ± 0.07	2847.9	342.5
235321.1-145857	358.33788	-14.98264	0.5 ⁵	2353.5-1457	0.823 ± 0.304	2.02 ± 0.30	3062.4	16.4
235604.0-002353	359.01671	-0.39825	0.283 ¹	new	0.300 ± 0.242	1.58 ± 0.37	3000.0	9.90
235612.2+403644	359.05067	40.61247	0.331 ¹	2356.2+4036	3.50 ± 0.38	1.94 ± 0.08	3196.4	220.7
235730.0-171803	359.37487	-17.30083	0.85 ³	2357.4-1718	1.25 ± 0.15	1.70 ± 0.08	5322.0	225.6
235825.2+382856	359.60496	38.48236	0.24 ⁵	2358.3+3830	8.48 ± 0.97	2.14 ± 0.10	2114.3	163.3
235836.8-180717	359.65346	-18.1215	0.39 ³	2358.5-1808	7.67 ± 0.68	1.83 ± 0.06	2561.1	430.2
235907.9-303740	359.78283	-30.62792	0.165 ¹	2359.0-3038	5.84 ± 0.54	1.80 ± 0.06	2787.5	424.5
235917.0+021520	359.821	2.25564	0.0 ³	new	0.540 ± 0.121	1.85 ± 0.14	5000.0	48.3
235919.5-204756	359.83138	-20.79892	0.096 ¹	2359.3-2049	6.84 ± 0.82	1.98 ± 0.09	2121.9	196.8
235955.0+314600	359.98042	31.76667	0.33 ⁵	new	0.854 ± 0.138	1.85 ± 0.12	5000.0	96.8